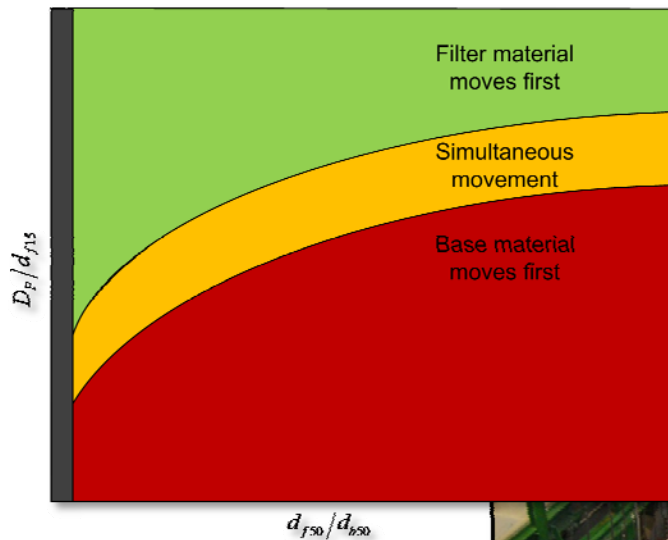


# STABILITY OF OPEN FILTER STRUCTURES



*MSc. Thesis*

*S.A.H. van de Sande*

*June 2012, Delft*

*REVISION, AUGUSTUS 2013*

Published through the Delft University of Technology Institutional Repository, based on Open Access. The author remains exclusive full ownership and exploitation rights.

Contact via: [stefan\\_van\\_de\\_sande@hotmail.com](mailto:stefan_van_de_sande@hotmail.com)

**Figures cover**, from left to right; 1) distinction between test results, 2) Environmental Fluid Mechanics Laboratory at Delft University of Technology, flume with model, 3) transport of filter material

# STABILITY OF OPEN FILTER STRUCTURES

*MSc. Thesis*

*S.A.H. van de Sande*

*JUNE 2012*

*REVISION, AUGUSTUS 2013*

**GRADUATION COMMITTEE:**

PROF. DR. IR. W.S.J. UIJTTEWAAL

IR. H.J. VERHAGEN

IR. J.P. VAN DEN BOS

IR. H.J. VERHEIJ

**DELFT UNIVERSITY OF TECHNOLOGY**

FACULTY OF CIVIL ENGINEERING AND GEOSCIENCES

SECTION HYDRAULIC ENGINEERING

**DELTA RES**



## ***MSC. THESIS: STABILITY OF OPEN FILTER STRUCTURES***

**ING. S.A.H. (STEFAN) VAN DE SANDE**

*Student number:* 1533304  
*Mail:* [stefan\\_van\\_de\\_sande@hotmail.com](mailto:stefan_van_de_sande@hotmail.com)  
*Mob.:* +31 (0)652656717  
*Address:* Zuideindseweg 13  
2645 BD Delfgauw

### ***GRADUATION COMMITTEE:***

**PROF.DR.IR. W.S.J. UIJTTEWAAL**

*Chairman of the committee*

*Delft University of Technology*

*Professor of Experimental Hydraulics, Head Environmental Fluid  
Mechanic Laboratory, Head Environmental Fluid Mechanics Section*

**IR. H.J. VERHAGEN**

*Supervisor*

*Delft University of Technology*

*Lecturer at the section of Hydraulic Engineering*

**IR. J.P. VAN DEN BOS**

*Supervisor*

*Delft University of Technology*

*Guest Lecturer at the section of Hydraulic Engineering*

**IR. H.J. VERHEIJ**

*Daily supervisor*

*Deltares*

*Senior advisor/researcher*

*Unit: Fresh water systems*

*Unit: River engineering and transport over water*



*“When dealing with water, first experiment then use judgement”*

*Leonardo da Vinci (1452-1519)*

*“Truth is what stands the test of experience”*

*Albert Einstein (1879-1955)*

**Keywords:** Bed protection, (open) filter (structure(s)), granular filter, geometrically open, design formula, riprap, model tests, flume experiments.

# ABSTRACT

---

Granular filters are used for protection against scour and erosion. For a proper functioning it is necessary that interfaces between the filter structure, the subsoil and the water flowing above the filter structure are stable. Stability means that there is no transport of subsoil material through the filter to the water above the filter, and that no filter material is removed by currents above the filter.

Three types of granular filters can be distinguished; 1) Geometrically closed filter structures, 2) Stable geometrically open filter structures, 3) Unstable geometrically open filter structures. This research is focusing on stable geometrically open filter structures.

Recently, a desk study has been carried out by Deltares resulting in a new theoretical formula for single layered geometrically open filter structures (CUR, 2010). Hoffmans improved the theoretical formula that had been founded by Deltares (Hoffmans G. , 2012)

The goal of this research was to verify the formula found by Hoffmans [2012] for structures loaded by currents (flow parallel to the filter construction). As part of the verification of the design formula ten flume experiments were performed in the Environmental Fluid Mechanic Laboratory at Delft University of Technology.

After the execution of the model tests an extensive analysis was made based on the performed model tests and model tests performed in the past (Bakker [1960], Haverhoek [1968], Wouters [1982], Konter et al. [1990], Van Huijstee and Verheij [1991] and Van Velzen [2012]).

The analysis showed that the formula is valid for single layered geometrically open filter structures loaded by currents. Two adjustments to the design formula are proposed:

1. The relative layer thickness fits better when related to the median sieve diameter of the filter material;
2. The alpha value proposed by Hoffmans [2012] is too high (new alpha values are 30% to 60% lower).

The original formula as proposed by Hoffmans [2012] gives unrealistic values for situations with wide graded filter material. Model tests showed that the relative layer thickness is better represented when related to the median sieve diameter of the filter material.

The design formula can be used for design purposes. The design of a single layered geometrically open filter structure can be schematized in two steps;

1. Firstly, determination of the material that should be used for the top-layer;
2. Secondly, determination of the layer-thickness of the filter/top-layer taking into account filter and base material characteristics.



# SUMMARY

---

Granular filters are used for protection against scour and erosion. For a proper functioning it is necessary that interfaces between the filter structure, the subsoil and the water flowing above the filter structure are stable. Stability means that there is no transport of subsoil material through the filter to the water above the filter, and that no filter material is removed by currents above the filter.

The following types of granular filters can be distinguished, based on two criteria; 1) base material can pass the pores in the filter material, 2) hydraulic load is larger than threshold value;

- Geometrically closed filter structures;
- Stable geometrically open filter structures;
- Unstable geometrically open filter structures.

This research is focusing on stable geometrically open filter structures.

Recently, a desk study has been carried out by Deltares resulting in a new theoretical formula for single layered geometrically open filter structures (CUR, 2010). Hoffmans improved the theoretical formula that had been founded by Deltares, resulting in the following formula (Hoffmans G. , 2012):

$$\frac{D_f}{d_{f15}} = \alpha_d \ln \left( \frac{\Delta_f d_{f50} \Psi_{cf} (1 - \gamma V_{Gf})}{\Delta_b d_{b50} \Psi_{cb} (1 - \gamma V_{Gb})} \right)$$

The goal of this research was to verify the above mentioned formula for structures loaded by currents (flow parallel to the filter construction). As part of the verification of the design formula ten tests were performed in the Environmental Fluid Mechanics Laboratory at Delft University of Technology.

Test number	$d_{b50}$ [ $\mu\text{m}$ ]	$d_{f50}$ [mm]	$d_{f50}/d_{b50}$ [-]	$D_f$ [mm]	Result
<b>To1</b>	309	8.57	27.73	20	$\mathbf{U_{b,c} > U_{f,c}}$
<b>To2a</b>	309	25.01	80.94	27	$\mathbf{U_{b,c} < U_{f,c}}$
<b>To2b</b>	309	25.01	80.94	27	$\mathbf{U_{b,c} < U_{f,c}}$
<b>To3</b>	309	25.01	80.94	61.5	$\mathbf{U_{b,c} \approx U_{f,c}}$
<b>To4</b>	633	25.01	39.51	27	$\mathbf{U_{b,c} \approx U_{f,c}}$
<b>To5</b>	309	17.86	57.80	8	$\mathbf{U_{b,c} < U_{f,c}}$
<b>To6a</b>	309	17.86	57.80	40	$\mathbf{U_{b,c} \approx U_{f,c}}$
<b>To7</b>	309	17.86	57.80	57	$\mathbf{U_{b,c} > U_{f,c}}$

*\* Test To6b and To6c are test situation with high turbulent intensities (tested base and filter material are similar to test To6a)*

**Table 1 Performed model tests (incl. results)**

The results of the model tests are divided in three categories;

- Base material moves at a lower critical velocity than the filter material ( $u_{b,c} > u_{f,c}$ );
- Base and filter material start to move at about the same critical velocity ( $u_{b,c} \approx u_{f,c}$ );
- Filter material moves at a lower critical velocity than the base material ( $u_{b,c} < u_{f,c}$ ).

After the execution of the model tests an extensive analysis was made based on the performed model tests and model tests performed in the past (Bakker [1960], Haverhoek [1968], Wouters [1982], Konter et al. [1990], Van Huijstee and Verheij [1991] and Van Velzen [2012]).

The analysis showed that the formula is valid for single layered geometrically open filter structures loaded by currents. Two adjustments to the design formula are proposed:

1. The relative layer thickness fits better when related to  $d_{f50}$  instead of  $d_{f15}$ ;
2. The alpha value proposed by Hoffmans [2012] is too high ( $\alpha_d=1.5$ ).

When the relative layer thickness is related to  $d_{f15}$  it gives unrealistic values for situations with wide graded filter material. Model tests showed that the relative layer thickness is better represented when related to the  $d_{f50}$  of the filter material.

Based on this research the following representation of the design formula for single layered geometrically open filter structures is proposed (the two adjustment mentioned above are included in this adjusted formula):

$$\frac{D_f}{d_{f50}} = \alpha_d \ln \left( \frac{d_{f50}}{d_{b50}} \frac{\Delta_f}{\Delta_b} \frac{\Psi_{c,f}}{\Psi_{c,b}} \frac{1 - \gamma V_{Gf}}{1 - \gamma V_{Gb}} \right)$$

With the following values for alpha;

- Deterministic approach:
  - $\alpha_d = 0.82$ , safe upper-limit;
  - $\alpha_d = 0.69$ , 90% confidence limit;
- Probabilistic approach; Log-normal distribution, with:
  - $\mu = -0.86$ ;
  - $\sigma = 0.38$ ;
  - $E(\alpha_d) = 0.46$ ;
  - $Var(\alpha_d) = 0.04$ .

The design formula can be used for design purposes. The design of a single layered geometrically open filter structure can be schematized in two steps;

- Firstly, determination of the material that should be used for the top-layer;

- Secondly, determination of the layer-thickness of the filter/top-layer taking into account filter and base material characteristics.

Further several recommendations are proposed for further research;

- Additional model tests to make the formula applicable for a wider range of situations;
  - Additional tests with wide graded filter materials;
  - Tests with geometrically open filter structures loaded by highly turbulent situations (e.g. behind bridge piles or a sill);
  - Tests were the geometrically open filter structures are loaded by waves;
  - Tests with geometrically open filter structures on a slope;
- Research into damping within granular layers;
- Research into multiple layered geometrically open filter structures.



# PREFACE

---

This thesis is a final report of a research project undertaken in order to obtain the degree of Master of Science at Delft University of Technology.

The thesis is about experimental research in order to obtain better insights into geometrically open filter structures and to improve the current design rules for geometrically open filter structures. The research was mainly conducted at the office of Deltares and the Environmental Fluid Mechanic Laboratory at Delft University of Technology. The performed research could not be achieved without the assistance of many people who I would like to thank.

First of all I would like to thank my graduation committee prof.dr.ir. W.S.J. Uijttewaai, ir. H.J. Verheij, ir. H.J. Verhagen and ir. J.P. van den Bos for their guidance and feedback during the project.

In addition I would like to thank all staff members from the Environmental Fluid Mechanic Laboratory for their help and support. Special thanks to Sander de Vree, Arie den Toom and Jaap van Duin.

Finally, I want to thank my parents and friends for their support throughout my studies.

*Delft, June 2012*

S.A.H. (Stefan) van de Sande

One year after graduation I made this updated version of my MSc thesis. In the original version there was a mistake in appendix B. This mistake has been corrected together with the tables and figures that changed as a consequence of the made correction.

I used the opportunity to rephrase some parts of the thesis to make them more clear and prevent wrong interpretations (e.g. the parts concerning statistics are revised).

The changes did not change the general conclusions, those are still valid.

Finally I would like to thank the persons who read my thesis and contacted me about the mistake and indecipherable parts.

*Gemonde, August 2013*

S.A.H. (Stefan) van de Sande



# TABLE OF CONTENTS

---

<b>ABSTRACT</b> .....	<b>II</b>
<b>SUMMARY</b> .....	<b>IV</b>
<b>PREFACE</b> .....	<b>VIII</b>
<b>NOMENCLATURE</b> .....	<b>XII</b>
ROMAN SYMBOLS.....	XII
GREEK SYMBOLS.....	XIII
FREQUENTLY USED INDICES .....	XV
ABBREVIATIONS .....	XV
COORDINATE SYSTEM .....	XVI
OTHER NOTATIONS.....	XVI
<b>FIGURES</b> .....	<b>XVII</b>
MAIN REPORT .....	XVII
APPENDIXES.....	XVIII
<b>TABLES</b> XIX	
MAIN REPORT .....	XIX
APPENDIXES.....	XX
<b>1 INTRODUCTION</b> .....	<b>2</b>
1.1 PROBLEM DEFINITION.....	3
1.2 OBJECTIVE.....	3
1.3 OUTLINE.....	4
<b>2 THEORETICAL BACKGROUND</b> .....	<b>6</b>
2.1 FAILURE MECHANISMS.....	6
2.2 HYDRAULIC LOAD .....	8
2.3 FLOW STABILITY .....	10
2.4 GRANULAR FILTERS .....	14
2.5 WIDE-GRADED FILTER MATERIAL.....	20
2.6 RESULTS PREVIOUS TESTS .....	20
<b>3 ANALYSIS OF THE NEW DESIGN FORMULA</b> .....	<b>22</b>
3.1 DERIVATION OF THE DESIGN FORMULA .....	22
3.2 PARAMETERS .....	25
3.3 COMPARISON WITH THE BAKKER-KONTER AND WÖRMAN FORMULA .....	31
<b>4 MODEL TEST SET-UP</b> .....	<b>34</b>
4.1 PARAMETER VARIATION .....	34
4.2 FLUME.....	35
4.3 SCALING .....	36
4.4 MEASUREMENTS.....	37
4.5 TEST SET-UP .....	42

4.6	TEST PROGRAM .....	45
4.7	MATERIAL PROPERTIES .....	48
4.8	EXECUTION OF THE MODEL TESTS .....	49
<b>5</b>	<b>TEST RESULTS .....</b>	<b>52</b>
5.1	HYDRAULIC CONDITIONS .....	52
5.2	TRANSPORT OF MATERIAL .....	57
5.3	DAMPING OF PRESSURE FLUCTUATIONS.....	64
5.4	HIGH TURBULENCE LEVELS .....	65
5.5	SOURCES OF ERRORS.....	69
<b>6</b>	<b>ANALYSIS AND DISCUSSION .....</b>	<b>72</b>
6.1	ANALYSIS ALPHA D AND RELATIVE LAYER THICKNESS .....	72
6.2	EFFECT OF HIGHER TURBULENT INTENSITY .....	80
6.3	MULTIPLE LAYERED BED PROTECTIONS .....	82
6.4	JUSTIFICATION SIMPLIFICATIONS .....	83
<b>7</b>	<b>DESIGN GUIDELINE.....</b>	<b>86</b>
7.1	DIMENSION TOP-LAYER MATERIAL .....	86
7.2	REQUIRED LAYER-THICKNESS .....	86
7.3	INSUFFICIENT DATA .....	87
7.4	LIMITATIONS .....	88
7.5	EXAMPLE.....	88
<b>8</b>	<b>CONCLUSIONS AND RECOMMENDATIONS.....</b>	<b>92</b>
8.1	CONCLUSIONS.....	92
8.2	RECOMMENDATIONS.....	95
	<b>REFERENCES .....</b>	<b>98</b>
	<b>PUBLICATIONS.....</b>	<b>100</b>
	<b>APPENDICES.....</b>	<b>102</b>
A	DATA PREVIOUS MODEL TESTS .....	A-2
B	MATERIAL PROPERTIES.....	B-10
C	DIMENSIONS ELASTOCOAST SLABS.....	C-16
D	VELOCITY METERS .....	D-18
E	TEST FACILITY.....	E-24
F	RESULTS MODEL TESTS .....	F-28
G	DEVIATION OF TRANSPORT MEASUREMENTS.....	G-38
H	SPECTRAL ANALYSIS.....	H-40

# NOMENCLATURE

---

## ROMAN SYMBOLS

Symbol	Unit	Description
$A$	$[m^2]$	Area
$a$	$[s/m]$	Forchheimer coefficient
$b$	$[m]$	Width
$b$	$\left[ \frac{s^2}{m^2} \right]$	Forchheimer coefficient
$C$	$[-]$	Coefficient
$C$	$\left[ \frac{\sqrt{m}}{s} \right]$	Chézy coefficient $\left[ C = 18 \log \left( \frac{12R}{k_r} \right) \right]$
$C_0$	$[-]$	Turbulence coefficient in Bakker-Konter formula
$c$	$[-]$	Coefficient in Klein-Breteler formula
$c_k$	$[-]$	Covariance coefficient (where $k = \text{lag}$ )
$c_v$	$\left[ \frac{m^2}{s} \right]$	Consolidation coefficient
$D$	$[m]$	Layer thickness
$d$	$[m]$	Diameter
$d_{n50}$	$[m]$	Median nominal diameter
$d_{nx}$	$[m]$	Nominal grain diameter, where $x\%$ of the mass has a smaller diameter
$d_x$	$[m]$	Grain diameter, where $x\%$ of the grains has a smaller diameter (sieve diameter)
$d_*$	$[-]$	Dimensionless particle diameter $\left[ d_* = d \left( \frac{\Delta g}{\nu^2} \right)^{1/5} \right]$
$E(x)$		Mean value of “ $x$ ”
$e$	$[-]$	Coefficient to take the difference between an open channel flow and flow within a granular filter into account (Bakker-Konter formula)
$F$	$[N]$	Force
$Fr$	$[-]$	Froude number
$F_s$	$[-]$	Conversion factor
$f$	$[Hz]$	Measuring frequency
$g$	$\left[ \frac{m}{s^2} \right]$	Acceleration of gravity $\left[ g = 9.81 \frac{m}{s^2} \right]$
$h$	$[m]$	Water depth
$I$	$[m^3]$	Volume
$i$	$[-]$	Gradient
$K$	$[-]$	Coefficient (Izbash)
$K$	$[-]$	Correction coefficient for granular layers placed against a wall
$k$	$\left[ \frac{m^2}{s^2} \right]$	Turbulent kinetic energy
$k$	$[-]$	Lag
$k_{f,s}$	$\left[ \frac{m^2}{s^2} \right]$	Turbulent energy due to gravity

Symbol	Unit	Description
$k_r$	[m]	Roughness of the bed (/wall) Granular bed: $k_r = 2d_{n50}$ Glass: $k_r = 3 \cdot 10^{-6}$
$L_d$	[m]	Damping length
$L_m$	[m]	Bakhmetev mixing length $\left[ L_m = \kappa z \sqrt{1 - \frac{z}{h}} \right]$
$l$	[m]	Length
$M$	[Nm]	Moment
$m$	[-]	Coefficient in Klein-Breteler formula
$N$	[-]	Number of samples
$n$	[-]	Porosity
$n_x$	[-]	Scaling factor (x indicates the parameter that is scaled)
$p$	$\left[ \frac{N}{m^2} \right]$	Pressure
$q$	[kg/s]	Amount of transported material
$q$	[N/m]	Distributed load
$R$	[m]	Hydraulic radius
$Re$	[-]	Reynolds number
$r$	[-]	Relative fluctuation/turbulence intensity
$r_0$	[-]	Depth averaged turbulent intensity
$r_k$	[-]	Autocorrelation coefficient (where k = lag)
$T$	[s]	Period (of the vortex)
$t$	[s]	Time
$u$	[m/s]	Velocity (velocity in the x direction)
$u_*$	[m/s]	Shear velocity $\left[ u_* = \bar{u} \frac{\sqrt{g}}{C} \right]$
$Var(x)$	[-]	The variance of "x" Variation coefficient representing the non-uniformity of the material
$V_G$	[-]	$\left[ V_G = 1 - \frac{d_{15}}{d_{50}} \right]$
$v$	[m/s]	Velocity in the y direction
$W$	[kg]	Weight
$W$	[m <sup>3</sup> ]	Modulus
$w$	[m/s]	Velocity in the z direction

## GREEK SYMBOLS

Symbol	Unit	Description
$\alpha$	[-]	Forchheimer coefficient
$\alpha$	[-]	Fitting coefficient
$\alpha_d$	[-]	Coefficient
$\alpha_k$	[-]	Coefficient
$\alpha_t$	[-]	Turbulence coefficient

Symbol	Unit	Description
$\alpha_v$	[-]	Coefficient $\left[ \alpha_v = \frac{1}{C_D} \left( \frac{2r_f^2}{\chi_k} \right)^2 \right]$
$\beta$	[-]	Forchheimer coefficient
$\beta$	[-]	Fitting coefficient
$\gamma$	[-]	Transport parameter $[\gamma = 0.625]$
$\Delta$	[-]	Under water relative material density $\left[ \Delta = \frac{\rho_s - \rho_w}{\rho_w} \right]$
$\eta$	[-]	Turbulence parameter
$\eta$	[-]	Ratio between shear stresses at the upper and lower level boundary of the filter
$\eta$	[-]	Relative load
$\kappa$	[-]	Von Kármán constant $[\kappa \approx 0.38]$
$\lambda$	[m]	Vortex length
$\mu$	[-]	Mean value
$\mu$	[-]	Parameter log-normal distribution
$\rho$	$\left[ \frac{kg}{m^3} \right]$	Density
$\rho_w$	$\left[ \frac{kg}{m^3} \right]$	Density of water $\left[ \rho_w = 999 \frac{kg}{m^3} \right]$
$\sigma$	[-]	Standard deviation
$\sigma$	[-]	Parameter log-normal distribution
$\sigma$	$\left[ \frac{N}{m^2} \right]$	Normal stress
$\sigma_s$	$\left[ \frac{N}{m^2} \right]$	Tensile strength
$\tau$	$\left[ \frac{N}{m^2} \right]$	Shear stress
$\tau_0$	$\left[ \frac{N}{m^2} \right]$	Mean shear stress
$\nu$	$\left[ \frac{m^2}{s} \right]$	Kinematic viscosity $\left[ \nu = 10^{-6} \frac{m^2}{s} (T = 20^\circ) \right]$
$\chi_k$	[-]	Turbulence coefficient $[\chi_k = 3.3]$
$\Psi$	[-]	Stability parameter
$\Psi_{Hoan}$	[-]	Stability parameter in Hoan formula $[\Psi_{Hoan,c} = 2.9]$
$\Psi_{Lm}$	[-]	Stability parameter in Hofland formula $[\Psi_{Lm,c} = 0.5]$
$\Psi_{wl}$	[-]	Stability parameter in Jongeling formula $[\Psi_{wl,c} = 4.4]$

## FREQUENTLY USED INDICES

<b>Indices</b>	<b>Description</b>
<i>b</i>	Base layer, base material
<i>bf</i>	Transition of the filter-base layer
<i>c</i>	Critical
<i>f</i>	Filter layer, filter material
<i>u</i>	Velocity in the x direction
<i>v</i>	Velocity in the y direction
<i>w</i>	Velocity in the z direction

## ABBREVIATIONS

<b>Abbreviation</b>	<b>Description</b>
ADV	Acoustic Doppler Velocimeter
EMS	Electromagnetic flow meter
eq.	Equation
LDA	Laser Doppler Anemometry
l.h.s.	Left Hand Side
r.h.s.	Right Hand Side
r.m.s.	Root Mean Square
std	
TU	University of Technology
T01S01	File encoding (discharge, pressure and transport measurements) T01: Test number S01: Situation number
T01S01L01H42	File encoding (ADV measurements) T01: Test number S01: Situation number L01: Location number H42: Height (as indicated on the ADV)

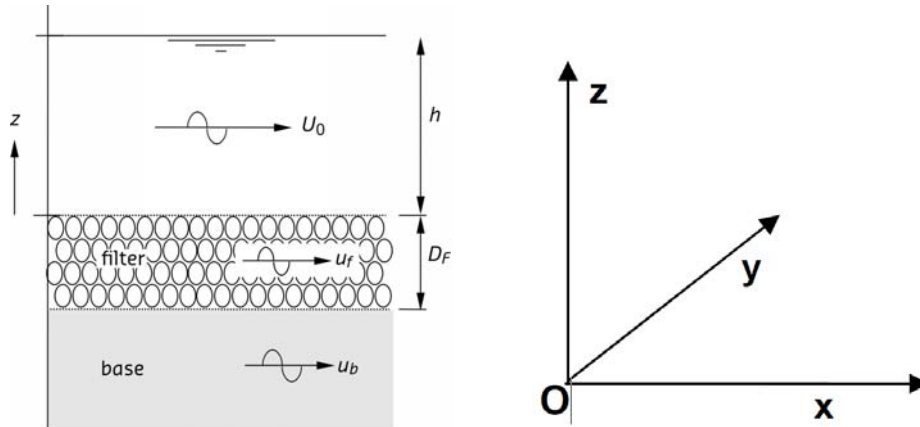
## COORDINATE SYSTEM

In this thesis a coordinate system is used in which;

- x = horizontal coordinate, in the direction of the flow
- y = horizontal coordinate, perpendicular to the flow
- z = vertical coordinate, positive upwards

Two different locations are used for  $z = 0$ ;

- $z=0$ , top of the filter layer
- $z=0$ , bottom of the flume (this one is used for the measurements, because the bottom is a fixed point)



## OTHER NOTATIONS

Notation	Description
$\bar{x}$	Averaged value of $x$
$x'$	(turbulent) fluctuation of $x$
$\langle x \rangle_y$	Spatial average over distance $y$

# FIGURES

---

## MAIN REPORT

Figure 2-1 Failure mechanisms .....	6
Figure 2-2 Distribution of shear stress.....	10
Figure 2-3 Forces on a grain in flow (Schierreck, 2004).....	10
Figure 2-4 Critical shear stress according to Shields (Shields, 1936).....	12
Figure 2-5 Types of granular filters .....	14
Figure 2-6 Possible design criteria for granular filters (Schierreck, 2004).....	15
Figure 2-7 Determination of the critical gradient according to Klein Breteler [1989] (CUR, 2010).....	18
Figure 2-8 The basics of the transport model by Den Adel (CUR, 2010).....	20
Figure 3-1 Distribution of the mean and characteristic load (CUR, 2010) .....	22
Figure 3-2 Critical Shields parameters according to Van Rijn (d calculated with $\nu=1.33 \cdot 10^{-6} \text{ m}^2/\text{s}$ and $\rho=2650 \text{ kg/m}^3$ ) (Schierreck, 2004) .....	28
Figure 3-3 Stability parameter $d^* = d_{50}(\Delta g / \nu^2)^{1/3}$ (CUR, 2010).....	28
Figure 3-4 Experimental data of Klar [2005] (Hoffmans G. , 2012).....	31
Figure 3-5 $D_F/d_{f50}$ versus the critical $d_{f50}/d_{b50}$ . The (linear) Wörman equation and the new logarithmic equation compared with measurements (Hoffmans G. , 2012).....	33
Figure 4-1 Determination critical velocity.....	34
Figure 4-2 Movement of filter material and base material.....	35
Figure 4-3 Flume with test set-up in the Environmental Fluid Mechanic Laboratory .....	36
Figure 4-4 Transport of filter material (black arrow indicates main flow direction) .....	37
Figure 4-5 Sieve in the drain of the flume .....	39
Figure 4-6 Sieve design (dimensions in cm) .....	39
Figure 4-7 Left: Sieve with lifting frame, Middle: Stack of sieves, Right: Sieve placed with a crane.....	40
Figure 4-8 Weighing the sand collected in a sieve.....	40
Figure 4-9 ADV, transmitter (blue part in the middle) and receivers (4 legs).....	42
Figure 4-10 Pressure meters (schematic representation).....	42
Figure 4-11 Sand bed between two concrete slabs with on top slabs of stones (glued together with elastocoast).....	45
Figure 4-12 Overview of the tests .....	47
Figure 4-13 Sill (left: top view (flow direction: from bottom to top), right: side view (flow direction: from left to right)), height sill: 6,5 cm .....	48
Figure 4-14 Round and rectangular piles used to increase the turbulent intensity.....	48
Figure 4-15 Materials, top: filter material (left: Yellow Sun 8-11, right: Yellow Sun 20-40), bottom: base material (left: m32, right: 0.50-0.80) .....	49
Figure 4-16 Flowchart model test.....	50
Figure 5-1 Single velocity measurement (To1So1Lo1H11), top: raw signal, bottom: despiked signal .....	53
Figure 5-2 Location of the cross-sections.....	53

Figure 5-3 Flow profiles test 1, situation 2 (To1So2)..... 54

Figure 5-4 Flow profiles at cross-section 1 and 2, left: To1So2, right: To4So6..... 55

Figure 5-5 Velocity profiles and turbulent intensities ..... 56

Figure 5-6 Vortex length ..... 56

Figure 5-7 Transport of filter material, test To1 (black arrow indicates main flow direction) ..... 57

Figure 5-8 Transport of base material..... 58

Figure 5-9 Sand (base material) transported through the filter layer ..... 59

Figure 5-10 Transport of base and filter material, test To1 ..... 60

Figure 5-11 Transport of base and filter material, test To2 ..... 60

Figure 5-12 Test results, simplified representation design formula, layer thickness;  $D_f/d_{f15}$  (used  $\alpha_d$  values are explained in chapter 6) ..... 62

Figure 5-13 Test results, layer thickness;  $D_f/d_{f15}$  (used  $\alpha_d$  values are explained in chapter 6) ..... 62

Figure 5-14 Test results, simplified representation design formula, layer thickness;  $D_f/d_{f50}$  (used  $\alpha_d$  values are explained in chapter 6) ..... 63

Figure 5-15 Test results, layer thickness;  $D_f/d_{f50}$  (used  $\alpha_d$  values are explained in chapter 6) ..... 63

Figure 5-16 Velocity profiles, up and downstream of the sill ..... 66

Figure 5-17 Turbulent intensities, up and downstream of the sill..... 67

Figure 5-18 Turbulent motion and erosion behind a round pile..... 68

Figure 5-19 Erosion behind a round pile (red lines indicate the diverging turbulent motion)..... 69

Figure 5-20 Erosion behind a rectangular pile ..... 69

Figure 5-21 Pressure tubes attached to the flume wall ..... 70

Figure 5-22 Left: Valve (discharge), Middle and right: Weir (manually) ..... 71

Figure 6-1 Distribution  $\alpha_d$  values (best-fit: log-normal distributions)..... 80

Figure 6-2 Damping in multiple layered geometrically open filter structures..... 83

Figure 7-1 Stability parameter  $d^* = d_{50}(\Delta g / \nu^2)^{1/3}$  ( $\nu \approx 10^{-6}$  m<sup>2</sup>/s) (CUR, 2010)..... 87

## APPENDIXES

Figure A-1 Sections as used within report Van Velzen [2012], the inner circle represents the pile, the outer circle the bed protection and the black arrow indicates the flow direction (Van Velzen, 2012) ..... A-8

Figure B-1 Sieve curves base and filter material ..... B-10

Figure C-1 Schematic representation of a lifted slab of filter material ..... C-16

Figure D-1 Measuring, Vectrino (ADV) (Nortek, 2009) ..... D-20

Figure D-2 Doppler shift (Wikipedia) ..... D-20

Figure D-3 Sideward looking ADV (left picture (Nortek, 2009)) ..... D-21

Figure D-4 Detailed drawing of the Vectrino (Nortek, 2009) ..... D-23

Figure E-1 Design model test (dimensions in cm) ..... E-26

Figure F-1 Transported filter material, test To1 (black arrow indicates main flow direction) ..... F-28

Figure F-2 Transport of base/filter material vs. average velocity, To1..... F-29

Figure F-3 Left: Retreating filter layer test To2b (black arrow indicates main flow direction), Right: Base layer after the test (after removing the filter layer, test To2a) ..... F-31

Figure F-4 Transport of base/filter material vs. average velocity, test T02a and T02b .....	F-31
Figure F-5 Transport of base/filter material vs. average velocity, test T03 .....	F-32
Figure F-6 Transport of base/filter material vs. average velocity, test T04 .....	F-33
Figure F-7 Winnowing (in large quantities) during test T05.....	F-34
Figure F-8 Transport of base/filter material vs. average velocity, test T06a .....	F-35
Figure F-9 Transport of base/filter material vs. average velocity, test T07 .....	F-36
Figure H-1 Autocorrelation velocity measurement .....	H-41
Figure H-2 Autocorrelation velocity measurement .....	H-43
Figure H-3 Distribution of the length scale, method 1 (based on 219 measurements).....	H-44
Figure H-4 Distribution of length scale for situations with high turbulence levels, method 1 (based on 24 measurements).....	H-44
Figure H-5 Distribution of the length scale, method 2 (based on 219 measurements).....	H-45
Figure H-6 Distribution of length scale for situations with high turbulence levels, method 2 (based on 24 measurements) .....	H-45

## TABLES

---

### MAIN REPORT

Table 2-1 Parameters according to Klein Breteler [1992] (Wolters, to be published).....	17
Table 3-1 Design formulas single layered geometrically open filter structures .....	32
Table 4-1 Properties flume .....	35
Table 4-2 Maximum length filter material slabs (to prevent breaking by own weight).....	44
Table 4-3 Weight of the filter material slabs .....	44
Table 4-4 Test situations.....	46
Table 4-5 Dimensions of the used obstructions .....	48
Table 4-6 Dimensions and density base material .....	49
Table 4-7 Dimensions and density filter material.....	49
Table 5-1 Results of the model test, categorized (colours represent locations as mentioned in Figure 4-2) .....	61
Table 5-2 Variation in the standard deviations of the measuring data .....	65
Table 6-1 Alpha values (ranked from high to low), related to the model tests.....	73
Table 6-2 Alpha values (ranked from high to low) for all model tests, relative layer thickness: $D_f/d_{f15}$ .....	75
Table 6-3 Alpha values (ranked from high to low) for all model tests, relative layer thickness: $D_f/d_{f50}$ .....	76
Table 6-4 Deterministic $\alpha_d$ values .....	77
Table 6-5 Distributions $\alpha_d$ values .....	80
Table 6-6 Log-normal distributions $\alpha_d$ values .....	80
Table 6-7 Relative density, stability parameter and shape factors.....	83
Table 7-1 Properties bed material.....	89

Table 7-2 Available granular materials ..... 89  
 Table 7-3 Results example ..... 91

## APPENDIXES

Table A-1 Base material used for all the tests (Bakker, 1960)..... A-3  
 Table A-2 Data model tests Bakker [1960], colours in the right column are  
 corresponding to situations as explained in paragraph 4.1 ..... A-3  
 Table A-3 Data model tests Haverhoek [1968] ..... A-4  
 Table A-4 Model tests Wouters [1982], colours in the right column are  
 corresponding to the situations as explained in paragraph 4.1 ..... A-4  
 Table A-5 Model tests Wörman [1989](Wörman, 1989) ..... A-5  
 Table A-6 Base material used for all the tests (Konter et al., 1990) ..... A-5  
 Table A-7 Model tests Konter et al. [1990], colours in the right column are  
 corresponding to situations as explained in paragraph 4.1 ..... A-6  
 Table A-8 Model tests Van Huijstee and Verheij [1991], colours in the right  
 column are corresponding to situations as explained in paragraph 4.1 ..... A-7  
 Table A-9 Model tests Dixen [2008] ..... A-7  
 Table A-10 Material properties model tests Van Velzen [2012] ..... A-8  
 Table A-11 Model tests Van Velzen [2012] ..... A-8  
 Table B-1 Results sieving base material: M32 ..... B-11  
 Table B-2 Results sieving base material: 0.50-0.80 ..... B-11  
 Table B-3 Density base material ..... B-12  
 Table B-4 Main properties base material ..... B-12  
 Table B-5 Dimensions filter material..... B-13  
 Table B-6 Density filter material ..... B-13  
 Table B-7 Pores, filter layer ..... B-14  
 Table C-1 Maximum length filter material slabs ..... C-17  
 Table D-1 Velocity meters ..... D-18  
 Table D-2 Used settings, Vectrino (ADV) ..... D-22  
 Table F-1 Data test T01..... F-28  
 Table F-2 Data test T02..... F-30  
 Table F-3 Data test T03..... F-32  
 Table F-4 Data test T04..... F-33  
 Table F-5 Data test T05..... F-34  
 Table F-6 Data test T06..... F-35  
 Table F-7 Data test T06..... F-36  
 Table G-1 Deviation of transported base material (average velocity = 0.35  
 m/s) ..... G-39  
 Table G-2 Deviation of transported base material (average velocity = 0.65  
 m/s) ..... G-39



# 1 INTRODUCTION

---

Granular filters are used for protection against scour and erosion. For a proper functioning it is necessary that interfaces between the filter structure, the subsoil and the water flowing above the filter structure are stable. Stability means that there is no transport of subsoil material through the filter to the water above the filter, and that no filter material is removed by currents above the filter.

The following types of granular filters can be distinguished, based on two criteria; 1) base material can pass the pores in the filter material, 2) hydraulic load is larger than threshold value;

- Geometrically closed filter structures;
- Stable geometrically open filter structures;
- Unstable geometrically open filter structures.

In practice geometrically closed filter structures are most used. The reason for using geometrically closed filters instead of geometrically open filter structures can be explained by;

- The knowledge about geometrically open filter structures is limited and there are no clear design rules;
- Geometrically closed filter structures is a proven technology;
- There are clear design rules for geometrically closed filter structures.

For the construction of a bed or slope protection, multiple filter layers are needed. When the principle of geometrically open filter structures is used, the number of filter layers needed can be reduced (in comparison with geometrically closed filter structures). Limiting the number of filter layers reduces the construction time (resulting in lower costs).

In the last decades some attempts were made to introduce a new formula or design method for geometrically open filter structures. But none of them were really adopted by the field of hydraulic engineers.

The most generally accepted formula till now is the formula of Wörman (1989). Wörman investigated open filter structures behind bridge piers. Wörman's tests were for a specific situation and it is not proven that the formula is valid in other situations.

Recently, a desk study has been carried out by Deltares resulting in a new theoretical formula for single layered geometrically open filter structures (CUR, 2010). Hoffmans improved the theoretical formula that had been founded by Deltares, resulting in the following formula (Hoffmans G. , 2012):

$$\frac{D_f}{d_{f15}} = \alpha_d \ln \left( \frac{\Delta_f d_{f50} \Psi_{cf} (1 - \gamma V_{Gf})}{\Delta_b d_{b50} \Psi_{cb} (1 - \gamma V_{Gb})} \right) \quad [1.1]$$

This report describes the validation of the theoretically derived formula. The validation is based on model tests, executed in the Environmental Fluid Mechanics Laboratory at Delft University of Technology.

## 1.1 PROBLEM DEFINITION

The new design formula for stable geometrically open filter structures (equation [1.1]) is based on a theoretical approach. Within the theoretical derivation of the new design formula, some assumptions and simplifications are made. Before the formula can be used for designing bed protections, the formula has to be verified. To verify the applicability of the design formula model tests have been performed.

Basic assumptions underlying the design formula;

- The design formula does not directly take load conditions into account. The formula is completely based on relative dimensions of base and filter material;
- The formula assumes that the top/filter layer is designed in such a way that it can withstand the design load conditions. With the damping of load within the filter layer and the relative dimensions of the filter/base layer the minimal required layer thickness of the filter can be calculated.

According to CUR [2010] and Hoffmans [2012] the formula is applicable for protection structures loaded with currents and waves. This research has focused on currents only. The effect of waves should still be tested.

## 1.2 OBJECTIVE

The objective of the research is verification of the new design formula for single layered stable geometrically open filter structures (equation [1.1]), resulting in the following research question:

*“Is the theoretically derived design formula for geometrically open filter structures (Hoffmans G. , 2012) in agreement with the test results for a situation where a single layered granular filter experiences a flow velocity parallel to the filter structure?”*

Sub-questions related to the main research question:

- (1) *What relevant tests were done in the past?*
- (2) *What are parameters of importance?*
- (3) *How is the flow velocity (load) related to the design formula?*
- (4) *What is/are the value(s) of the coefficient  $\alpha_d$  ?*

## 1.3 OUTLINE

This report starts with a literature study/theoretical background of the different aspects related to this research (chapter 2).

In chapter 3 the design formula [1.1] is elaborated. First the derivation of the design formula is explained, followed by an extensive analysis of each of the parameters. The chapter concludes with a comparison with other design formulas for single layered geometrically open filter structures.

Chapter 4 discusses the mode set-up. The results of these tests are presented in chapter 5. Followed by chapter 6, where the results are used to discuss the design formula.

Chapter 7 gives a simple guideline for the design of single layered geometrically open filter structures.

The last chapter, chapter 8, presents the conclusions as well as some recommendations for further research.



## 2 THEORETICAL BACKGROUND

---

This chapter gives a brief summary of theory, literature, previous researches and tests related to this research. This overview is not complete and for details of the theory one is advised to read the original documents.

The chapter will start with an introduction concerning the possible failure mechanisms (paragraph 2.1). After explaining the possible failure mechanisms, theory about hydraulic load will be given (paragraph 2.2). In relation to the two most important failure mechanisms (shear failure and winnowing), theory about the stability of the top layer (paragraph 2.3) and the various types of filter constructions (paragraph 2.4) are explained.

In paragraph 2.5 information is given about the categorization of (wide) graded materials.

The last paragraph of this chapter (paragraph 2.6) is dedicated to all the previous model tests, related to this research, that have been executed in the past.

### 2.1 FAILURE MECHANISMS

Granular protections are used to prevent a bed from eroding. So when the bed beneath the granular protection layer is eroding, it can be seen as a failure of the protection.

There are multiple possibilities in which a granular protection can fail. A distinction can be made between three main failure mechanisms (see Figure 2-1);

- Shear failure;
- Winnowing;
- Edge failure.

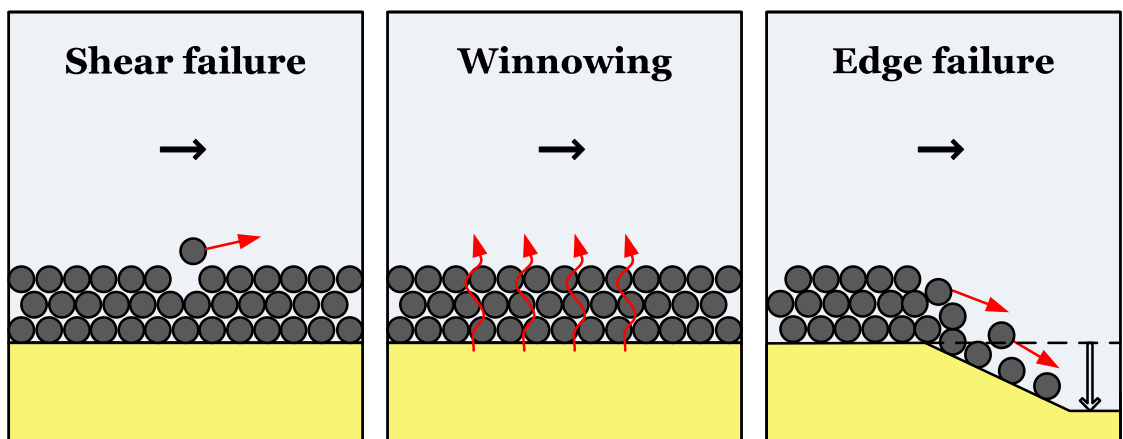


Figure 2-1 Failure mechanisms

### 2.1.1 SHEAR FAILURE

Shear failure arises when the load on a grain becomes larger than the resistance. When the load on a grain is larger than its resistance, it will start to move. This elementary balance of forces is valid for all the grains (filter and base material). The elementary balance of forces is explained in paragraph 2.3.1.

When the force on a stone becomes too large it starts to move, this movement continues until the resistance becomes larger than the load. Then the stone starts to settle again.

Limited movement of grains will not directly result in failure of a protection. As long as the transport rate is the same over the bed protection (and there is enough supply of material) the layer thickness will not decrease (Bosboom & Stive, 2011). This principle is used for transport filters.

When shear failure of the top layer occurs the filter layer becomes thinner, which reduces the damping within the filter and makes it easier for bed material to move through the filter (in case of a geometrically open filter structure). It goes without saying that when the load is strong enough to wash away the complete filter structure, erosion of the bed material will also occur afterwards.

To prevent shear failure, several design rules are available for the design of top layers. These design rules will be presented in paragraph 2.3.

### 2.1.2 WINNOWING

In case of geometrically open filter structures the protection of the base material is based on the damping of the load within the filter layer. The damping of the load results in lower forces beneath the filter than above the filter. The forces have to be damped in such a way that the force beneath the filter (on the transition of filter and base material) is not large enough to bring the grains of the bed material into movement.

When the damping is limited, the load conditions can bring the grain particles into movement. This can lead to washing out of base material through the filter layer. This mechanism is known as winnowing.

Besides washing out of particles through the filter layer, the material can also be transported inside the pores of the filter material.

To prevent winnowing attention has to be paid to the design of the filter layer(s). An introduction into the design of filter structures is given in paragraph 2.4.

### 2.1.3 EDGE FAILURE

The edge of a protection is a sensitive part. Special attention has to be paid to this part of the protection. A possible cause of failure of the edge of the protection is erosion behind the protection. When erosion behind the protection occurs, the bed lowers and finally the bed protection slides into the scour hole. Edge failure is not taken into account in this research. For more information

about edge failure one is referred to e.g. research about falling aprons (e.g. (Van Velzen, 2012)).

## 2.2 HYDRAULIC LOAD

A distinction can be made between two different hydraulic load conditions, namely currents (continuous load) and waves (cyclic load). This research takes only currents (continuous loads) into account.

For the validation of the design formula for cyclic loads (waves) additional research is needed.

This paragraph gives no introduction into the basics of currents and fluid mechanics, but focuses on turbulence and the development of shear stresses in the water column. For information about basic fluid mechanics, the following literature is recommended; “CT2100 Vloeistofmechanica” (in Dutch) (Battjes, 2002), “Principles of Fluid Flow and Surface Waves in Rivers, Estuaries, Seas and Oceans” (Van Rijn, 2011).

### 2.2.1 TURBULENCE

According to Hinze [1975], turbulence is defined as follows: “*Turbulent fluid motion is an irregular motion, but statistically distinct average values can be discerned and can be described by laws of probability*” (Schierreck, 2004). To do so, the velocity is averaged over a period of time. The velocity/pressure can be written as the combination of an average velocity and a fluctuation:

$$\begin{aligned} u &= \bar{u} + u' \\ v &= \bar{v} + v' \\ w &= \bar{w} + w' \\ p &= \bar{p} + p' \end{aligned} \tag{2.1}$$

The period over which the velocity is averaged should be long enough to smoothen out the turbulence (larger than the large scale eddies) but shorter than general changes in the velocity.

The average of the fluctuations is by definition zero ( $\overline{u'} = 0$ ). So to indicate the intensity of the turbulence the root-mean-square (r.m.s.) value is taken. The relative fluctuation intensities ( $r$ ), are the r.m.s. values of all directions related to the main flow component (in this report the main flow direction is the x-direction):

$$r_u = \frac{\sqrt{\overline{u'^2}}}{\bar{u}}, \quad r_v = \frac{\sqrt{\overline{v'^2}}}{\bar{u}}, \quad r_w = \frac{\sqrt{\overline{w'^2}}}{\bar{u}} \tag{2.2}$$

The kinetic energy in a turbulent flow is given as:

$$k = \frac{1}{2} \left( \overline{u'^2} + \overline{v'^2} + \overline{w'^2} \right) \tag{2.3}$$

According to Klar [2005] the turbulence in the pores is approximately uniform in all directions (Hoffmans G. , 2012):

$$\sqrt{\overline{u'^2}} \approx \sqrt{\overline{v'^2}} \approx \sqrt{\overline{w'^2}} \quad [2.4]$$

Resulting in:

$$k_f = \frac{3}{2} \overline{u'^2} \quad [2.5]$$

The local relative turbulence intensity in the filter layer is defined as (Hoffmans G. , 2012):

$$r_f(z) = \frac{\sqrt{k_f(z)}}{\overline{u}(z)} \quad [2.6]$$

### 2.2.2 SHEAR STRESSES

The (Reynolds) stresses within the flow can be obtained from the Reynolds averaged Navier-Stokes equations. The Navier-Stokes equations are the most complete set of equations available for motion within fluids. After Reynolds averaging the Navier-Stokes equation the following normal and shear stresses can be obtained from them (Van Rijn, 2011):

*Normal stresses*

$$\sigma_{xx} = 2\rho_w \nu \frac{\partial \overline{u}}{\partial x} - \rho_w \overline{u'u'}$$

$$\sigma_{yy} = 2\rho_w \nu \frac{\partial \overline{v}}{\partial y} - \rho_w \overline{v'v'}$$

$$\sigma_{zz} = 2\rho_w \nu \frac{\partial \overline{w}}{\partial z} - \rho_w \overline{w'w'}$$

*Shear stresses*

$$\tau_{xy} = \tau_{yx} = \rho_w \nu \left( \frac{\partial \overline{u}}{\partial y} + \frac{\partial \overline{v}}{\partial x} \right) - \rho_w \overline{u'v'}$$

$$\tau_{xz} = \tau_{zx} = \rho_w \nu \left( \frac{\partial \overline{u}}{\partial z} + \frac{\partial \overline{w}}{\partial x} \right) - \rho_w \overline{u'w'}$$

$$\tau_{yz} = \tau_{zy} = \rho_w \nu \left( \frac{\partial \overline{v}}{\partial z} + \frac{\partial \overline{w}}{\partial y} \right) - \rho_w \overline{v'w'}$$

[2.7]

The shear stress at height z in a steady flow can be described as follows (Van Rijn, 2011):

$$\tau_z = \rho_w \nu \frac{\partial \overline{u}}{\partial z} - \rho_w \overline{u'w'} \quad [2.8]$$

The shear stress in equation [2.8] consists of two parts, the first part is the viscous part (viscous shear stress ( $\tau_v$ )) and the second part is the turbulent part (Reynolds stress ( $\tau_t$ )).

Equation [2.8] describes a linear distribution in z-direction (Van Rijn, 2011), as visualized in Figure 2-2. The viscous part of the shear stress is only of importance close to the boundary. For rough bottoms (such as the experiments described within this report) the viscous part is not of importance for the major

part of the flow, in that case the shear stress can be described as a Reynolds stress only:

$$\tau_z = -\rho_w \overline{u'w'} \quad [2.9]$$

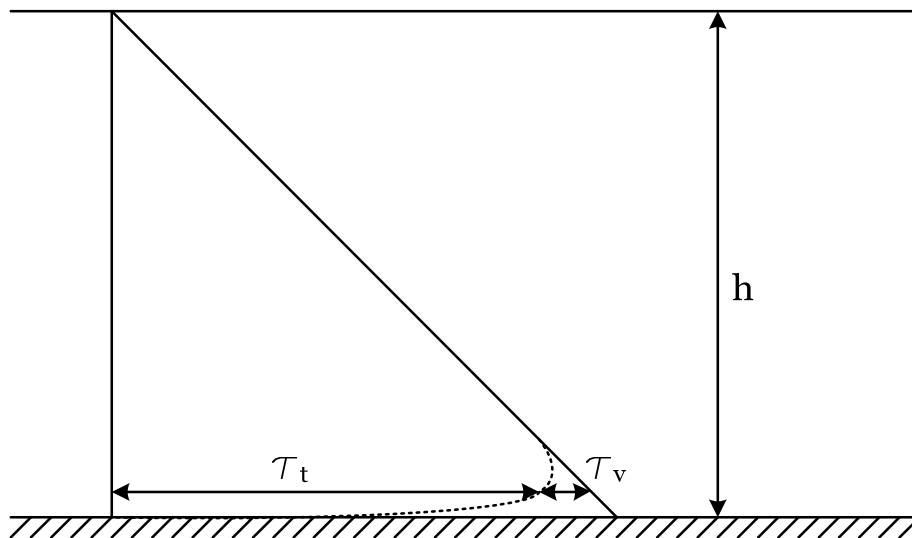


Figure 2-2 Distribution of shear stress

## 2.3 FLOW STABILITY

This paragraph gives an introduction into the stability of the top layers, where the top layer is loaded by a flow parallel to the top layer.

### 2.3.1 BASIC EQUATIONS

Within this paragraph the stability of loose non-cohesive grains in a situation with horizontal flow will be elaborated (based on (Schierreck, 2004)).

To understand the stability of grains in a turbulent flow it is necessary to understand the forces that make the stone move. The forces that are important for the stability of the grain are given in Figure 2-3.

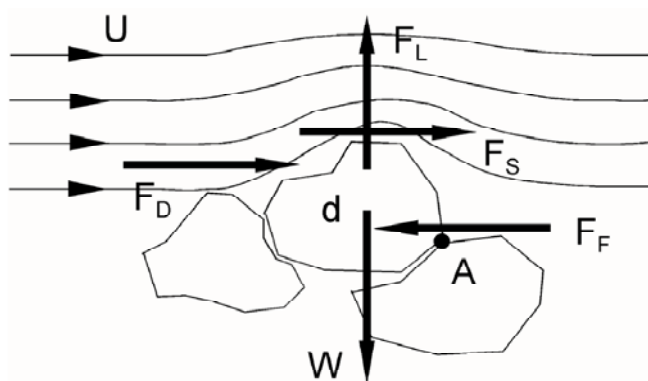


Figure 2-3 Forces on a grain in flow (Schierreck, 2004)

When the velocity becomes larger than a certain critical velocity the forces on the grain are no longer in equilibrium and the grain starts to move. The forces that will bring the grain into movement are:

$$\left. \begin{aligned} \text{Drag force: } F_D &= \frac{1}{2} C_D \rho_w u^2 A_D \\ \text{Shear force: } F_S &= \frac{1}{2} C_F \rho_w u^2 A_S \\ \text{Lift force: } F_L &= \frac{1}{2} C_L \rho_w u^2 A_L \end{aligned} \right\} F \approx \rho_w u^2 d^2 \quad [2.10]$$

In the above mentioned formulas  $C_i$  are coefficients of proportionality and  $A_i$  is the exposed surface area. Since the surface of a grain is proportional to the square of a representative diameter ( $d$ ) of the grain the load can be expressed in terms of  $d$ .

When the forces are in equilibrium, the grain will not move. An equilibrium in forces:

$$\left. \begin{aligned} \sum H = 0 & \quad F_D + F_S = F_F \\ \sum V = 0 & \quad F_D = W \\ \sum M = 0 & \quad F_D \cdot O(d) + F_S \cdot O(d) = W \cdot O(d) \end{aligned} \right\} \rho_w u^2 d^2 \approx (\rho_s - \rho_w) g d^3 \quad [2.11]$$

This results in the following relation:

$$u_c^2 \approx \left( \frac{\rho_s - \rho_w}{\rho_w} \right) g d = \Delta g d \rightarrow u_c^2 = K \Delta g d \quad [2.12]$$

Izbash [1930] did experiments and defined the K-factor (Schierreck, 2004). This resulted in the following expression:

$$\Delta d = 0.7 \frac{u_c^2}{2g} \quad [2.13]$$

The Izbash formula does not take the depth into account and he did not define the location of the critical velocity. So the formula is presented as a tool for a first estimation.

### 2.3.2 SHIELDS

For uniform flow conditions Shields [1936] gives the following relation (Schierreck, 2004):

$$\Psi_c = \frac{\tau_c}{(\rho_s - \rho_w) g d} = \frac{u_*^2}{\Delta g d} = f(\text{Re}_*) = f\left(\frac{u_* d}{\nu}\right) \quad [2.14]$$

Figure 2-4 gives the relation between the dimensionless shear stress and the particle Reynolds number. For high  $\text{Re}_*$  numbers,  $\Psi_c$  is no longer dependent on  $\text{Re}_*$  and becomes constant with a value of 0,055.

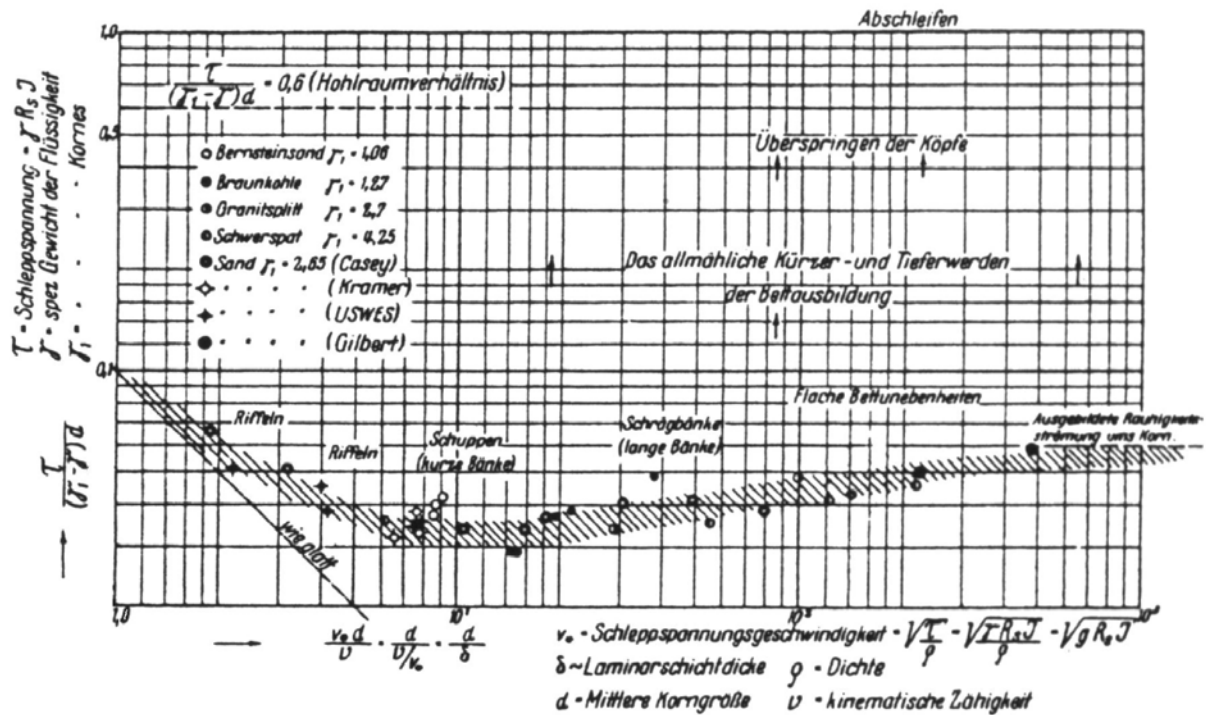


Abb. 6.

Schleppspannungsbeiwert  $\frac{\tau}{(\gamma_s - \gamma) d}$  gegen die Reynold'sche Zahl des Kornes  $\frac{v_* d}{\nu}$ .

Figure 2-4 Critical shear stress according to Shields (Shields, 1936)

To create a more practical applicable version of the Shields formula, the shear velocity is replaced by a mean velocity  $\left( u_* = \bar{u} \sqrt{\frac{g}{C}} \right)$  (which is easier to measure):

$$\Psi_c = \frac{\bar{u}_c^2 g}{\Delta g d_{n50} C^2} \rightarrow d_{n50} = \frac{\bar{u}_c^2}{\Psi_c \Delta C^2} \quad [2.15]$$

### 2.3.3 HOFFMANS

An alternative for the design formula of Shields [1936] is the design formula of Hoffmans (Van Velzen, 2012):

$$d_{50} = 0.7 \frac{(r_0 \bar{u}_c)^2}{\Psi_c \Delta g} \quad [2.16]$$

The formula of Hoffmans is applicable for uniform flow conditions, where the turbulent properties are introduced by bed shear stresses. (For highly turbulent situations the formula has not yet been validated).

The most important difference with the Shields formula is the introduction of the relative turbulent intensity. In this formula [2.16] the diameter of the stone is directly related to the turbulent intensity of the flow. For situations without high turbulent levels, where the turbulence intensity is related to the bed shear stress,

the formula of Shields [2.15] takes turbulent properties indirectly into account by the roughness of the bottom protection (which is included in the Chézy coefficient).

An estimate of the depth averaged turbulent intensity can be made by:

$$r_0 = 1.2 \frac{\sqrt{g}}{C} \quad [2.17]$$

#### 2.3.4 NON-UNIFORM FLOW

Hoan [2008] did research into the stability parameter under non-uniform flow conditions. His research is based on earlier researches by Jongeling et al. [2004] and Hofland [2005]. Jongeling et al., Hofland and Hoan extended the Shields relation [2.14] for turbulent situations (Hoan, 2008).

According to Hoan [2008], the Shields stability parameter is not sufficient to represent the forces on a grain in non-uniform flow. A correction factor does not physically explain the influence of turbulence. The methods described beneath include the fluctuations (turbulence) in the flow.

Jongeling et al. [2004] found a criterion for non-uniform flow (Hoan et al., 2007):

$$\psi_{wl} = \frac{\left\langle (\bar{u} + \alpha_t \sqrt{k})^2 \right\rangle_{hm}}{\Delta g d_{n50}} \quad [2.18]$$

With  $\alpha_t = 6$  and  $h_m = 2d_{n50} + 0.2h$

Hofland [2005], defined a large eddy near the bottom in order to determine the stability coefficient (based on the equation of Jongeling et al., 2004) (Hoan et al., 2007):

$$\psi_{Lm} = \frac{\max \left[ \left\langle \bar{u} + \alpha_t \sqrt{k} \right\rangle_{Lm} \frac{L_m}{2} \right]^2}{\Delta g d_{n50}} \quad [2.19]$$

With  $\alpha_t = 6$  and  $L_m = \kappa z \sqrt{1 - \frac{z}{h}}$

Hoan [2008], found:

$$\psi_{Hoan} = \frac{\left\langle (\bar{u} + \alpha_t \sigma(u))^2 \sqrt{1 - \frac{z}{h}} \right\rangle_h}{\Delta g d_{n50}} \quad [2.20]$$

A practical representation of the formula of Hoan [2008]:

$$d_{n50} = \frac{\left\langle (\bar{u} + \alpha_t \sigma(u))^2 \sqrt{1 - \frac{z}{h}} \right\rangle_h}{\Delta g \psi_{Hoan,c}} \quad [2.21]$$

With  $\alpha_t = 3$  and  $\psi_{Hoan,c} = 2.9$

## 2.4 GRANULAR FILTERS

When base material of a bed or bank has the tendency to erode a granular filter can be used to protect the bed/bank against erosion. Granular filters can be split up in three categories (see also Figure 2-5), namely;

- Geometrically closed (sand-tight) filters: no transport of base material is physically possible;
- Stable geometrically open (sand-tight) filters, also called hydrodynamically sand tight filters: the hydraulic load is less than the threshold value for incipient motion (of the base material);
- Instable geometrically open filters/transport filters/hydraulically sand-open filters: the hydraulic load is occasionally larger than the threshold value.

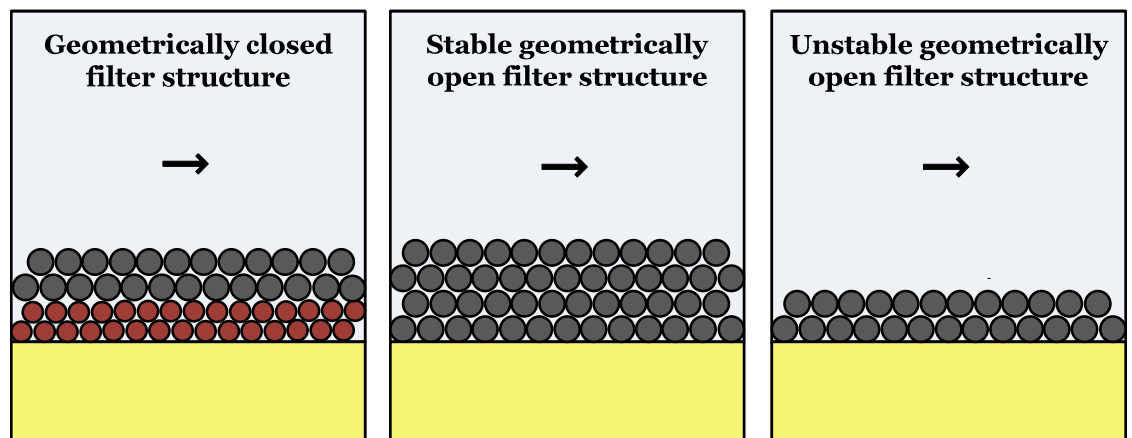
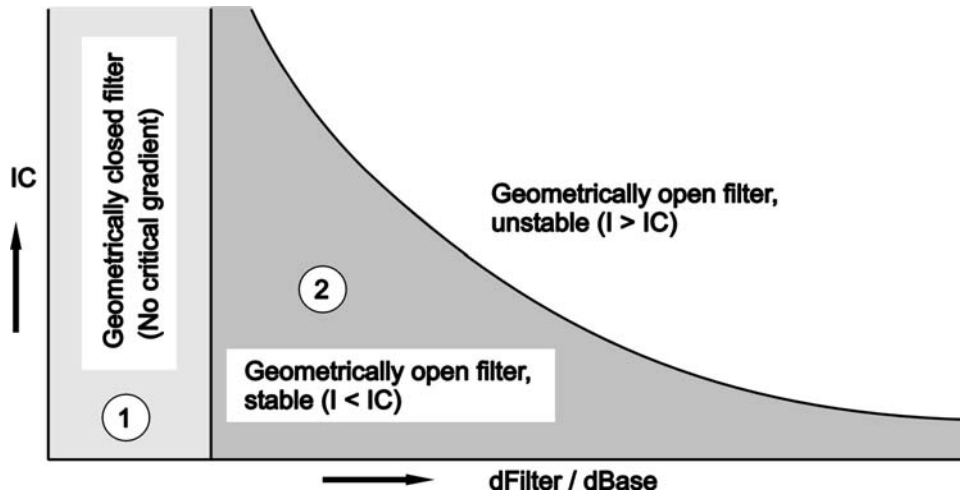


Figure 2-5 Types of granular filters

Figure 2-6 gives a graphical distinction of the three types of filter structures. In this figure I represent the mobility parameter and IC represents the stability parameter.

The three types of granular filters are explained in paragraph 2.4.1 - 2.4.3. Because the research is focused on stable geometrically open filters, the geometrically closed filters and instable geometrically open filters will only be discussed briefly.



**Figure 2-6 Possible design criteria for granular filters (Schiereck, 2004)**

The top layer of any granular filter, the armour layer, should contain stones that are large enough to withstand the load induced by the flow. The calculation of the required nominal diameter of the armour stones is explained in paragraph 2.3.

#### 2.4.1 GEOMETRICAL CLOSED FILTERS

Geometric closed filters or sand-tight filters can prevent erosion independent of the hydraulic load, simply because the material of each layer is physically not able to pass the above lying layer. So the base material is physically not able to pass the filter layer on top of the base material. And so on up to the armour layer. This usually means that the filter consists of several filter layers. To form a geometrically closed filter, the filter should not only meet the condition for retention of base material, but also for internal stability and permeability (Schiereck, 2004);

$$\text{Stability: } \frac{d_{f15}}{d_{b85}} < 5 \quad \text{Int. Stability: } \frac{d_{60}}{d_{10}} < 10 \quad \text{Permeability: } \frac{d_{f15}}{d_{b15}} > 5$$

A geometrically closed filter often results in an uneconomical design. Multiple (thin) layers are needed, which are time consuming to construct. Another problem is the flow velocity during construction, it will be a problem to prevent loss of material during placing of the fine material (the first filter layer(s)).

#### 2.4.2 STABLE GEOMETRICAL OPEN FILTERS

Stable geometrical open filters or hydraulically sand-tight filters prevent erosion of the base material by reducing the hydraulic load within the filter layer. The hydraulic load should be damped within the filter in such a way that the load at the interface between filter and base material is smaller than the resistance of the base material. If the load is damped enough, the base material will not pass the filter, even though it is physically able to. Compared with the geometrically closed filters, stable geometrical open filters are easier to construct, because

fewer layers are needed. They are also easier to repair. However, they do introduce a lot more uncertainties and require usually a larger layer thickness.

Within literature, four different methods for designing stable geometrically open filter structures can be found. The new design formula (CUR, 2010)(Hoffmans G. , 2012) will be discussed in detail in chapter 3. The other three design methods will be discussed in the upcoming paragraphs. The design methods:

- Klein Breteler [1989];
- Bakker-Konter [1994];
- Wörman [1989];

All the methods have been designed for permanent load conditions.

An analogy of the new design formula with the formulas of Bakker-Konter [1994] and Wörman [1989] is that none of them directly takes a load condition into account. All the formulas are based on the relation between the base and filter material.

#### 2.4.2.1 VELOCITY IN A POROUS MEDIUM

The velocity in general is seen as the driving load for transport of material. The flow velocity within porous media (e.g. filters) is related to the gradient via the Forchhem equation [2.22] (Schierreck, 2004). When the gradient is multiplied by the density of the fluid and the gravitational constant, the gradient can be expressed by a pressure gradient.

$$i = au_f + bu_f |u_f| \tag{2.22}$$

For laminar flow conditions (e.g. in sand layers) the second term of [2.22] can be neglected, the equation transforms then into Darcy's law for laminar ground water flow. For turbulent flow, which is usually the case, the second term becomes dominant and the gradient becomes proportional to the flow velocity squared.

The parameters  $a$  and  $b$  in equation [2.22] are the Forchheimer coefficients. These coefficients are dimensional and contain several parameters. Van Gent [1995] suggested the following descriptions of the Forchheimer coefficients (Wolters, to be published);

$$a = \alpha \frac{(1-n)^2}{n^3} \frac{v}{gd_{n50}} \tag{2.23}$$

$$b = \beta \frac{(1-n)}{n^3} \frac{1}{gd_{n50}} \tag{2.24}$$

Van Gent [1995] recommended the following values (Wolters, to be published);

$$\alpha = 1000$$

$$\beta = 1.1$$

#### 2.4.2.2 KLEIN BRETELER

Based on measurements Klein Breteler [1989] and den Adel [1992] derived the following relationship for the critical filter velocity (stationary current) (Wolters, to be published):

$$u_{c,f} = \left( \frac{n_f}{c} \left( \frac{d_{f15}}{\nu} \right)^m \sqrt{\psi_{c,b} \Delta g d_{b50}} \right)^{1/(1-m)} \quad \text{valid for } 0.1 < d_{b50} < 1 \text{ mm} \quad [2.25]$$

The coefficients  $m$  and  $c$  depend on the grain diameter of the base material and are given in Table 2-1.

$d_{b50}$ [mm]	$c$ [-]	$m$ [-]
0.1	1.18	0.25
0.15	0.78	0.20
0.2	0.71	0.18
0.3	0.56	0.15
0.4	0.45	0.11
0.5	0.35	0.07
0.6	0.29	0.04
0.7	0.22	0
0.8	0.22	0
1.0	0.22	0

**Table 2-1 Parameters according to Klein Breteler [1992] (Wolters, to be published)**

For situations with a sloping interface some additional terms can be added (see (Wolters, to be published)). A more practical representation of the design method of Klein Breteler is given in Figure 2-7. With this figure the dimensions of the base and filter material, the porosity of the filter layer and the slope angle the critical gradient can be determined.

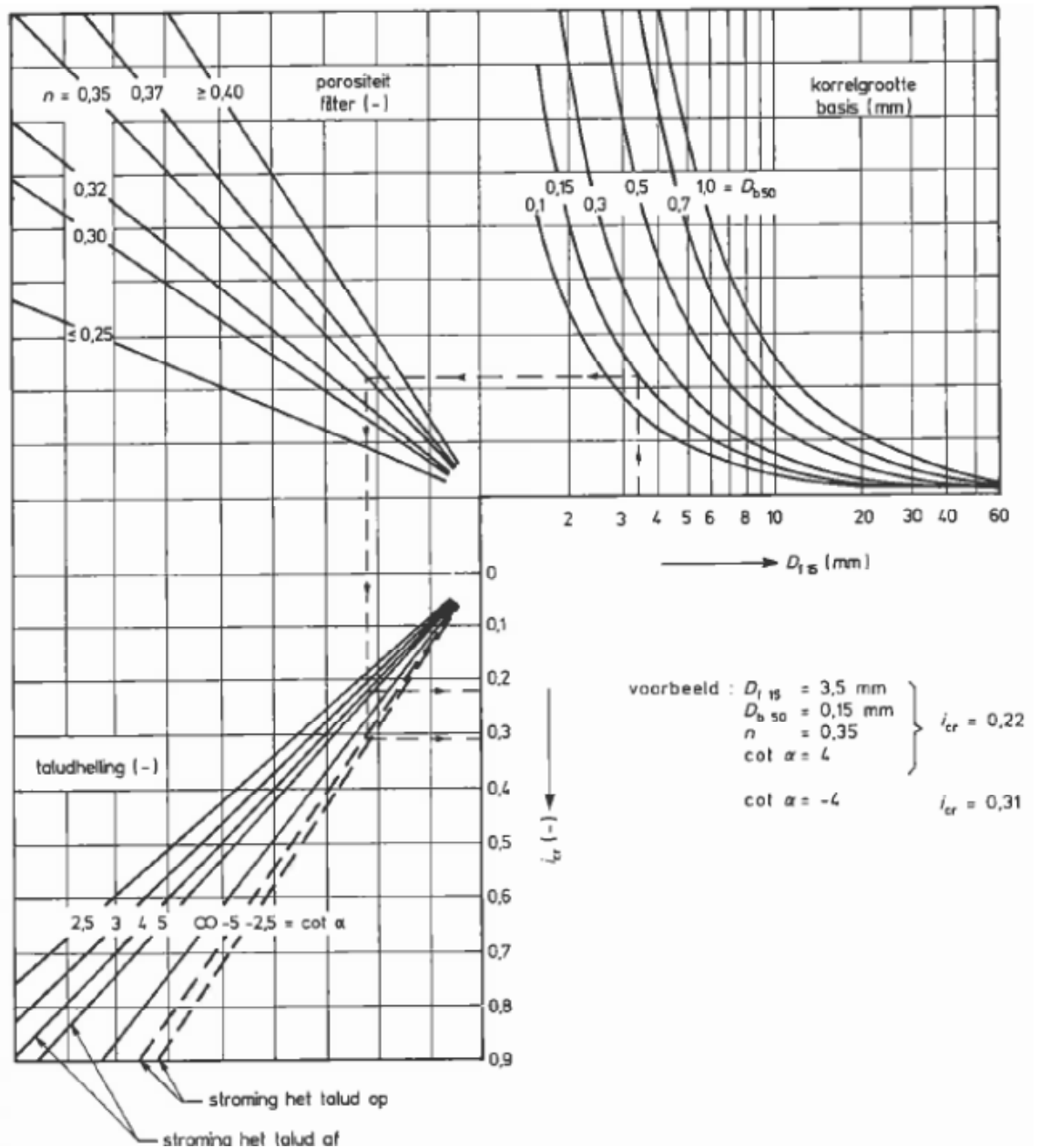


**Figure 2-7 Determination of the critical gradient according to Klein Breteler [1989] (CUR, 2010)**

Klein Breteler treated the flow in the filter like an open channel flow. He did not take the entrainment of turbulent pressure and velocity fluctuations from the flow above the filter into account. This restriction is correct in a situation with a block revetment, which causes a strong damping of turbulence, but can be incorrect in the case of granular filter material (CUR, 2010).

Because Klein Breteler neglected the entrainment of turbulent fluctuations, the formula is not applicable for granular filters.

### 2.4.2.3 BAKKER-KONTER

Bakker & Konter did include turbulent fluctuations within their design formula. The fluctuations are represented by the hydraulic radius ( $R$ ) and thus related to the dimensions of the cross-section of the situation in the flume (or

river, etc.). Because the influence is related to the cross-section, only turbulent fluctuations for uniform flows are taken into account. The high turbulent energy levels of non-uniform flows are not taken into account, which makes the formula only applicable in case of uniform flow conditions. The formula of Bakker-Konter (CUR, 2010):

$$\frac{d_{f15}}{d_{b50}} = \frac{2.2}{C_0 e^2} \frac{R}{d_{f50}} \frac{\Psi_{c,b} \Delta_b}{\Psi_{c,f} \Delta_f} \quad [2.26]$$

Where  $C_0$  [-] is a turbulence coefficient that varies from 6 to 100, with a commonly used value of 15. The variable  $e$  [-] is a coefficient that takes the difference between an open channel flow and flow within a granular filter into account. The average value of  $e$  is 0.24 (CUR, 2010).

#### 2.4.2.4 WÖRMAN

Wörman investigated granular open filter structures around bridge piers. The flow around bridge piers is a non-uniform flow. The model tests of Wörman are presented in appendix A. With the model tests Wörman derived the following formula for single layered open filter structures (CUR, 2010):

$$\frac{D_f}{d_{f15}} = 0.16 \frac{\Delta_f}{\Delta_b} \frac{n_f}{1-n_f} \frac{d_{f85}}{d_{b85}} \quad [2.27]$$

For large ratios between the filter and base material  $\frac{d_{f50}}{d_{b50}} > 50$ , equation [2.27] gives an overestimation of the required filter layer thickness for large ratios between the sieve diameter of the filter and base material (see also Figure 3-5). CUR 233 [2010] indicates a better fit with a constant of 0.08 for situations with  $\frac{d_{f50}}{d_{b50}} > 50$  (Wolters, to be published):

$$\frac{D_f}{d_{f15}} = 0.08 \frac{\Delta_f}{\Delta_b} \frac{n_f}{1-n_f} \frac{d_{f85}}{d_{b85}} \quad [2.28]$$

#### 2.4.3 UNSTABLE GEOMETRICAL OPEN FILTERS

When the grains of the filter layer are even larger (relative to the grains of the under layer) than for geometrically open filters, the filter layer is not stable anymore. The loading is reduced, but not enough to prevent transport of the grains of the base material, resulting in erosion of base material (transport through the filter). If the amount of erosion is known beforehand and the necessity of maintenance is accepted, this type of filter layer can be economic. The filter is cheaper because fewer filter layers are needed and the difference in grading between base material and filter material is considerable. On the other hand maintenance will be necessary. (Ockeloen, 2007)

Den Adel [1994] developed a description for the amount of transported base material as a function of time. He assumed that particles were either in rest or in motion with the same velocity as the water in the pores (local flow velocity). This principle is given in Figure 2-8.

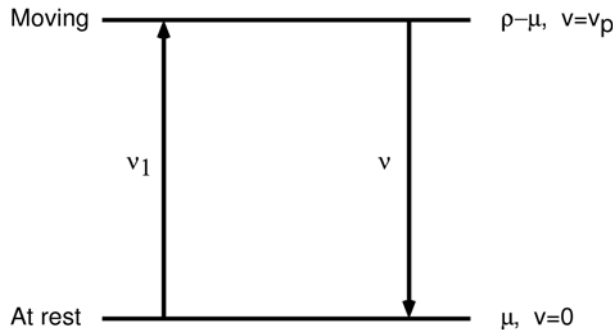


**Figure 2-8 The basics of the transport model by Den Adel (CUR, 2010)**

## 2.5 WIDE-GRADED FILTER MATERIAL

Based on practice two gradations of filter material/armour stone are distinguished within the framework of granular filter structures (CUR, 2010);

- Standard gradation  $\frac{d_{85}}{d_{15}} < 2.5$
- Wide gradation  $\frac{d_{85}}{d_{15}} > 2.5$

The above made distinction is used in the theoretical derivation of the new design rule for geometrically open filter structures (CUR, 2010). This distinction will also be used in this report.

The Rock Manual gives a different definition for the gradation of filter material/armour stone (CIRIA, CUR, & CETMEF, 2007);

- Narrow gradation  $\frac{d_{85}}{d_{15}} < 1.5$
- Wide gradation  $1.5 < \frac{d_{85}}{d_{15}} < 2.5$
- Very wide gradation  $\frac{d_{85}}{d_{15}} > 2.5$

## 2.6 RESULTS PREVIOUS TESTS

In the past, several researchers performed model tests with geometrically open filter structures. By combining the results of the researches with the results from this research, a larger data set can be created. From this set of tests better sustained conclusions can be drawn.

The following model tests are taken into account;

- Bakker [1960]
- Haverhoek [1968]
- Wouters [1982]
- Wörman [1989]
- Konter et al. [1990]
- Van Huijstee and Verheij [1991]
- Dixen [2008]
- Van Velzen [2012]

Haverhoek [1968], Wouters [1982], Van Huijstee and Verheij [1991] and Dixen [2008] did tests for uniform flow conditions. The model tests from Wörman [1989] and Van Velzen [2012] are both used to measure the effects of piles (e.g. bridge piles) on the stability of geometrically open filters.

The tests performed by Bakker [1960] and Konter et al. [1990] contain both, situations tested under uniform and non-uniform flow conditions.

The data of the above mentioned tests/researches is given in appendix A.

# 3 ANALYSIS OF THE NEW DESIGN FORMULA

## 3.1 DERIVATION OF THE DESIGN FORMULA

The derivation of the new design formula (CUR, 2010)(Hoffmans G. , 2012) is done in three steps. Each step will be explained briefly;

- Step 1: Applying the hypothesis of Grass
- Step 2: Damping of turbulent energy
- Step 3: Required thickness of a stable filter construction

### 3.1.1 STEP 1: APPLYING THE HYPOTHESIS OF GRASS

The hypothesis of Grass gives a characteristic load (Figure 3-1) and a characteristic strength/erosion resistance:

- Characteristic load:  $\tau_{0,k} = \tau_0 + \gamma\sigma_0$
- Characteristic strength:  $\tau_{c,k} = \tau_c + \gamma\sigma_c$

Where  $\sigma_0$  is given by:  $\sigma_0 = V_c \tau_0$

When we use Shields (paragraph 2.3.2) to express the shear stress, the shear stress can be expressed as:

$$\tau_c = (\rho_s - \rho_w) g d_{n50} \Psi_c = \rho_w g d_{n50} \Delta \Psi_c \quad [3.1]$$

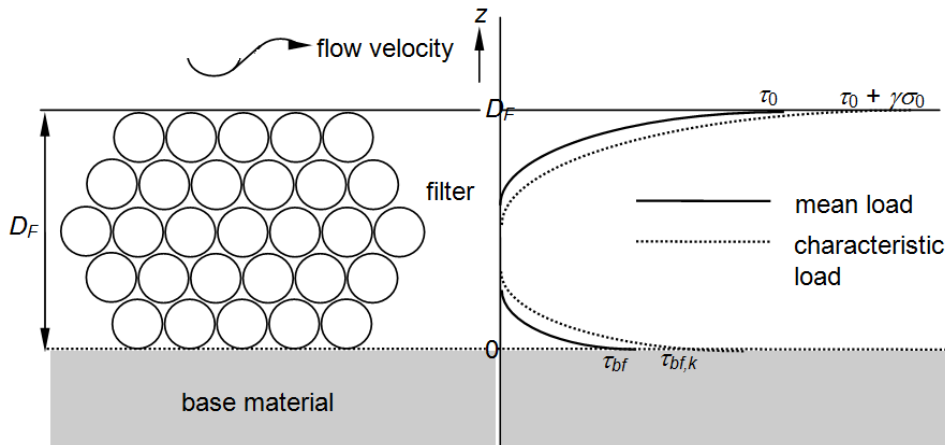


**Figure 3-1 Distribution of the mean and characteristic load (CUR, 2010)**

When assuming a relative strength relation between the strength at the bottom (top of the filter) and the strength at the transition of the filter and the

base layer  $\left(\eta_c = \frac{\tau_{c,bf}}{\tau_c}\right)$ , it is implicitly assumed that movement of the base layer will not occur as long as the top layer is stable. When using this relation the movement of the top layer and the base layer will theoretically start at the same load condition (velocity).

The relative strength  $(\eta_c)$  is defined as the ratio of the mean strength of the base layer  $(\tau_{c,bf})$  at the transition of the filter-base layer and the mean strength at the top of the filter layer  $(\tau_c)$  (Hoffmans G. , 2012):

$$\eta_c = \frac{\tau_{c,bf}}{\tau_c} = \frac{d_{b50}}{d_{f50}} \frac{\Delta_b}{\Delta_f} \frac{\Psi_{c,b}}{\Psi_{c,f}} \quad [3.2]$$

The same relation can be elaborated for the characteristic strength of the base material  $(\tau_{c,bf,k})$  and the characteristic strength of the filter material  $(\tau_{c,f,k})$ :

$$\eta_c = \frac{\tau_{c,bf,k}}{\tau_{c,f,k}} \quad [3.3]$$

With;

$$\tau_{c,bf,k} = \tau_{c,b} + \gamma\sigma_{c,b} = \rho g d_{b50} \Delta_b \Psi_{c,b} (1 - \gamma V_{Gb}) \quad [3.4]$$

$$\tau_{c,f,k} = \tau_{c,f} + \gamma\sigma_{c,f} = \rho g d_{f50} \Delta_f \Psi_{c,f} (1 - \gamma V_{Gf}) \quad [3.5]$$

Combining equation [3.4] and [3.5] with equation [3.3] results in:

$$\eta_c = \frac{\tau_{c,bf}}{\tau_c} = \frac{d_{b50}}{d_{f50}} \frac{\Delta_b}{\Delta_f} \frac{\Psi_{c,b}}{\Psi_{c,f}} \frac{1 - \gamma V_{Gb}}{1 - \gamma V_{Gf}} \quad [3.6]$$

Equation [3.6] can be rewritten to:

$$\frac{d_{f50}}{d_{b50}} = \frac{1}{\eta_c} \frac{\Delta_b}{\Delta_f} \frac{\Psi_{c,b}}{\Psi_{c,f}} \frac{1 - \gamma V_{Gb}}{1 - \gamma V_{Gf}} \quad [3.7]$$

Equation [3.7] has been derived by Verheij et al. [2000] (CUR, 2010).

### 3.1.2 STEP 2: DAMPING OF TURBULENT ENERGY

The damping of turbulence in the filter layer can be described as a decrease of local turbulent energy  $(k_f)$  over the depth. Based on the storage equation, the balance of forces, the Forchheimer equation, the hypothesis of Boussinesq and a relation for the eddy viscosity the penetration of the turbulent energy  $(k_f)$  is described as follows:

$$k_f(z) = k_{f,s} + (k_b - k_{f,s})e^{\frac{z}{L_d}} \quad [3.8]$$

The derivation of equation [3.8] is given in Hoffmans [2012].

With the following relation for the damping length:

$$L_d = \alpha_d d_{f15} \quad [3.9]$$

For load penetration of wind and ship waves in granular and block revetments Bezuijen and Köhler found the following relation for the damping length (Hoffmans G. , 2012):

$$L_d = \sqrt{\frac{T_p c_v}{\pi}} \quad [3.10]$$

In equation [3.10],  $T_p$  represents the pressure period and  $c_v$  the consolidation coefficient.

The  $\alpha_d$  parameter will be evaluated in paragraph 3.2.

The relative load can be given by (Hoffmans G. , 2012):

$$\eta = \frac{k_f(z)}{k_b} \approx e^{\frac{z}{L_d}} = e^{\frac{z}{\alpha_d d_{f15}}} \quad [3.11]$$

This simplification can be made because  $k_{f,s} \ll k_b$ .

### 3.1.3 STEP 3: REQUIRED THICKNESS OF A STABLE FILTER CONSTRUCTION

Equation [3.6] gives a relation between the filter layer and the base layer and implicitly assumes that the base layer is stable if the filter layer is stable.

In the filter the turbulence energy will be damped. Because of the damping the load on the base material will be significant smaller than the load on the top of the filter. The damping of the turbulent fluctuations in the filter is given by equation [3.11]. The damping is related to the thickness of the filter layer and as we are interested in the load at the top of the base layer  $z$  can be replaced by the filter thickness ( $z = -D_f$ ). In that case equation [3.11] can be rewritten to:

$$\eta \approx e^{\frac{-D_f}{\alpha_d d_{f15}}} \quad [3.12]$$

Combining equation [3.6] and [3.12] results in (Hoffmans G. , 2012):

$$\frac{D_f}{d_{f15}} = \alpha_d \ln \left( \frac{d_{f50}}{d_{b50}} \frac{\Delta_f}{\Delta_b} \frac{\Psi_{c,f}}{\Psi_{c,b}} \frac{1 - \gamma V_{Gf}}{1 - \gamma V_{Gb}} \right) \quad [3.13]$$

The design formula as given in equation [3.13] is the design formula as derived in the book of Hoffmans (Hoffmans G. , 2012). Previous to the derivation of Hoffmans, Verheij derived almost the same design formula (CUR, 2010) (equation [3.14]). The difference between the two design formula is within the  $\alpha_d$  parameter;

- In the equation as derived by Hoffmans the coefficient ( $\alpha_d$ ) is linear;
- In the equation as derived by Verheij the coefficient ( $\alpha_k$ ) is logarithmic.

$$\frac{D_f}{d_{f15}} = 2 \ln \left( \alpha_k \frac{d_{f50}}{d_{b50}} \frac{\Delta_f}{\Delta_b} \frac{\Psi_{c,f}}{\Psi_{c,b}} \frac{1 - \gamma V_{Gf}}{1 - \gamma V_{Gb}} \right) \quad [3.14]$$

Both, Hoffmans (Hoffmans G. , 2012) and Verheij (CUR, 2010), used the following assumptions to simplify their formulas ([3.13] and [3.14]);

$$\frac{\Delta_f}{\Delta_b} = 1 \qquad \frac{\Psi_{c,f}}{\Psi_{c,b}} = 1 \qquad \frac{1 - \gamma V_{Gf}}{1 - \gamma V_{Gb}} = 1 \qquad \frac{d_{f50}}{d_{f15}} = 1.25$$

These simplifications result in the following simplified representation of formula [3.13]:

$$\frac{D_f}{d_{f50}} = \frac{\alpha_d}{1.25} \ln \left( \frac{d_{f50}}{d_{b50}} \right) \quad [3.15]$$

### 3.2 PARAMETERS

Within this paragraph the influence of the different parameters of equation [3.13] will be evaluated. The following parameters/relations will be evaluated;

- Relative layer thickness  $\frac{D_f}{d_{f15}}$ ;
- Relative diameter  $\frac{d_{f50}}{d_{b50}}$ ;
- Relative density  $\frac{\Delta_f}{\Delta_b}$ ;
- Relation stability parameters  $\frac{\Psi_{c,f}}{\Psi_{c,b}}$ ;
- Grading coefficient  $\frac{1 - \gamma V_{Gf}}{1 - \gamma V_{Gb}}$ ;
- Damping coefficient  $\alpha_d$ .

### 3.2.1 RELATIVE LAYER THICKNESS

According to model tests done by Van Os [1998], the mean and standard deviation of the velocity in the filter layer decreases only to a depth of 1.5 times the nominal diameter of the filter material. Thicker filter layers will not result in lower velocities at the transition between the filter and base layer.

Based on experiments of Klar [2005] the effective layer thickness for damping of turbulent energy is 4 to 5 times the nominal diameter of the filter material.

From a practical point of view layers of stone material are at least two times the nominal diameter of the filter material.

Besides the velocity also the distance the sand particle has to travel is of importance. A thicker filter layer results in a longer path to travel for sand particles. Turbulent eddies in the filter layer result in pressure fluctuations. These fluctuations can pickup sand particles and carry them through the filter layer. When sand particles are carried out of the filter layer, they will be carried away by the flow in the channel. The pressure fluctuations through eddies are of short duration. During this short period the sand particle can be lifted and transported. When the pressure fluctuation and/or the fluctuation time is not large enough the sand particle will not be carried completely through the filter. After the short fluctuation the sand particle will sink and settle again in the base layer. When the sand particle is lifted to the higher part of the filter layer it can be picked up by other eddies/fluctuations and transported out of the filter layer.

A thick filter layer can prevent erosion, even if the pressure fluctuations are large enough to erode the sand bed. The pressure fluctuations are of short duration and are not able to transport the particles through the complete filter layer.

The dimension of the pores are normative for the pore velocity and the development of eddies in the filter layer. In larger pores larger velocities and eddies can develop. Normative for the dimensions of the pores are the small stones in the filter material.

### 3.2.2 RELATIVE DIAMETER

The relative diameter  $\left(\frac{d_{f50}}{d_{b50}}\right)$  gives the relation between the diameter of the base and filter material.

The geometrically closed filter rules are based on the relation between the dimensions of the filter layer and the base layer (see paragraph 2.4.1). Within geometrically closed filters it is physically not possible for particles of the base layer to pass the filter layer. Within geometrically open filters it is physically possible for the particles to pass the filter layer. Logically it is easier for particles to pass through large gaps than through small gaps. So to prevent erosion of the base layer the relation between the filter material and the base material  $\left(\frac{d_{f50}}{d_{b50}}\right)$  should be as small as possible.

Besides preventing erosion of the base material, the filter material has to be stable. The filter material has to be large enough to withstand the forces of the flow in the channel above the filter. The minimal required stone diameter for the filter layer can be calculated with Shields (equation [2.15]):

$$d_{f50} = \frac{\bar{u}_{c,f}^2}{\Psi_{c,f} \Delta_f C^2} \quad [3.16]$$

Combining equation [3.16] and equation [3.13], the design formula can be related to the velocity in the channel:

$$\frac{D_f}{d_{f15}} = \alpha_d \ln \left( \frac{\bar{u}_{c,f}^2}{d_{b50} \Delta_b \Psi_{c,b} C^2} \frac{1 - \gamma V_{Gf}}{1 - \gamma V_{Gb}} \right) \quad [3.17]$$

It is of important to notice the contradiction between the two main criteria for the diameter of the filter material. On the one hand the filter material has to be large enough to withstand the forces of the flow in the channel, on the other hand the filter material has to be small enough to prevent erosion of the bed material.

Because of the contradiction mentioned above a designer must be aware of the influence of an overdimensioned design. When calculating the minimal stone diameter for the filter/top layer it is common to choose a slightly larger stone class (a class that is standard available and probably somewhat larger than the required stone dimension). The larger stones are better to prevent erosion of the filter layer, but on the other hand a filter of larger stones has larger pores. Larger pores makes it easier for bed material to pass through the filter material. **So when using larger stones, also a thicker filter layer is needed.**

### 3.2.3 RELATIVE DENSITY

The relative density of the base and filter material is of importance for the resistance against erosion. Lighter material will erode more easily than heavy material.

Equation [3.3] gives a relation between the shear force at the top of the filter layer and the base material. This relation is, as explained in paragraph 3.1, the fundament of the design formula (equation [3.3]). Because the formula is based on the relation between the stability of the filter layer and the stability of the base layer, the relation between the relative weight of the filter and base material has to be taken into account (the load which is taken indirectly into account by the diameter of the filter material has to be translated to a load related to the base material).

### 3.2.4 RELATION STABILITY PARAMETERS

The stability parameter or Shields parameter is related to the shear velocity as can be seen in Figure 2-4. Van Rijn replaced the particle Reynolds-number by a dimensionless particle diameter ( $d^*$ ) resulting in Figure 3-2.

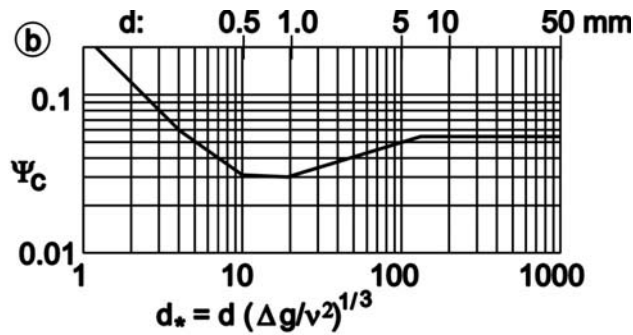


**Figure 3-2 Critical Shields parameters according to Van Rijn (d calculated with  $v=1.33 \cdot 10^{-6} \text{ m}^2/\text{s}$  and  $\rho=2650 \text{ kg/m}^3$ ) (Schierreck, 2004)**

Based on Shields, Rouse developed a formulation of the transport parameter. Breusers went even further, he made a distinction between 7 different phases of particle transport. Figure 3-3 is representing the 7 phases of particle transport as defined by Breusers, ranged from phase 1: “Occasional particle movement at some locations” to phase 7: “General transport”. The graphs of Shields and Van Rijn (Figure 3-2) are in accordance with phase 6: “Continuous particle movement at all locations” (Schierreck, 2004).

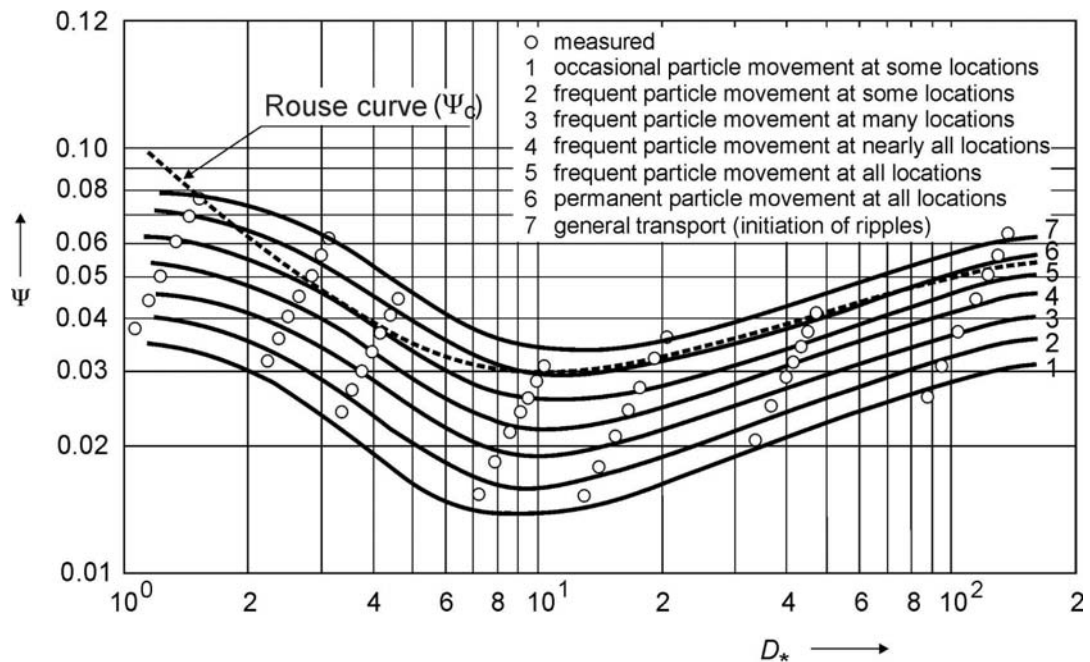


**Figure 3-3 Stability parameter  $d^* = d_{50}(\Delta g/v^2)^{1/3}$  (CUR, 2010)**

As can be seen in Figure 3-2 and Figure 3-3 the critical Shields parameter only varies to a certain grain diameter (to a diameter of approximately 6 to 7 mm). For larger diameters the Shields parameter becomes constant with a value depending on the allowable transport of particles.

When the diameter of filter material is, in practice and in this research, larger than ~7 mm the critical stability parameter for the filter layer can be taken as a constant. For phase 1 resulting in  $\Psi_{c,f} = 0.03$  (for phase 6 resulting in  $\Psi_{c,f} = 0.055$ ).

Within this research only types of sand as base material are taken into account (smaller particles than sand particles are not taken into account in this research because of their cohesive properties). The dimension of sand particles varies from  $62.5 \mu\text{m}$  (very fine sand) to  $2 \text{ mm}$  (very course sand). When these dimensions are taken into account, the critical stability parameter for the base material varies for the start of movement (phase 1) between  $\Psi_{c,b} = 0.015$  and  $\Psi_{c,b} = 0.035$ . When the original Shields curve is used for the design of the filter structure, the stability parameters for the base material would lay in the range from  $\Psi_{c,b} = 0.03$  to  $\Psi_{c,b} = 0.07$ .

When the base layer is made of sand, the relation between the critical stability parameter of the filter material and the critical stability parameter of the base material varies between  $\frac{\Psi_{c,f}}{\Psi_{c,b}} = 0.79$  and  $\frac{\Psi_{c,f}}{\Psi_{c,b}} = 2$ . This variation depends on the particle dimensions of the bed material and on the chosen phase of allowable transport.

According to (CUR, 2010) realistic values for the relation between the critical stability parameter of the filter material and the critical stability parameter of the base material are between  $\frac{\Psi_{c,f}}{\Psi_{c,b}} = 1.3$  and  $\frac{\Psi_{c,f}}{\Psi_{c,b}} = 1.5$ .

### 3.2.5 GRADING COEFFICIENT

The  $V_G$  factor represents the non-uniformity of the material. It represents the grading of the material, defined as the relation between the smaller particles ( $d_{15}$ ) and the sieve diameter ( $d_{50}$ ) of the filter material:

$$V_G = 1 - \frac{d_{15}}{d_{50}} \quad [3.18]$$

The influence of particle grading on the stability depends on the difference of grading between the filter and the base layer. When the base material is for example wider graded than the filter material ( $V_{Gb} > V_{Gf}$ ), the relative strength is less than in the situation where base and filter material have the same grading. And when the filter material is more graded than the base material ( $V_{Gb} < V_{Gf}$ ) the relative strength is greater than in a situation where base and filter material have the same grading.

Gamma represents the transport parameter. Grass found that sand ( $V_{Gf} \approx 0.3$ ), within a uniform flow is completely stable for  $\gamma=1$ , while a significant transport of sand particles was observed for  $\gamma=0$ . Based on his experiments, he reported that with  $\gamma=0.625$  the criterion of Shields for initial movement of sand was met up to a size of  $250 \mu\text{m}$  (CUR, 2010).

### 3.2.6 DAMPING COEFFICIENT

The damping of turbulent energy in the filter layer is represented by the damping coefficient  $\alpha_d$  :

$$\alpha_d = \sqrt{\frac{\alpha_v}{C_D}} \quad [3.19]$$

In the book “The influence of Turbulence on Scour and Erosion”, appendix B11 (Hoffmans G. , 2012) the damping parameter is derived. The derivation results in the following representation of the damping parameter:

$$\alpha_d = \frac{2r_f^2}{C_D \chi_k} \quad [3.20]$$

The damping is related to the relative turbulent intensity in the filter ( $r_f$ ), the drag coefficient ( $C_D (=1)$ ) and a turbulence coefficient ( $\chi_k (=3.3)$ ).

Figure 3-4 represents the damping of turbulent energy in the filter layer. The damping of turbulent energy decreases the further it penetrates into the filter layer (Figure 3-4). According to experiments of Klar [2005] the damping occurs only in the layer of the first 4 to 5 times the nominal diameter of the granular material. Thicker layers do not result in a better damping of turbulent energy.

For layer thicknesses of more than 4 to 5 times the nominal diameter experiments of Klar [2005] resulted in values for  $k_f / u_*^2$ , varying from 0.15 to 0.25 (Hoffmans G. , 2012). This results in  $\alpha_d$  values varying from 0.85 to 1.35. Hoffmans used a safe upper limit to determine the  $\alpha_d$  value. He used  $k_f / u_*^2 = 0.3$  resulting in  $\alpha_d = 1.5$  (Hoffmans G. , 2012).

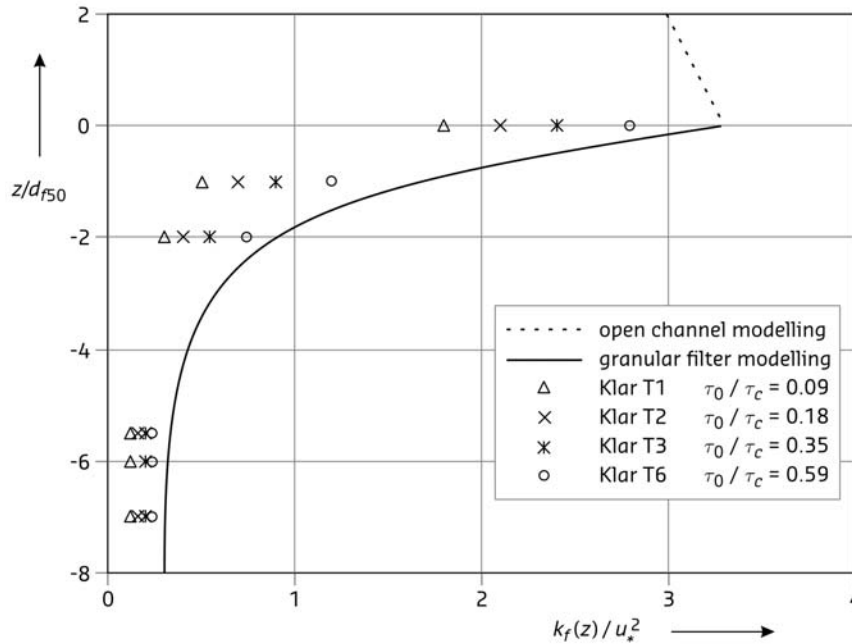


Figure 3-4 Experimental data of Klar [2005] (Hoffmans G., 2012)

### 3.3 COMPARISON WITH THE BAKKER-KONTER AND WÖRMAN FORMULA

This paragraph describes the similarities and differences between equation [3.13], the Bakker-Konter formula (equation [2.26]) and the formula of Wörman (equation [2.27]).

The most important similarity between all three design formulas is that they are all based on the relation between the properties of filter and base material. In all cases the load is taken into account indirectly. Based on the load the top-layer has to be chosen (designed with a suitable formula (e.g. Shields)). With the properties of the chosen material, the filter can be designed with one of the formulas (Hoffmans, Bakker-Konter or Wörman).

When taking a closer look at the design formulas, the parameters can be categorized in the following categories;

- Layer thickness of the filter layer;
- Relative material properties (filter versus base material properties);
- Load parameters;
- Fitting parameters (e.g.  $\alpha_d$ ).

Table 3-1 gives an analysis of the three design formulas. A distinction is made between the categories mentioned above.

Formula	Layer thickness	Material properties	Load	Fitting parameters
<b>Bakker-Konter</b> $\frac{1}{d_{f15}} = \frac{C_0 e^2 R}{2.2} \frac{d_{f50}}{d_{b50}} \frac{\Psi_{c,f}}{\Psi_{c,b}} \frac{\Delta_f}{\Delta_b}$	$\frac{1}{d_{f15}}$	$\frac{d_{f50}}{d_{b50}}, \frac{\Delta_f}{\Delta_b}, \frac{\Psi_{c,f}}{\Psi_{c,b}}$	R	$\frac{C_0 e^2}{2.2}$
<b>Wörman</b> $\frac{D_f}{d_{f15}} = 0.16 \frac{\Delta_f}{\Delta_b} \frac{n_f}{1-n_f} \frac{d_{f85}}{d_{b85}}$	$\frac{D_f}{d_{f15}}$	$\frac{d_{f85}}{d_{b85}}, \frac{\Delta_f}{\Delta_b}, \frac{n_f}{1-n_f}$		0.16
<b>Hoffmans</b> $\frac{D_f}{d_{f15}} = \alpha_d \ln \left( \frac{d_{f50}}{d_{b50}} \frac{\Delta_f}{\Delta_b} \frac{\Psi_{c,f}}{\Psi_{c,b}} \frac{1-\gamma V_{Gf}}{1-\gamma V_{Gb}} \right)$	$\frac{D_f}{d_{f15}}$	$\frac{d_{f50}}{d_{b50}}, \frac{\Delta_f}{\Delta_b}, \frac{\Psi_{c,f}}{\Psi_{c,b}}, \frac{1-\gamma V_{Gf}}{1-\gamma V_{Gb}}$		$\alpha_d$

**Table 3-1 Design formulas single layered geometrically open filter structures**

The Bakker-Konter formula does not take the layer thickness of the filter into account, this in contrast to the other two design formulas. This is the major reason the Bakker-Konter formula is not suitable for design purposes.

One of the normative parameters is the relative dimension of the filter and base material. The diameter/dimension of the filter material is a reflection of the load conditions, this parameter is determined based on the load conditions (paragraph 2.3). The ratio between filter and base material determines how easily base material can pass the filter layer. This relation between the dimensions of filter and base material is dominant in all three formulas (when the grading of the filter and base material is equal,  $d_{f85}/d_{b85} = d_{f50}/d_{b50}$ ).

The ratio between the relative density of filter and base material is represented within each formula. Other material properties are differently represented in the various design formulas. These parameters (the relative stability parameter, porosity of the filter material and relative shape factor) have only a limited influence on the result.

The main difference between the design formulas of Hoffmans and Wörman is the relation between the layer thickness and the material properties (which indirectly represent the load condition). In Wörman formula the layer thickness and the ratio between the filter and base material is linear whereas this relation is logarithmic within Hoffmans's formula. This difference is clearly visible in Figure 3-5. Hoffmans's formula gives a better fit in relation to model tests (Figure 3-5, Figure 5-12 and Figure 5-14).

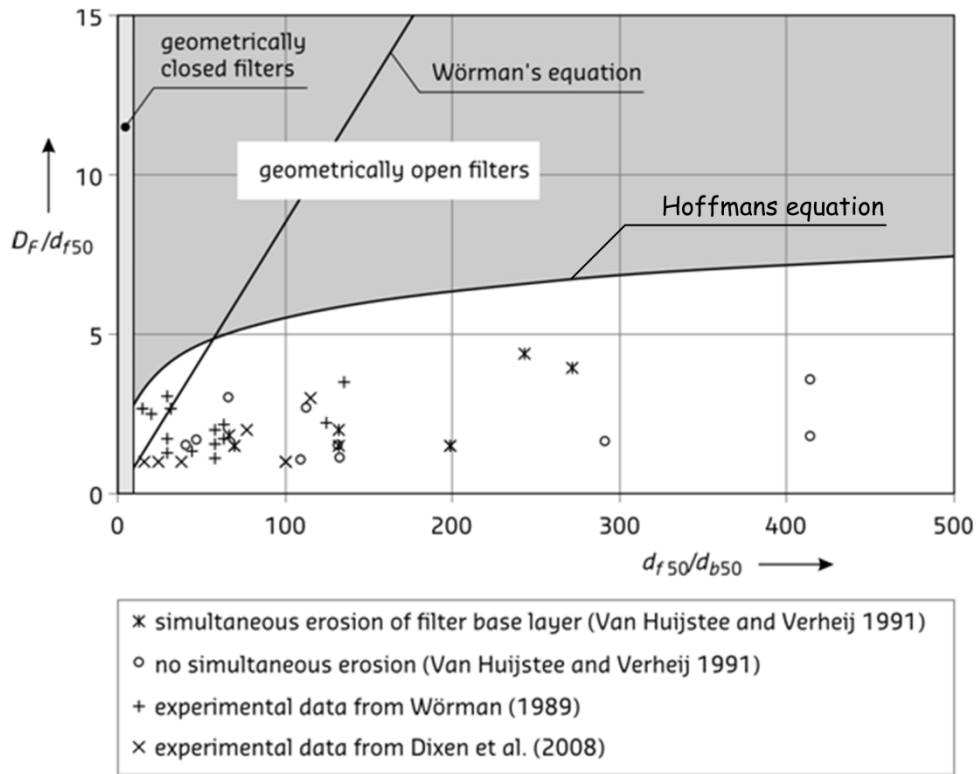


**Figure 3-5  $D_F/d_{f50}$  versus the critical  $d_{f50}/d_{b50}$ . The (linear) Wörman equation and the new logarithmic equation compared with measurements (Hoffmans G. , 2012)**

## 4 MODEL TEST SET-UP

---

The goal of the model tests was to test the new design formula [3.13]. This chapter will describe the model tests which were performed in the period January till March 2012. First the elements which have been examined within the model tests to verify the design formula will be described. Further on the facility, the scaling rules, the situations that are tested, the materials, the measurements and the model test set-up will be discussed.

### 4.1 PARAMETER VARIATION

Implicitly the design formula assumes that if a filter is designed with the formula the base material is stable if the filter material is stable. This is based on damping within the filter (paragraph 3.1).

This means that if the filter layer has the thickness that has been calculated with the design formula, the movement of the filter material and the base material will start at the same moment (same critical velocity). When the filter layer is less thick, the base material will start to move/erode before movement of filter material will occur. And also the other way around, when the layer of filter material is thicker than needed, the filter material will start to move/erode before movement of base material will start.

To test the relation as described above, both the transport of filter material and base material had to be measured. To determine the critical velocity, all the different models are tested with ascending velocities, starting with a velocity significantly lower than the critical velocity for the filter material, as can be calculated with Shields or Hoffmans (formula [2.14] and [2.15]), after which the velocity was increased step by step until significant erosion of base and/or filter material occurred.

Beforehand, one can expect that the erosion of material is limited until a certain critical velocity. When the velocity becomes higher than the critical velocity, the amount of erosion/movement will increase significantly, as shown in Figure 4-1.

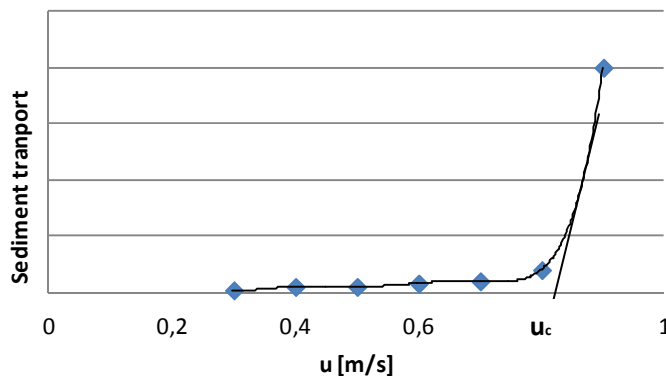


**Figure 4-1 Determination critical velocity**

The results can be split up in three categories (see Figure 4-2);

- Base material moves at a lower critical velocity than the filter material (red area in Figure 4-2);
- Base and filter material start to move at about the same critical velocity (orange area in Figure 4-2);
- Filter material moves at a lower critical velocity than the base material (green area in Figure 4-2).

With the results split up in the different categories the design formula can be proven (and eventually changes can be made to the design formula).

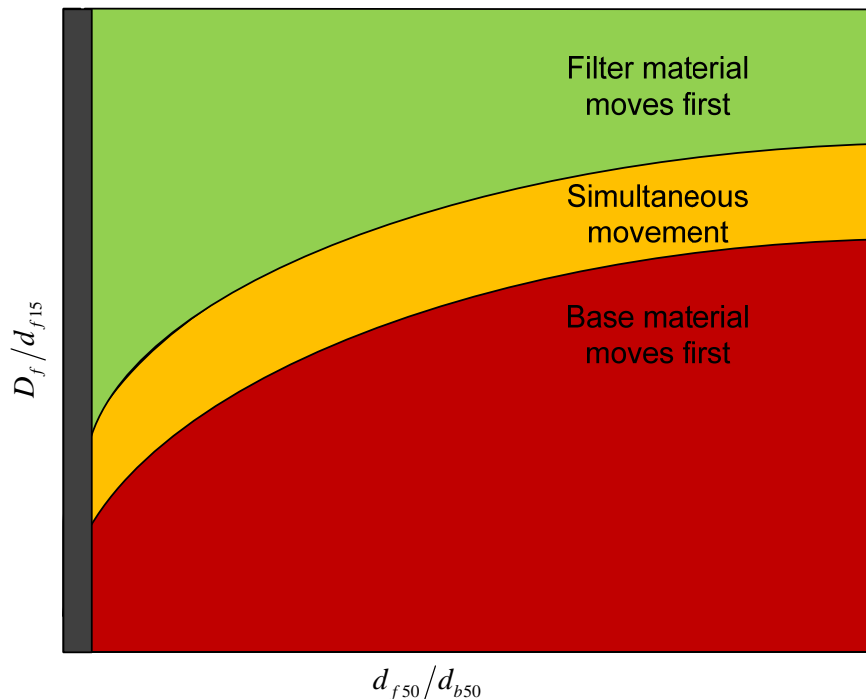


Figure 4-2 Movement of filter material and base material

## 4.2 FLUME

The tests were elaborated in a 12 meter long flume in the Environmental Fluid Mechanics Laboratory at Delft University of Technology. Table 4-1 gives an overview of the most important properties of the flume. In Figure 4-3 some pictures of the flume (with model test set-up) are given to get an impression.

Flume	
Length	12 m
Width	40 cm
Depth	40 cm
Max. discharge	~ 100 l/s

Table 4-1 Properties flume



**Figure 4-3 Flume with test set-up in the Environmental Fluid Mechanic Laboratory**

### 4.3 SCALING

Physical models are a powerful tool to get better insight into physical behaviour, but a negative point that has to be overcome is the effect of scaling. Within models it is impossible to scale all the properties (e.g. the gravitational force and the viscosity of water are properties which are hard to scale). When using model tests, scaling rules can be used to scale a situation to a model.

Scaling rules are dimensionless relations between the primary variables; length, mass and time. Which scaling rule should be applied depends on the dominant force that should be scaled properly.

Scale rules can be expressed with dimensionless numbers. The two most frequently used scaling rules are (Schierreck, 2007);

$$\text{Froude:} \quad Fr = \frac{u^2}{gh} \rightarrow \frac{n_u}{\sqrt{n_g n_l}} = 1 \quad [4.1]$$

$$\text{Reynolds:} \quad Re = \frac{ul}{\nu} \rightarrow \frac{n_u n_l}{n_\nu} = 1 \quad [4.2]$$

This research focuses on the validation of equation [3.13]. This formula is based on dimensionless parameters ( $\Delta, \psi, \gamma, V_g$ ) and relative dimensions ( $D_f/d_{f15}, d_{f50}/d_{b50}$ ). This makes the formula insensitive to scaling.

Of importance are the relative dimensions ( $D_f/d_{f15}, d_{f50}/d_{b50}$ ). To create a similar relation between the diameter of the filter and base material, both have to be scaled with the same factor. The possibility to scale the base material is limited. Smaller particles than  $60 \mu m$  become silt and are cohesive, giving a very different behaviour.

The load in equation [3.13] is taken into account indirectly by the dimension of the filter material. Determination of the required stone size can be done with for example the formula of Izbash (eq. [2.13]). With the Buckingham Pi Theorem

(Hughes, 1993) the scaling rule(s) of importance can be determined. In this research Froude scaling is of importance.

The gravitational force cannot be scaled, resulting in scaling of the dimensions and the velocity (load). The scaling of the dimensions is related to the scaling of the velocity as:

$$n_v = \sqrt{n_l} \quad [4.3]$$

## 4.4 MEASUREMENTS

To determine whether filter and base material start to move at the same time or that one of the materials is moving at a lower critical velocity than the other material, it is important to measure the amount of material transport in relation to the velocity. In the following paragraphs the measurement methods for determining the transport of filter and base material, the velocity and pressure fluctuations are explained.

### 4.4.1 TRANSPORT OF FILTER MATERIAL

The transport of filter material was measured visually. To be able to count the moved stones, a section of the filter layer was constructed with painted stones. After each load condition (velocity) the number of moved stones were counted (Figure 4-4). When the transported stones for each load condition are plotted in a graph, it results in a graph like in Figure 4-1.



**Figure 4-4 Transport of filter material (black arrow indicates main flow direction)**

There the formulas of Shields [2.14] and Hoffmans [2.15] are tested and verified, the results measured for movement of filter material have to be in agreement with the calculated values. So for each test the theoretical start of movement is calculated and added to the results. Appendix F shows that the measured start of movement and the calculated start of movement are accordant.

#### 4.4.2 TRANSPORT OF BASE MATERIAL

A couple of methods can be used to measure transport of sand material. The most obvious method is placing a filter/sieve to filter all the sediment out of the water. An alternative method is using a suction tube to take a sample out of the water and measuring the amount of sediment in the water taken out of the flume by the suction tube. A third method is an indirect measurement. After each step the settlement of the bed is measured, from the measured settlement of the bed the amount of sediment transport can be determined.

Within the experiments the velocity is increased till a significant amount of sediment (and filter material) transport is measured. Before the critical velocity is reached, the amount of sediment transport is limited (see Figure 4-1). With the indirect measurement method, measuring the settlement, the small amounts of sediment transport cannot be measured, which makes this method unsuitable for this experiment.

The problem with the suction tube is that it only takes a sample at a certain location in the flume. When the tube is placed close to the bed, one can expect to measure more sediment than when the tube is placed at a higher location in the water. Especially for the small amounts of sediment transport the deviation of the measurements could be extremely large.

Because of the above mentioned, the measuring method used for this research was a sieve/filter. The sieve catches all the sediment that is transported to the end of the flume. A limitation of the sieve is the hydraulic permeability.

The sieve was placed behind the flume (see appendix E). Within the tube behind the flume, there is a narrowing. The sieve was placed on top of this narrowing. The water that leaves the flume leaves the flume throughout the tube behind the flume. In this way all the water had to go through the sieve, which filtered all the sediment out of the water.

The sieve cloth that was used had openings that were small enough to filter out even the finest particles of the m32 sand (the finest base material). The sieve had openings of 106  $\mu\text{m}$ . The hydraulic permeability of the sieve had to be as large as possible, to limit the impoundment on top of the sieve. The chosen type of sieve had a maximum amount of open spaces (57% of its surface) and was the most permeably type of sieve available.

A water level will rise on top of the sieve, resulting in a larger gradient over the sieve, till the input of water is equal to the permeability of the sieve. Higher velocity (resulting in larger discharges) results in a higher water level on top of the sieve. The water level inside the tube should not affect the water level inside the flume. As long as the water level on top of the stack of sieves is limited, it does not influence the water level in flume.

As the sieves were made especially for these experiments, there are no figures about the permeability of the sieves. With the formula of Torricelli, and the percentage of open space in the sieve, the thickness of the water layer on top of the filter was calculated. Besides the theoretical calculation, small tests had been executed (before the model tests were executed) to determine permeability of the

sieves. The theoretical approach as well as the experiments pointed out that the sieves are permeable enough for the highest velocities during the model tests.

The sieves are constructed in such a way that they fit exactly in the tube behind the flume (Figure 4-5). The design of the sieve is given in Figure 4-6.



**Figure 4-5 Sieve in the drain of the flume**

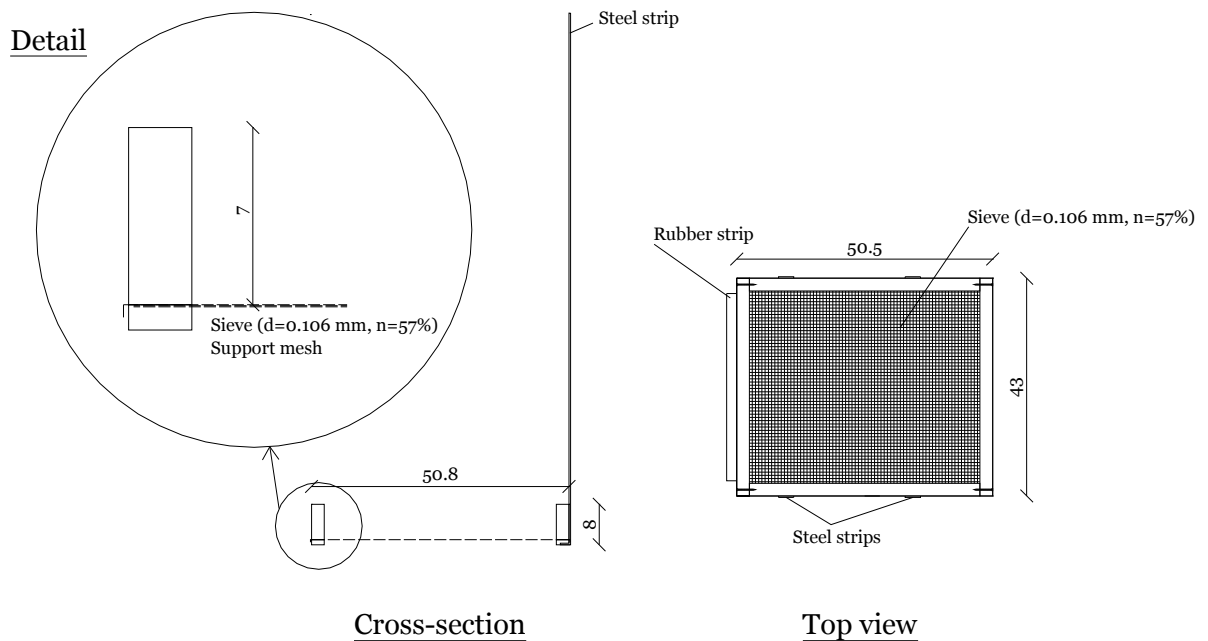


**Figure 4-6 Sieve design (dimensions in cm)**

The amount of sediment has to be measured after each step (each velocity). There are two options to do this;

- The experiment has to be stopped, the sieve is taken out and another sieve is placed (it is not possible to pull out the sieve when there is water on top of it);
- A new sieve is placed on top of the previous one. The first sieve contains the sediment from the first step and no more sediment will be added to this sieve. The new sieve is filtering the sediment of the next step out of the water (the size of the openings of all the sieves are same).

The second method is time saving and also gives fewer problems with the test. Every time the flow is stopped, the water level has to be held constant in the flume by bringing the valve at the end of the flume up and closing the water supply. This will result in a translation wave within the flume. Also every time the experiment is continued, the starting of the flow will influence the experiment. By placing the sieves on top of each other, these effects can be minimized.

The sieves are designed in such a way that they can be placed by a crane (Figure 4-7).



**Figure 4-7 Left: Sieve with lifting frame, Middle: Stack of sieves, Right: Sieve placed with a crane**

After each test, the material filtered out of the water by each sieve is collected in a smaller filter (coffee filters were used). After drying the material it was weighed (Figure 4-8). The used coffee filters have a weight of 1,60 gram. This weight was abstracted from the measured weight, resulting in a net weight of transported material.



**Figure 4-8 Weighing the sand collected in a sieve**

#### 4.4.3 VELOCITY

To measure the velocity, different devices can be used. Simple ways to measure the velocity are by discharge meter or miniature impellor. A discharge meter is used to determine the discharge through the flume. This meter is used

to set the right discharge/velocity during the tests and the meter is used to calculate the average velocity during the test.

For more accurate (local) velocity measurements the following equipment can be used (a description/explanation about the equipment is given in appendix D);

- Pitot tube;
- Electromagnetic flow meter (EMS);
- Acoustic Doppler Velocimetry (ADV);
- Laser Doppler Anemometry (LDA).

To be able to measure turbulent fluctuations in the flow, the sampling rate should be high enough. The sampling rate of the EMS is high enough to measure the large scale eddies, but small scale turbulent fluctuations cannot be measured. To get a good image of the turbulent intensities the sampling rate of the instrument should be high enough, bringing us to the ADV or LDA.

Both the ADV and the LDA are working as a result of reflection on particles (this reflection is experiencing a Doppler shift). To be able to measure with these types of instruments, sufficient small particles have to be present in the water.

The reliability of the measurement with the ADV and LDA depends on the amount of small particles. To generate reliable measurements, extra particles are added to the water. To increase the number of particles in the water, Kaolinite (Chinese Clay) is added. The kaolinite is dissolved in the water and added to the water at the beginning of the flume (see drawing appendix E). Kaolinite is extremely fine material ( $d_{50} = 2 \sim 3 \mu m$ ), which is even dissolved during low velocities. The material is also much smaller than the dimensions of the openings in the sieve. So the particles do not influence the measurement of transported base material.

From a practical point of view, the ADV is chosen to do the velocity measurements. The transmitter and receiver of the ADV are connected to each other (Figure 4-9). In the case of the LDA the transmitter and receiver are two loose elements. Those elements should be placed very carefully, to guarantee that the receiver receives the signal from the transmitter. Because the velocity profiles measurements should be obtained at different locations, the measurement equipment should be easy to move, which makes the ADV more favourable in comparison with the LDA.

The velocity meter is used to measure (the development of) the flow profile and to measure near bed velocity and turbulent fluctuations.

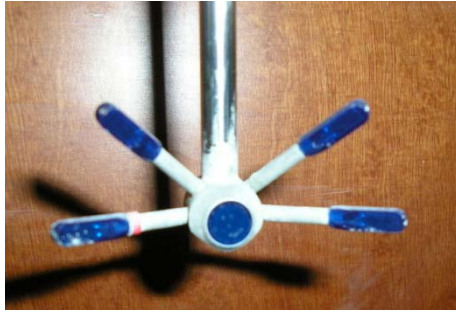


**Figure 4-9 ADV, transmitter (blue part in the middle) and receivers (4 legs)**

#### 4.4.4 PRESSURE

To measure the damping of turbulent fluctuations in the filter layer, pressure meters were installed. The pressure tubes were installed in such a way they measure the absolute pressure and the relative pressure (see Figure 4-10).

To prevent the tubes from clogging the tubes were placed in the same section as the section where the transport of stones was measured. In this part of the flume no fine sediment is present which reduces the change of clogging. For the location of the pressure tubes see the drawing of model set-up in appendix E.

Beforehand there was already some doubt about the accuracy of the equipment and the effect of the local situation. During the analysis of the measurements, it was found that the fluctuations introduced by the equipment are dominant and that no general conclusion can be drawn. This will be discussed/explained in paragraph 5.3.

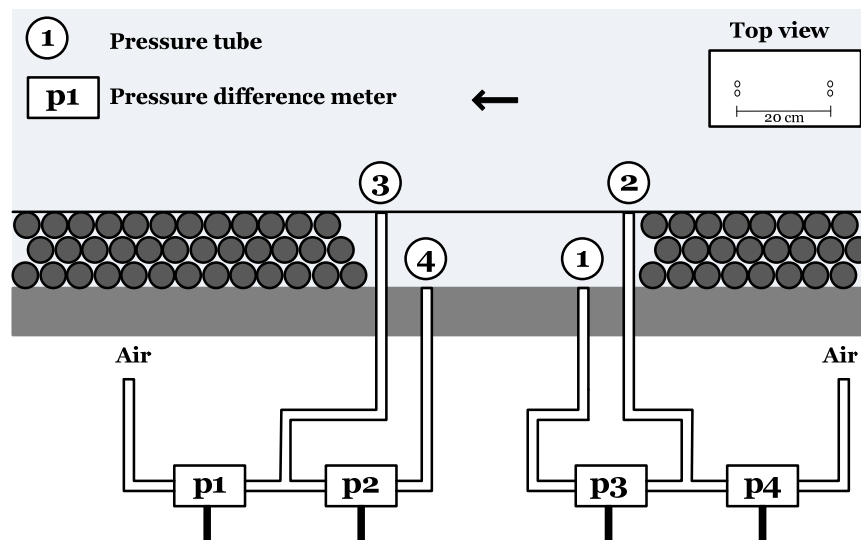


**Figure 4-10 Pressure meters (schematic representation)**

## 4.5 TEST SET-UP

The design drawing of the model test can be found in appendix E. In this paragraph the choices made within the design are explained.

#### 4.5.1 SEPARATE TEST SECTIONS

The sections to measure transport of filter material and base material are separated. This to prevent the measurements from effecting each other.

Only a small section of the flume will be used to place a base layer. The base layer is placed between two concrete slabs. Besides enclosing the section with sand/base material, the concrete slabs also minimize the amount of stones/filter material that is needed in front of the test section.

The stones on top of the base layer were glued together with elastocoast. This was to prevent degradation of the filter layer thickness. A thinner filter layer results in more erosion of the base material. If there would be erosion of the filter material on top of the base material and sediment transport would be measured, the erosion could not be linked anymore to the originally filter layer thickness.

#### 4.5.2 LOCATION

The test section was placed to the end of the flume as far as possible. By placing this test section completely at the end of the flume, the time that sand particles had to settle again is limited. And the distance sand particles had to travel before entering the sieve was limited.

The last 0.50 meter of the flume was not used as test section because of the undesired effect of the spillway.

When heavy erosion of the filter material would occur, there would be a transition at the location where the loose stones end/the slabs created with elastocoast start. To limit the effect of this possible transition an extra slab of stones glued with elastocoast was placed in front of the test section (the test section for base material transport).

The locations of the test sections are given in the drawing in appendix E.

#### 4.5.3 DIMENSIONS

The dimensions of all the parts of the model, also given in the drawing in appendix E, in anti-chronological order (from the end of the flume to the front);

- 0.5 meter: Concrete slab with on top a slab of filter material glued together with elastocoast. This part of the flume is experiencing influence from the spillway;
- 1.0 meter: Test section. Base layer (sand) with on top a slab of filter material glued together with elastocoast. This part of the section is to investigate the erosion of the base layer (under a granular layer). According to experiments of Klein Breteler et al. [1992], the transport of base material is, for sections with a dimension of 1 meter or more, independent of the length of the test section (Wolters, to be published);
- 0.5 meter: Transition between the test sections. Concrete slab with on top a slab of filter material glued together with elastocoast. This to prevent a transition at the start of the test section when heavy erosion of the loose filter material occurs;

- 0.2 meter: Transition with a filter layer of loose material. To prevent that the transition of loose material and the slabs of filter material is located within the test section for transport of filter material;
- 0.2 meter: Test section. Filter layer with painted filter material. The colour makes it possible to count the stones that moved during the test. Within this section also the pressure meters are installed;
- 3.0 meter: Layer of filter material with the same height as the test sections. This layer is to let the velocity profile develop completely. The section has a length of 10 times the maximum water depth;
- At the beginning of the flume: A pile of corrugated plates to damp the turbulent fluctuations of the extremely turbulent flow that is entering the flume. Followed by a floating plate to damp small waves (waves generated by the flow entering the flume).

#### 4.5.4 DIMENSIONS FILTER MATERIAL SLABS

The slabs made of filter material are thin, which makes them vulnerable for breaking during lifting. To prevent breaking because of its own weight, the maximal length has been calculated in appendix C, the results are given in Table 4-2.

By calculating the maximum length, the slabs are represented as a beam on two support points. Where the support points are representing the points at which the plate is lifted. The weight of the slab is the force that generates the bending moment that has to be resisted. The calculation is worked out in appendix C.

$D_f$ [mm]	$l_{max}$ (Yellow Sun) [cm]	$l_{max}$ (Yellow Sun) [cm]
20	141	139
30	172	170
100	314	311

**Table 4-2 Maximum length filter material slabs (to prevent breaking by own weight)**

To be safe a length of 50 cm is chosen for all the slabs, resulting in the dimensions and weight as given in Table 4-3. The dimensions are also chosen in such a way that the slabs can be lifted by hand.

$D_f$ [mm]	Length [mm]	Width [mm]	Weight [kg]
20 <sup>*1</sup>	500	394	7.0
27 <sup>*1</sup>	500	394	7.9
40 <sup>*2</sup>	500	394	11.9
57 <sup>*2</sup>	500	394	17.3
61.5 <sup>*1</sup>	500	394	18.0
*1 : Yellow Sun			
*2 : Basalt			

**Table 4-3 Weight of the filter material slabs**

#### 4.5.5 CONSTRUCTION

As preparation to the test all the instruments were installed and tested. The positions of all the elements and measurement equipment are given in the drawing in appendix E.

The base and filter materials were placed in the following order (see also Figure 4-16);

- Base layer (sand);
- Slabs of filter material;
- Loose filter material (incl. painted filter material).

The sand was placed in-between the concrete slabs. To make it possible to equal the sand bed, a strip of timber was constructed on each side against the wall of the flume. This strips had the exact height of the base layer and could be used to equalize the base layer. The strips of timber also prevented erosion close to the flume wall (at this location there was a joint between the slabs of filter material and the wall).



**Figure 4-11 Sand bed between two concrete slabs with on top slabs of stones (glued together with elastocast)**

### 4.6 TEST PROGRAM

Within the test program variations were made in three main properties to bound the design curve;

- Ratio between the filter material and the base material;
- (Relative) layer thickness;
- Turbulent energy level.

During the tests the situations were adapted to the new findings.

#### 4.6.1 RATIO BETWEEN FILTER AND BASE MATERIAL

To cover the complete area of application, different filter/base material ratios were used.

When both the filter and base material are coarser with the same factor (keeping the ratio constant), Formula [3.13] implies that the required relative filter layer thickness is equal.

#### 4.6.2 (RELATIVE) LAYER THICKNESS

Paragraph o explained that there is still some uncertainty about the value of the damping parameter. To validate the damping parameter the layer thicknesses is varied.

Layer thicknesses were chosen such that all the three possible types of results (see Figure 4-2) were represented within the tests.

#### 4.6.3 TESTS

The tests executed to validate the design formula [3.13] are given in Table 4-4. The tests are also graphically given in Figure 4-12.

During the execution of the tests in the laboratory it was clear that the original design formula was giving an overestimation of the minimal layer thickness. During the testing, the designs of the test situations were adapted to the revised design curve (based on the data till that moment). The final series of tests are comparable with previous model tests (Figure 4-12).

In Figure 4-12 a comparison is made with previous test from; Bakker [1960], Haverhoek [1968], Wouters [1982], Wörman [1989], Konter et al. [1990], Van Huijstee and Verheij [1991], Dixen [2008] and Van Velzen [2011]. Information about those tests can be found in appendix A.

Test number	Base material	Filter material	$d_{f50}/d_{b50}$ [-]	$D_f/d_{f15}$ [-]	$D_f$ [mm]
<b>To1</b>	A <sub>b</sub>	A <sub>f</sub>	27.73	2.70	20
<b>To2a</b>	A <sub>b</sub>	C <sub>f</sub>	80.94	1.20	27
<b>To2b*1</b>	A <sub>b</sub>	C <sub>f</sub>	80.94	1.20	27
<b>To3</b>	A <sub>b</sub>	C <sub>f</sub>	80.94	2.74	61.5
<b>To4</b>	B <sub>b</sub>	C <sub>f</sub>	39.51	1.20	27
<b>To5*2</b>	A <sub>b</sub>	B <sub>f</sub>	57.80	0.50	8
<b>To6a</b>	A <sub>b</sub>	B <sub>f</sub>	57.80	2.51	40
<b>To6b*2,3</b>	A <sub>b</sub>	B <sub>f</sub>	57.80	2.51	40
<b>To6c*2,4</b>	A <sub>b</sub>	B <sub>f</sub>	57.80	2.51	40
<b>To7</b>	A <sub>b</sub>	B <sub>f</sub>	57.80	3.58	57

\*1 : Filter material above the test section for sediment transport not fixed with elastocoast (in contrast to the other tests)  
 \*2 : Sediment transport is determined visually  
 \*3 : Situation with high turbulence levels, high turbulent levels created by a sill  
 \*4 : Situation with high turbulence levels, high turbulent levels created by rectangular and round piles

**Table 4-4 Test situations**

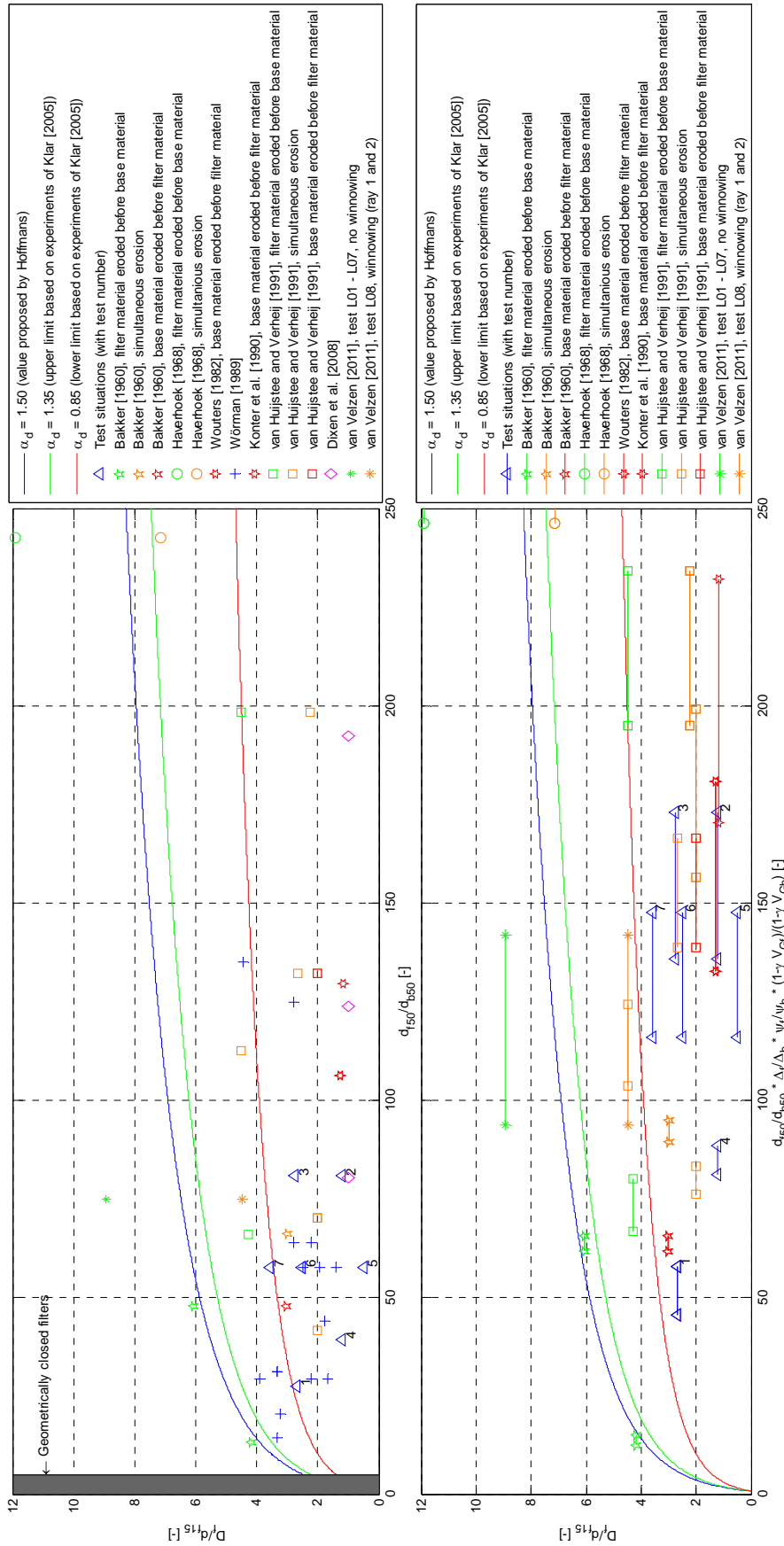


Figure 4-12 Overview of the tests



#### 4.6.4 HIGHLY TURBULENT FLOW

Test To6b and To6c were tests with an increased level of turbulent energy. In the first situation (To6b) the increased level of turbulent energy was generated by a sill (Figure 4-13), in the second situation (To6c) the increased level of turbulent energy was generated by piles (Figure 4-14). The dimensions of the obstructions are given in Table 4-5.

Test	Type of obstruction	Dimensions
To6b	Sill	Height: 65 mm
To6c	Round	Diameter: 110 mm
	Rectangular	Length x width 90 x 40 mm
	Rectangular	Length x width 65 x 40 mm

**Table 4-5 Dimensions of the used obstructions**



**Figure 4-13 Sill (left: top view (flow direction: from bottom to top), right: side view (flow direction: from left to right)), height sill: 6,5 cm**



**Figure 4-14 Round and rectangular piles used to increase the turbulent intensity**

#### 4.7 MATERIAL PROPERTIES

For the model tests two types of base material and three types of filter material were used.



**Figure 4-15 Materials, top: filter material (left: Yellow Sun 8-11, right: Yellow Sun 20-40), bottom: base material (left: m32, right: 0.50-0.80)**

#### 4.7.1 BASE MATERIAL

Two types of sand were used as base material. The dimensions of the sand are given in Table 4-6. The sieve curves, density and the way these are determined are given in appendix B.

Type	$d_{15}$ [ $\mu\text{m}$ ]	$d_{50}$ [ $\mu\text{m}$ ]	$d_{85}$ [ $\mu\text{m}$ ]	$\rho_b$ [ $\text{kg}/\text{m}^3$ ]
<b>A<sub>b</sub></b> m32	248	309	389	2630
<b>B<sub>b</sub></b> 0.50-0.80	523	633	739	2527

**Table 4-6 Dimensions and density base material**

#### 4.7.2 FILTER MATERIAL

For the filter material stones of the type Yellow Sun and Basalt were used. Three different types with a normal grading are used, Yellow Sun 8-11, Yellow Sun 20-40 and Basalt 16-22. The sieve curves and measurement are given in appendix B.

Type	$d_{15}$ [mm]	$d_{50}$ [mm]	$d_{85}$ [mm]	$d_{90}$ [mm]	$d_{n15}$ [mm]	$d_{n50}$ [mm]	$d_{n85}$ [mm]	$d_{n90}$ [mm]	$\rho_f$ [ $\text{kg}/\text{m}^3$ ]
<b>A<sub>f</sub></b> Yellow Sun 8-11	7.42	8.57	9.99	10.41	6.53	7.54	8.79	9.16	2633
<b>B<sub>f</sub></b> Basalt 16-22	15.93	17.86	19.91	20.47	14.02	15.72	17.52	18.02	2960
<b>C<sub>f</sub></b> Yellow Sun 20-40	22.45	25.01	27.23	27.83	19.75	22.01	23.96	24.49	2633

**Table 4-7 Dimensions and density filter material**

## 4.8 EXECUTION OF THE MODEL TESTS

The model tests (inclusive preparations) were executed in 3 months (January till March 2012). Every test was executed following a certain scheme. The execution of each model test is schematically (step by step) given in Figure 4-16.

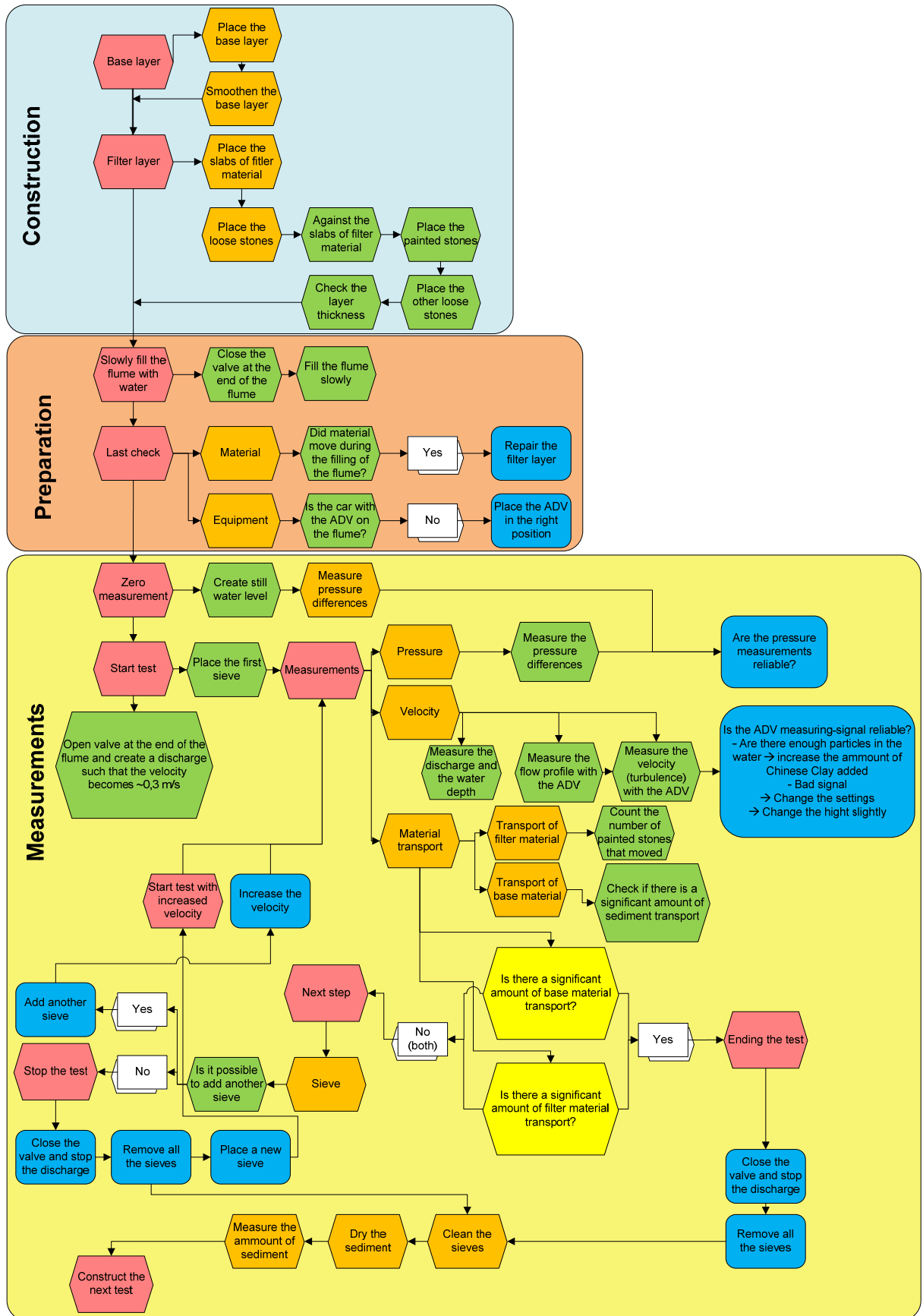


Figure 4-16 Flowchart model test



# 5 TEST RESULTS

---

This chapter together with appendix F, G and H presents the results of the model tests.

The chapter is split in five sections. The first paragraph presents the hydraulic conditions/velocity measurements of the model tests. The second paragraph the transport of material, followed by the third paragraph explaining the pressure measurements inside the filter. In paragraph four some extra attention is paid to the two tests with high turbulent levels (T06b and T06c). The final paragraph is giving some errors and limitations related to the measurements and model set-up.

## 5.1 HYDRAULIC CONDITIONS

The hydraulic conditions of each test are based on velocity measurements which were obtained with an ADV. The following paragraphs consecutively deal with the measurements themselves, the flow profiles and the turbulent properties of the flow.

### 5.1.1 VELOCITY MEASUREMENTS

With the use of the Vectrino (ADV) the instantaneous velocity is measured. The Vectrino measured instantaneous velocities with a sampling frequency of 25 Hz. This results in a measuring signal as given in the top graph in Figure 5-1.

The Vectrino obtained the velocity from a Doppler shift of a reflected acoustic signal. The acoustic signal is reflected by small particles in the water. When a signal is not reflected by a particle and/or reflections from outside the sampling volume are picked up by the receiver extreme values are registered. These extreme values are visible in the top graph in Figure 5-1. The extreme values are eliminated with a despiking function (Matlab script), resulting in the signal given in the lower graph in Figure 5-1.

The despiked signal is used for determination of velocity and turbulence properties.

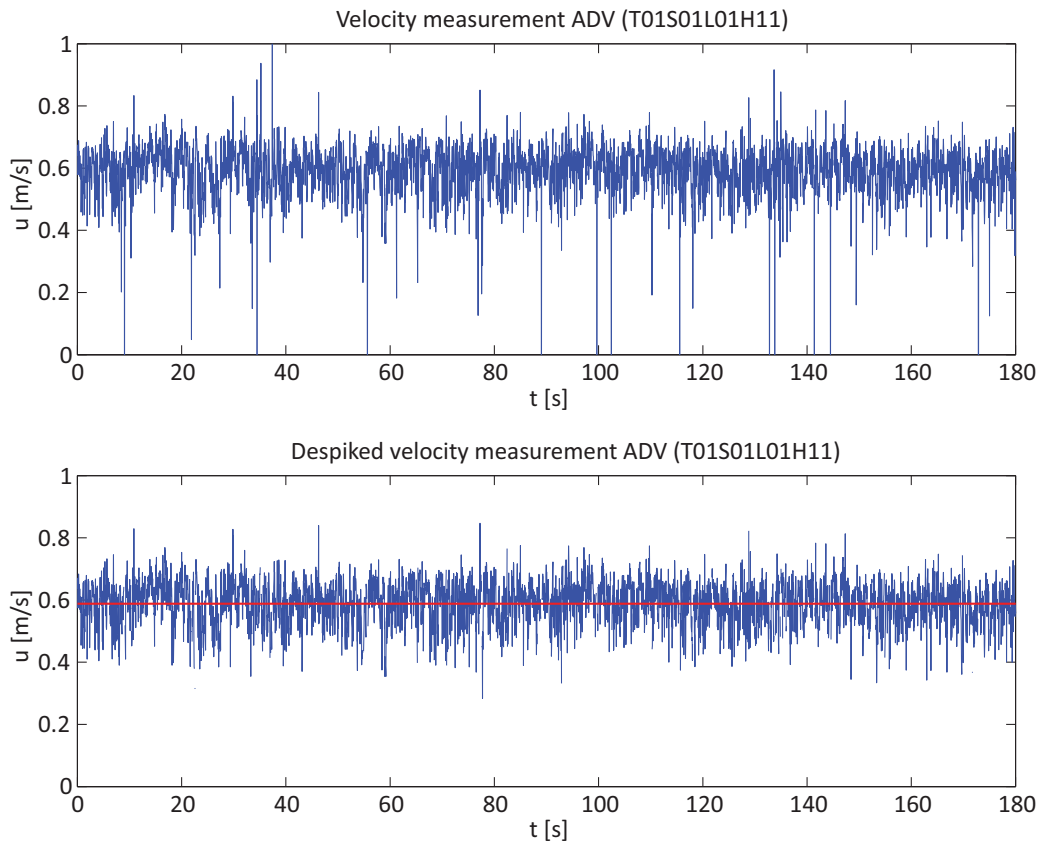


**Figure 5-1 Single velocity measurement (T01S01L01H11), top: raw signal, bottom: despiked signal**

### 5.1.2 FLOW PROFILES

With the Vectrino (ADV) measurements are made at three different cross-sections. The locations of the cross-sections are given in Figure 5-2. Cross-section 1 and 2 are taken at locations above the filter layer. Cross-section 1 is made 0,5 meter upstream of the first test section. Cross-section 3 is upstream in comparison to the part of the flume that is protected with filter material.

The flow profile should be fully developed before the first test section. By measuring the flow profile just before the test section and a second time downstream of the first measurement, the measurements can be compared.

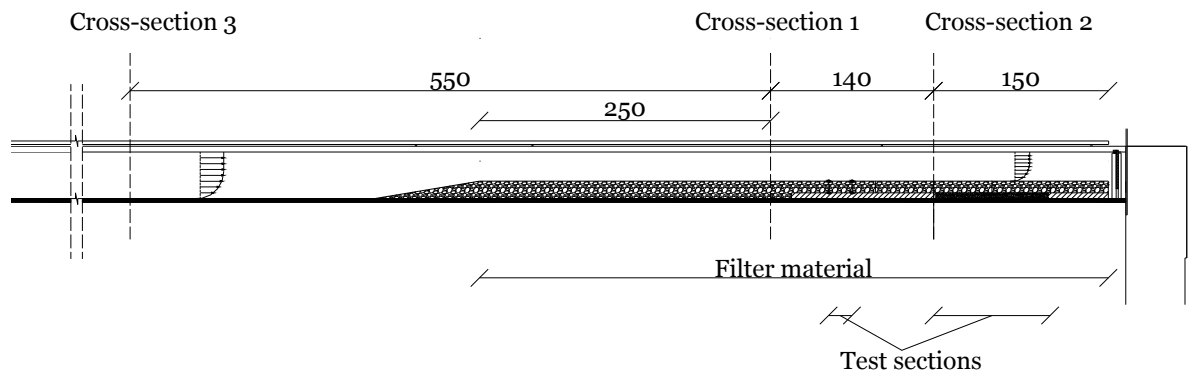


**Figure 5-2 Location of the cross-sections**

With the Vectrino (ADV) measurements are obtained from just above the filter layer up to the water surface. With the averaged velocities at all the locations the flow profiles, as given in Figure 5-3, are generated.

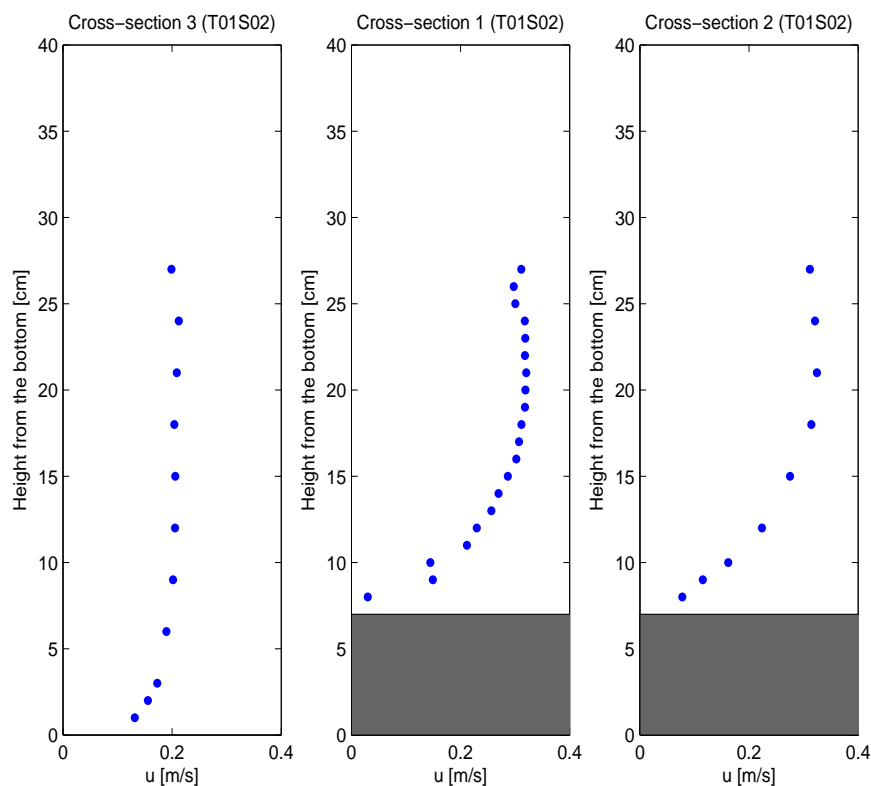


**Figure 5-3 Flow profiles test 1, situation 2 (To1So2)**

The development of the flow profile is related to the shape of the flow profile. When the flow profile is fully developed the shape of the flow profile will not change between cross-section 1 and 2.

When the data of cross-section 1 and 2 is plotted in one figure (see Figure 5-4, left figure) it shows that the shapes of the profiles are nicely correlated. From this correlation can be concluded that the profile is already fully developed at cross-section 1 (cross-section 1 is situated before the test sections). So the flow is completely developed above the test sections (it can be concluded that the adaptation area is long enough).

The flow profiles as given in Figure 5-3 are made during a relative low flow velocity. To cover the complete area of velocities used during the tests, the comparison of the flow profiles has to be made for the lowest velocity as well as for the highest velocity. To cover this complete range of velocities, flow profiles are made for test To1So2 (low velocity) and To4So6 (high velocity).

Figure 5-4 gives the comparison of the flow profile at cross-section 1 (blue dots) and cross-section 2 (red dots). For both situations (low and high velocity) the flow profiles give a completely developed flow profile.

As known from the basics of fluid mechanics a pressure difference is needed to get a flow. So the flow velocity is related to a gradient of the water level. There the model tests are executed in a horizontally placed flume (no gradient in the bed), the water depth is smaller near the end of the flume. A smaller water depth, results in a higher velocity. This acceleration can be seen in Figure 5-4 as a shift in the flow profiles. This shift is hardly visible for low velocities (left figure), but increases with the velocity, resulting in a clear gradient for the highest velocities (right figure).

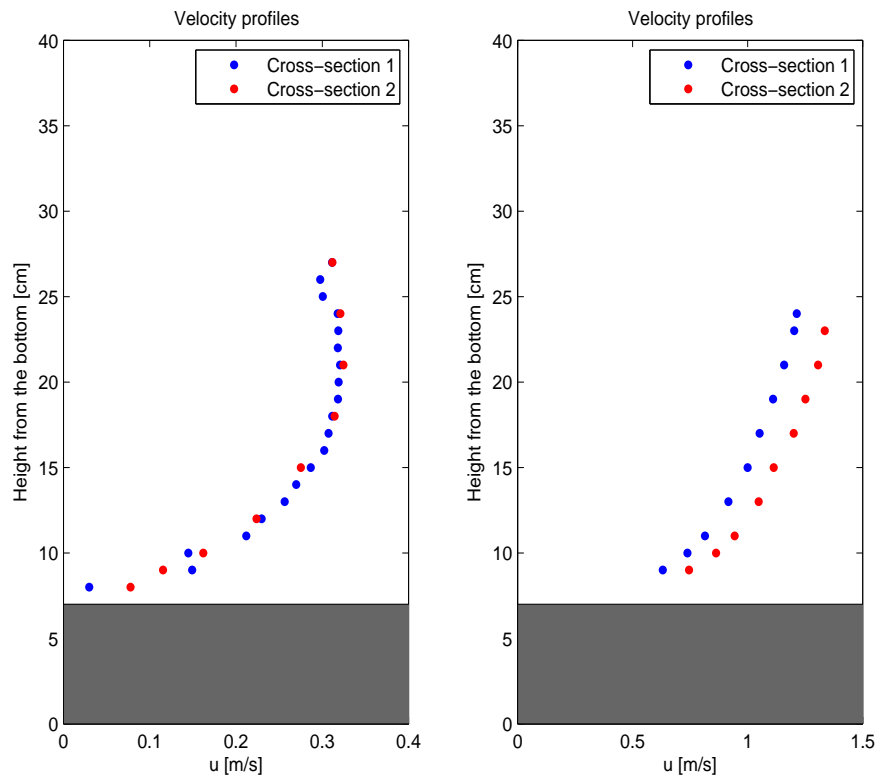


**Figure 5-4** Flow profiles at cross-section 1 and 2, left: To1So2, right: To4So6

### 5.1.3 TURBULENCE

From the measurement records the flow profiles and the turbulent properties of the flow are obtained (Figure 5-5). The turbulent intensities are larger near the rough bed (where the average velocities are smaller).

The velocity profiles and turbulent intensities are nicely correlated, except for some measurements close to the bed. Especially the turbulent intensities in the z-direction near the bed are poorly correlated. This is probably related to the quality of the measurements near the bed. The manufacturer indicated that the quality of the measurements in z-direction are of less quality compared to the measurements in x- and y-direction (Nortek, 2004).

Velocity fluctuations are commonly assumed to be about 10% to 20% of the average velocity. This assumption is confirmed by Figure 5-5.

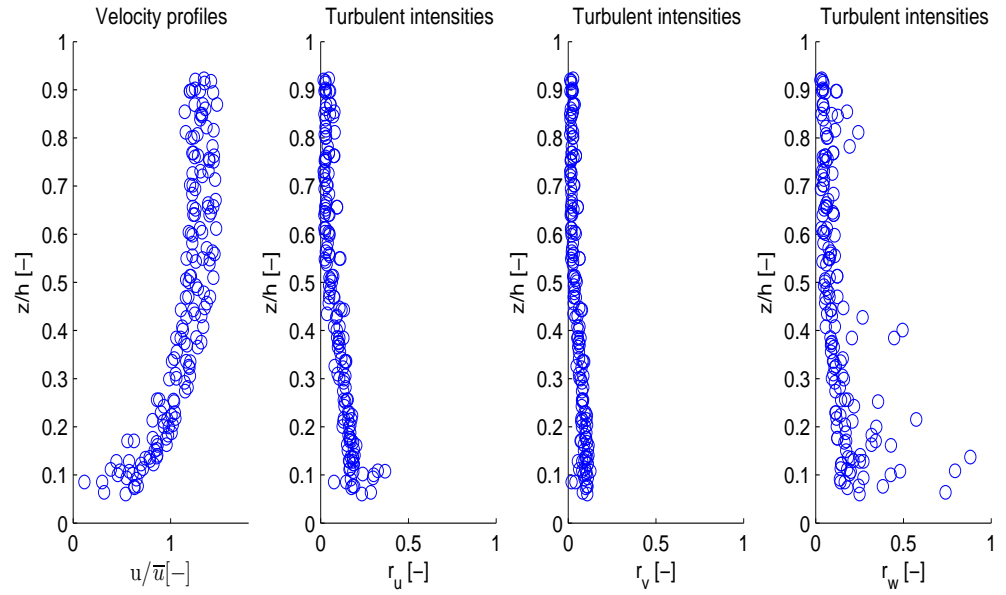


**Figure 5-5 Velocity profiles and turbulent intensities**

With the use of autocorrelation functions the length scale of the vortices in the flow is estimated. The determination of the length scale is explained in appendix H. The spectral analysis results in the distribution of average vortex lengths ( $\lambda$ ) as given in Figure 5-6 (the situations with increased turbulent intensities are excluded in this figure). The average vortex has a length of several centimetres.

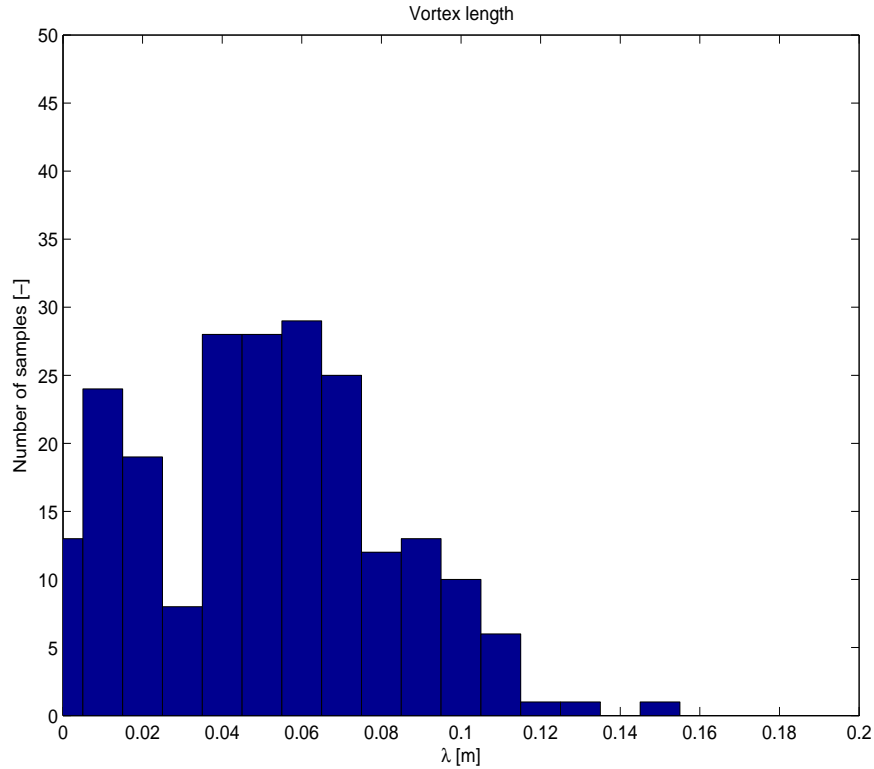


**Figure 5-6 Vortex length**

## 5.2 TRANSPORT OF MATERIAL

The transport of base and filter material is measured for every test (except test T05, T06b and T06c) and each load condition (velocity).

In this paragraph, first the way transport occurs is described and further on the amount of transport and the results.

### 5.2.1 TRANSPORT OF FILTER MATERIAL

The stability of a stone in the filter layer is related to the shear stress, as has been mentioned by Shields (Schierck, 2004). When the shear stress exceeds a critical value the stone starts to move.

With the use of the formulas of Shields (equation [2.15]) and Hoffmans (equation [2.16]) a theoretical start of movement can be calculated. The Shields parameters belonging to phase 1 and 6 are used to calculate the theoretical lower and upper boundary of the start of filter material transport. In paragraph 3.2.4 a distinction is made between the 7 phases of transport (see Figure 3-3). These lower and higher boundaries are given as vertical lines in Figure 5-10 and Figure 5-11 (and in the figures in appendix F).

The calculation of the critical velocities with the stability parameter is proven technology and the measured critical velocities should be in accordance with the calculated critical velocity. Based on the test results (appendix F) one can conclude that the measurements are corresponding with the theoretical calculated critical velocities.



**Figure 5-7 Transport of filter material, test T01 (black arrow indicates main flow direction)**

### 5.2.2 TRANSPORT OF BASE MATERIAL

The amount of sand measured is the amount of sand that is filtered out of the water at the end of the flume. Sand that is transported for a small distance but did not end in the sieve at the end of the flume is not taken into account (/is not measured). This makes the measurement not 100% reliable, the measured amounts of sand transport should be handled with care.

For the transport of sand a distinction is made between two ways of transport, namely; bed transport and winnowing. Figure 5-8 gives a schematic representation of the two ways sand is transported.

In the case of bed transport, the sand is picked up by the flow through the filter, but the sand is not transported completely through the filter. The increased velocity (turbulent fluctuation) is limited in time and after the velocity has become lower, the sand settles again. This is a continuous process, by which the sand can finally be transported to the end of the flume.

In the case of winnowing, the sand is picked up and transported through the filter. When the sand is completely out of the filter it is loaded by the channel flow. These high loading conditions (in comparison with the load beneath the filter layer) result in a suspended load. The sand is transported directly to the end of the flume, where it is filtered out of the water. Of course the distinction between these two types of transport is in practice not so clear and there are forms of transport in between.

When we simplify the situation, one can say that all the sand that is moved completely through the filter (winnowing) is collected in the sieve. This is in contrast with the bed transport. The sand that is moved by bed transport, moves part by part to the end of the flume. This is a time consuming process. At the end of the test, there will still be sand inside the filter layer, sand that moved out of the test section by bed transport but did not reach the sieve. This part of the sand is not taken into account. Figure 5-9 shows a picture of the sand that is transported through the filter layer, but did not end up in the sieve. In this picture the filter layer is removed, which gives a clear view on the remaining sand under the filter layer.

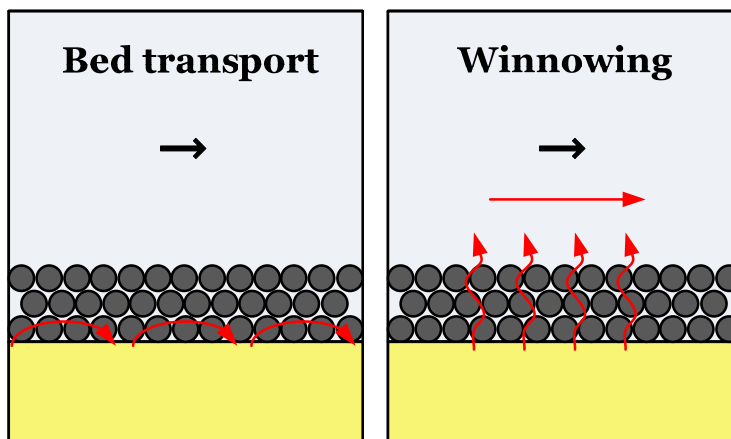
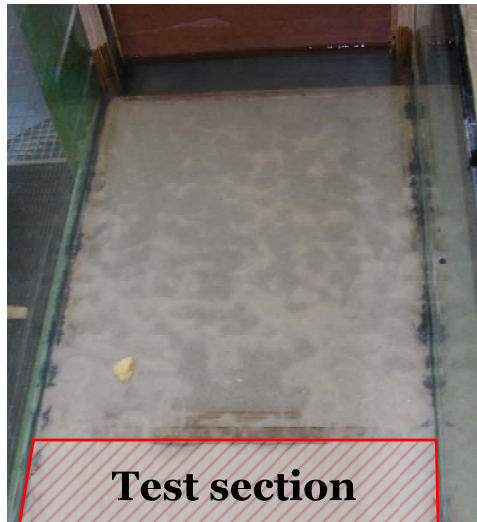


Figure 5-8 Transport of base material



**Figure 5-9 Sand (base material) transported through the filter layer**

### 5.2.3 RESULTS

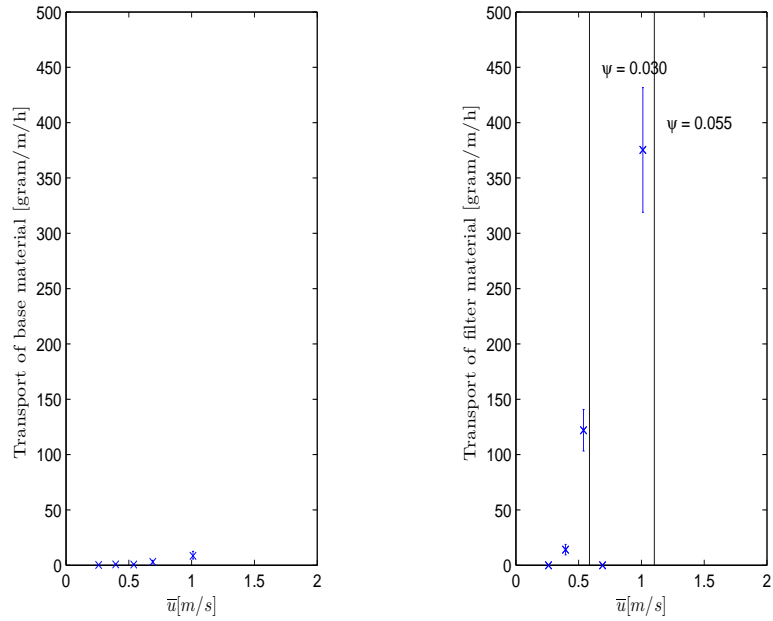
By measuring the amount of transport and plotting this against the velocity, the critical velocity can be determined. The critical velocity of the base and filter material can be compared after which a distinction can be made between three types of situations.

The tests can be split up in three categories (see Figure 4-2);

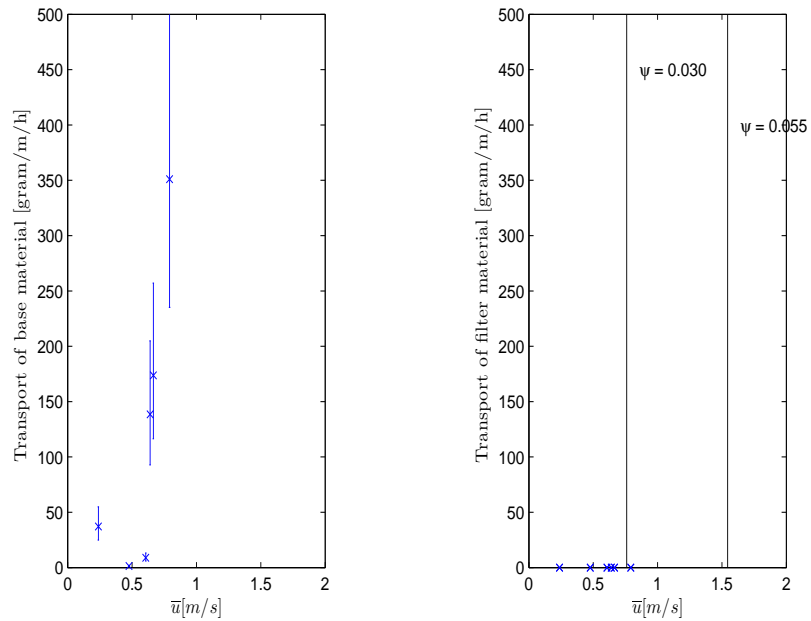
- Base material moves at a lower critical velocity than the filter material (red area in Figure 4-2);
- Base and filter material start to move at about the same critical velocity (orange area in Figure 4-2);
- Filter material moves at a lower critical velocity than the base material (green area in Figure 4-2).

Figure 5-10 represents the results of test T01. Clearly visible in this figure is that there is significant amount of transported filter material and that there is almost no transport of base material.

Figure 5-11 represents the results of test T02. In this situation transport of base material starts before the transport of filter material starts.



**Figure 5-10 Transport of base and filter material, test T01**



**Figure 5-11 Transport of base and filter material, test T02**

Figures like Figure 5-10 and Figure 5-11 are made for each test (see appendix F). With the use of these figures, each test can be placed in one of the three categories. The result of each test is given in Table 5-1, where each test is categorized.

Test	$u_{c,b} < u_{f,c}$ (red area)	$u_{c,b} \approx u_{c,f}$ (orange area)	$u_{b,c} > u_{c,f}$ (green area)
<b>To1</b>			X
<b>To2a</b>	X		
<b>To2b</b>	X		
<b>To3</b>		X	
<b>To4</b>		X	
<b>To5</b>	X		
<b>To6a</b>		X	
<b>To7</b>			X

*The results of test To6a and To6b are discussed in paragraph 5.4*

**Table 5-1 Results of the model test, categorized (colours represent locations as mentioned in Figure 4-2)**

The results, together with results from previous researches, are plotted in Figure 5-12 to Figure 5-15.

Test results

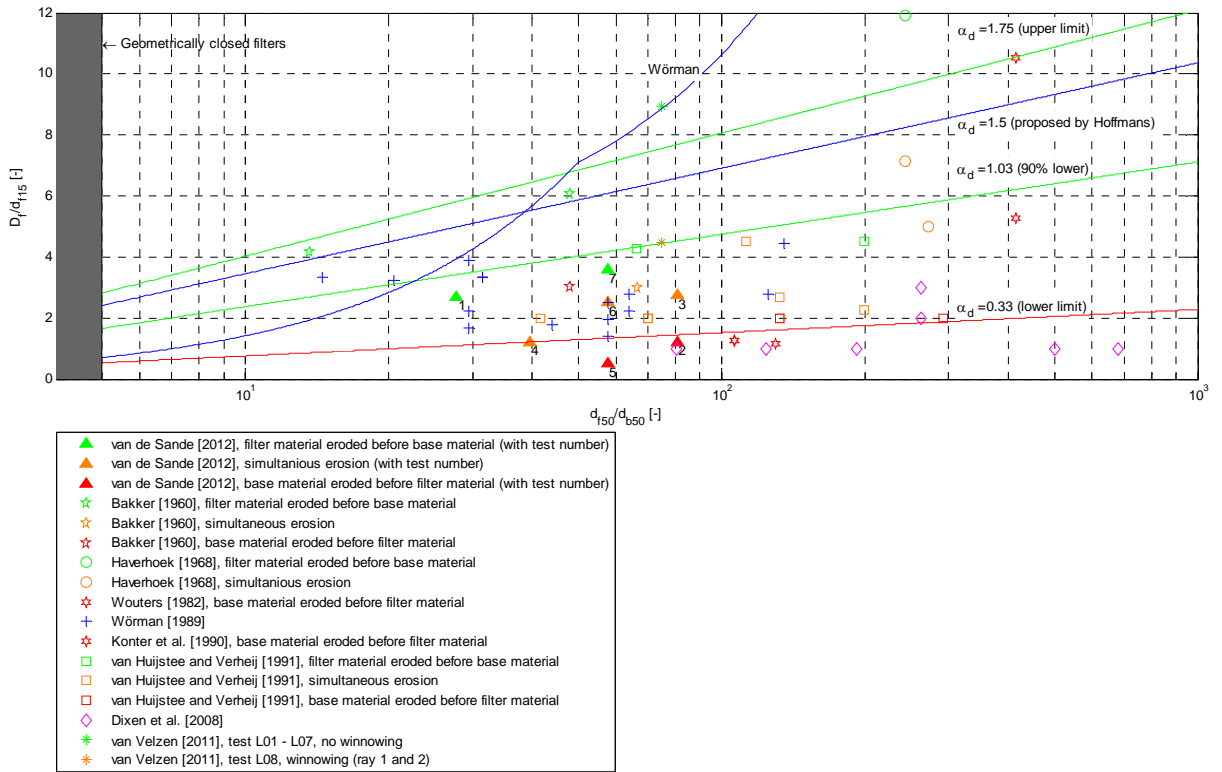


Figure 5-12 Test results, simplified representation design formula, layer thickness;  $D_f/d_{f15}$  (used  $\alpha_d$  values are explained in chapter 6)

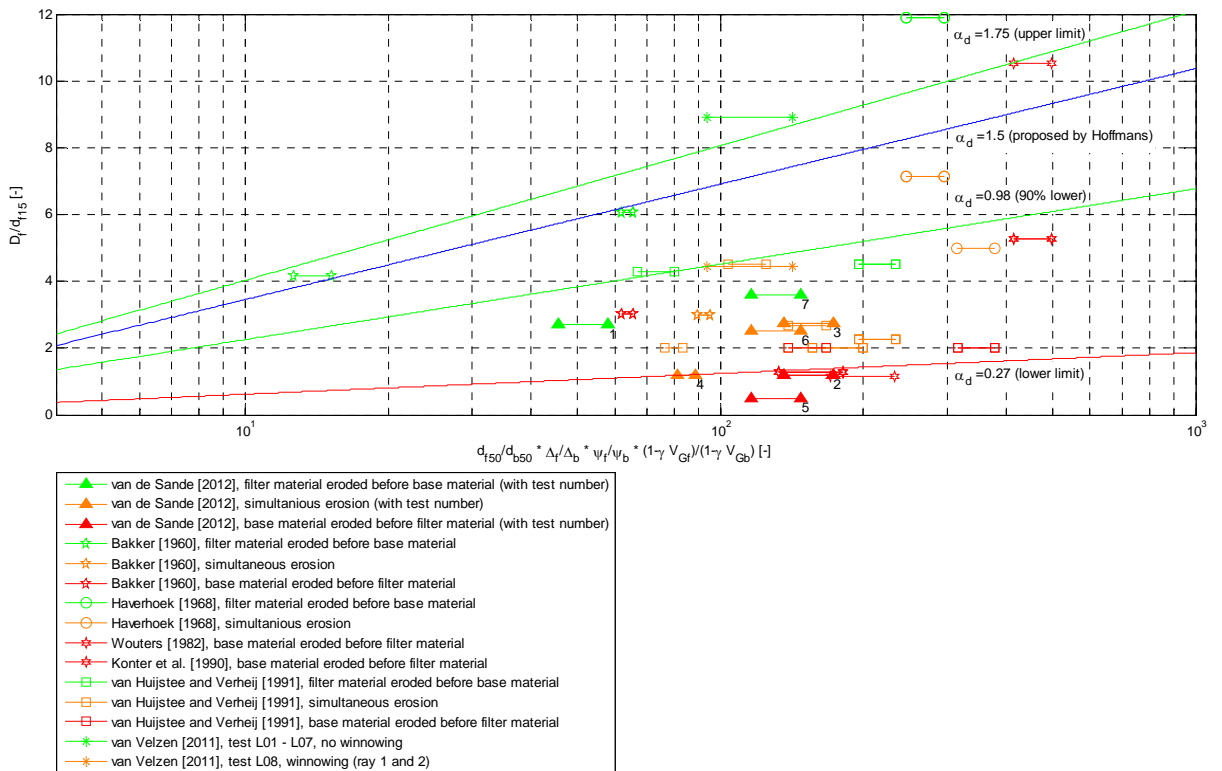


Figure 5-13 Test results, layer thickness;  $D_f/d_{f15}$  (used  $\alpha_d$  values are explained in chapter 6)

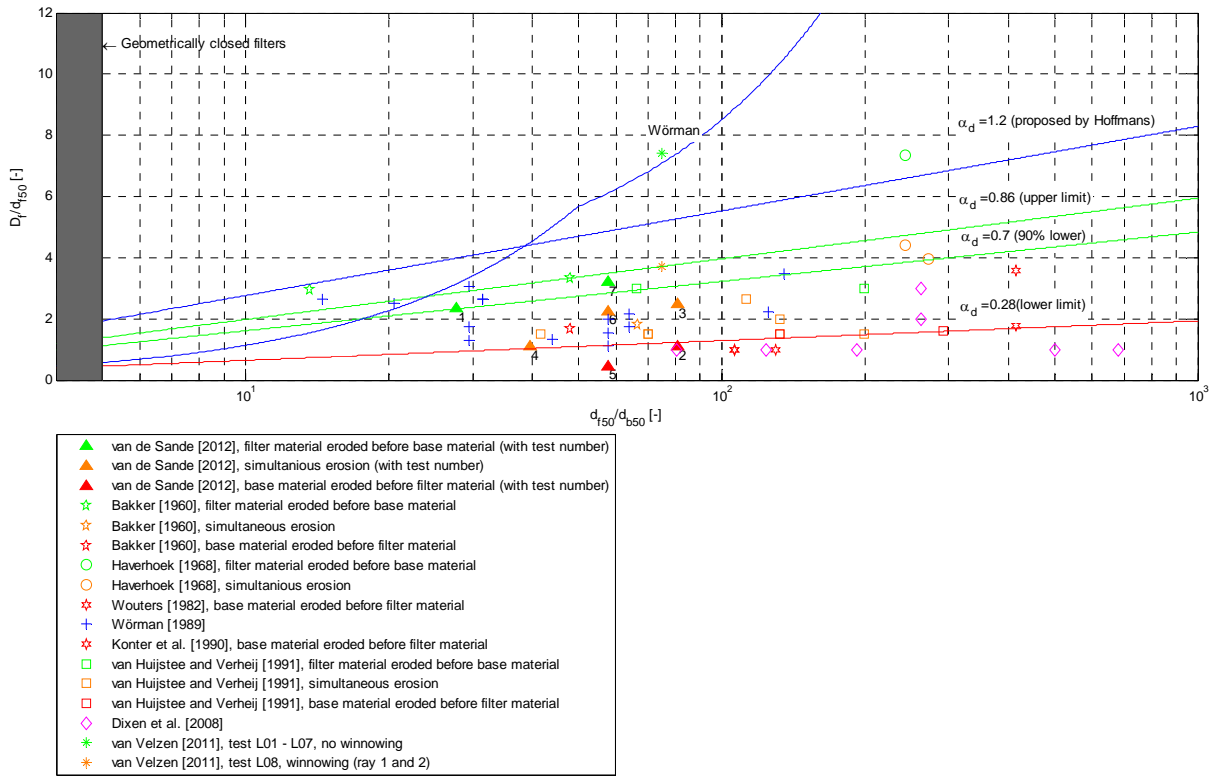


Figure 5-14 Test results, simplified representation design formula, layer thickness;  $D_f/d_{f50}$  (used  $\alpha_d$  values are explained in chapter 6)

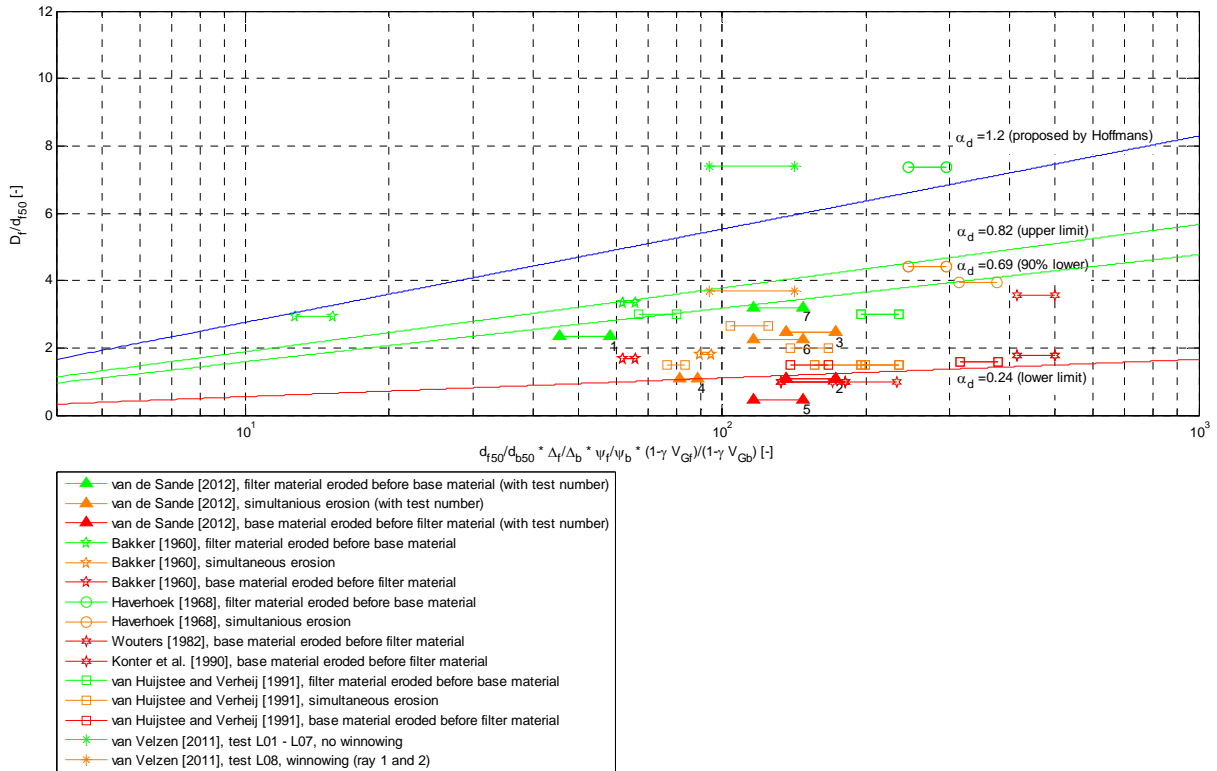


Figure 5-15 Test results, layer thickness;  $D_f/d_{f50}$  (used  $\alpha_d$  values are explained in chapter 6)

## 5.3 DAMPING OF PRESSURE FLUCTUATIONS

Within the model four pressure difference meters were installed (see Figure 4-10). Pressure difference meter p1 and p4 measured the pressure difference between the pressure just above the filter layer and the open air. Pressure difference meter p2 and p3 measured the pressure difference over the filter layer.

For each type of measurements the accuracy is determined. For the pressure measurements, the fluctuations in the record can be divided into two sources;

- Fluctuations introduced by the measuring equipment itself;
- Fluctuations caused by fluctuations in the load (turbulence).

Besides fluctuations in the measuring record, there are also differences introduced by the local situations. The measurement is influenced by the way the stones of the filter layer are placed around the measuring point. This fluctuation in space results in a shift in the measuring record (shift in mean value).

To be able to determine the influence of turbulent fluctuations, the fluctuations introduced by the measuring equipment should be small in comparison with the fluctuations introduced by the variation in load (turbulence). To compare the fluctuations introduced by the measuring equipment with the fluctuations introduced by the turbulence, the measurements can be split in two groups;

- Measurements performed with still water;
- Measurements performed with flowing water.

There are no turbulent fluctuations when the water is standing still. So the fluctuations measured in these situations can be assigned to the measurement equipment. When the water is flowing, both the fluctuations of the measuring equipment and the fluctuations introduced by turbulence are measured. By comparing the fluctuations in the records with still water with the fluctuations in the record with flowing water, the magnitude of the fluctuations related to the measuring equipment and turbulence can be compared.

The standard deviation of 53 measurement records is determined and split up in two categories; still water and flowing water. The minimum, mean and maximum standard deviation from the measurement records in each category is given in Table 5-2.

The standard deviation within the measurement records are of the same order of magnitude for still and flowing water. This means that the fluctuations related to the measurement equipment dominate the fluctuations in the measurement record.

Since the fluctuations are dominated by the measurement equipment, the data cannot be used for the determination of the influence/damping of turbulent motion. The pressure measurements can be used for determination the water depth. The water depth is related to the mean value of pressure meter p1 and p4.

Pressure difference meter	Still water			Flowing water		
	Min. $\sigma$ [Volt]	Mean $\sigma$ [Volt]	Max. $\sigma$ [Volt]	Min. $\sigma$ [Volt]	Mean $\sigma$ [Volt]	Max. $\sigma$ [Volt]
<b>p1</b>	0.097	0.307	0.526	0.070	0.205	0.478
<b>p2</b>	0.083	0.115	0.161	0.124	0.335	0.626
<b>p3</b>	0.020	0.037	0.083	0.018	0.075	0.157
<b>p4</b>	0.087	0.250	0.460	0.018	0.091	0.163

**Table 5-2 Variation in the standard deviations of the measuring data**

To be able to measure the turbulent fluctuations other types of measuring equipment should be used, measuring equipment with a high level of accuracy and a high measurement frequency. The measurement frequency has to be large enough to measure the eddies with small time scales.

Instruments that are able to measure turbulent fluctuations are for example the Acoustic Doppler Velocimeter (ADV) and the Laser Doppler Anemometry (LDA) (see also paragraph 4.4.3 and appendix D). This type of measurement equipment needs a certain sampling volume. This sampling volume is larger than the pores available inside the filter layer. To be able to measure with those type of equipment the pores should be made artificially larger at the location of the measurement. Larger pores are influencing the flow inside the filter structure. So the measurement would not be related to the filter anymore, but to the artificially large pore where the measurement was obtained. Van Os [1998] did measurements inside filter structures with a Laser Doppler Anemometry. He also encountered the problem of increased pore dimensions.

A good example of measuring turbulent fluctuation inside pores/granular structures is the research of Klar [2005]. Klar used an endoscopic 3D particle-tracking system. He measured the turbulent properties of the flow inside filter structures at multiple locations, from which he obtained the damping of turbulent energy in the filter. The result of his research is given in Figure 3-4.

The equipment used by Klar [2005] was not available for this research. With the measurements obtained from the pressure difference meters, the results of Klar cannot be checked.

## 5.4 HIGH TURBULENCE LEVELS

This paragraph focuses on test To6b and To6c (the two tests with increased turbulence intensities) and the comparison of those two tests with the other tests. The velocity is measured during test To6b only.

### 5.4.1 HYDRAULIC PROPERTIES

For test To6b velocities were measured at five different cross-sections. The first cross-section is 70 cm upstream of the sill. The second one is above the sill and the last three are downstream of the sill at 40 cm, 70 cm and 130 cm. The velocity profiles and turbulent intensities for the five cross-sections are given in Figure 5-16 respectively Figure 5-17.

The shapes of the velocity profiles and the development of turbulent intensity over the height at the cross-sections 70 cm up-stream and 120 cm downstream of the sill are comparable with the shapes of the velocity profiles

and turbulent intensities given in normal situations (Figure 5-5). Those cross-sections are considered as fully developed.

Above the sill the flow is accelerating, resulting in an increased velocity and decreased turbulent intensities. Directly behind the sill the flow is decelerating and the turbulent intensities are increasing again. The velocity profiles changes until an equilibrium logarithmic profile is reached again.

Above and directly behind the sill there is a net downward motion. This can be seen in the decreased water level behind the sill. The velocity, as result of the sill, is supercritical directly behind the sill (there is no cross-section at a location with super critical flow). A hydraulic jump is the result of the transition from super- to subcritical flow.

The influence of the hydraulic jump is clearly visible in the cross-section 40 cm downstream of the sill. The measurement most on top of this cross-section, which is taken just below the hydraulic jump (no measurements could be made inside the hydraulic jump) gives an significant lower average velocity (in comparison with the other measurements at this cross-section) and an increased turbulent intensity.

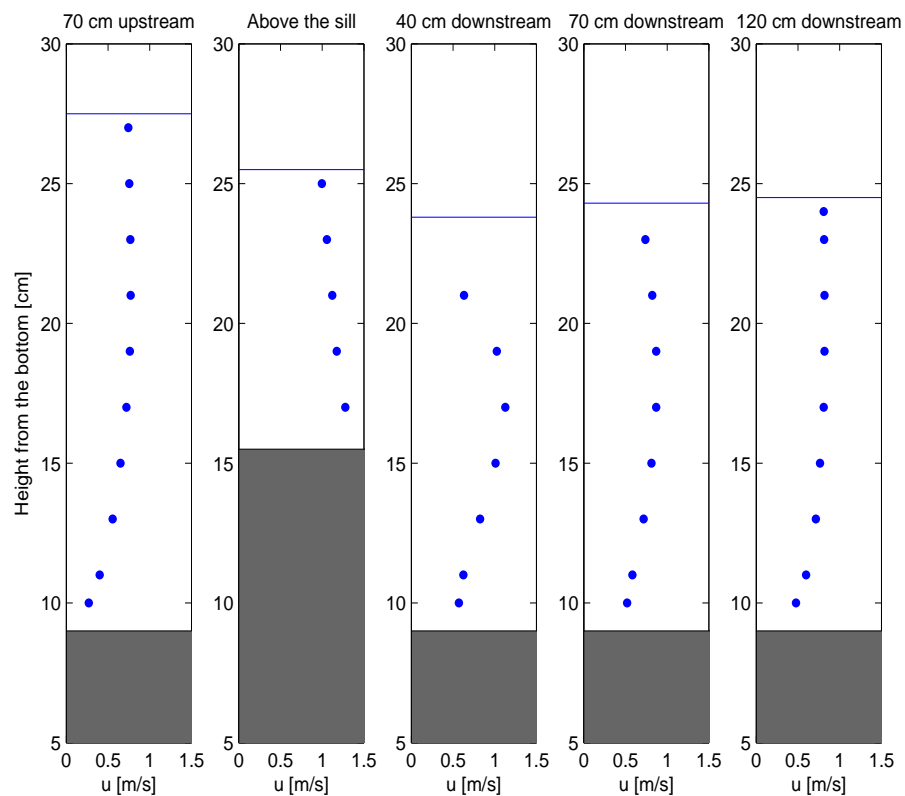


**Figure 5-16 Velocity profiles, up and downstream of the sill**

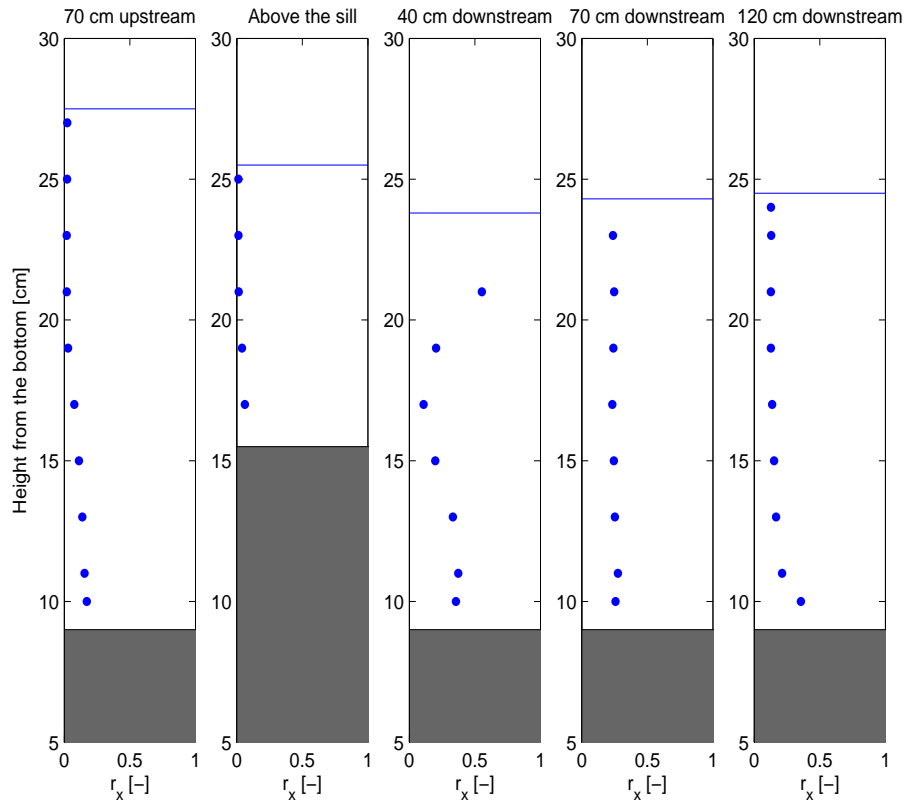


**Figure 5-17 Turbulent intensities, up and downstream of the sill**

#### 5.4.2 TRANSPORT OF MATERIAL

For both tests (T06b and T06c), situations were tested which were stable without the obstacles (no movement of base and/or filter material). After placing the obstacles (the sill (T06b)/pile (T06c)) erosion of base material occurred.

The sill was placed on a foundation just in front of the fixed part of the filter. A foundation was there to prevent water from flowing under the sill. The piles were placed on top of the fixed part of the filter. This location was also the location where the base material was located. For both tests transport of base material was observed after placing the obstacle. Because the filter material was fixed no transport of filter material could be measured.

Figure 5-18, Figure 5-19 and Figure 5-20 show the erosion of base material behind a pile.

The sill resulted in increased velocity and turbulent intensity (Figure 5-16 and Figure 5-17). After the sill was placed, erosion occurred around the location of the reattachment point. Because both the velocity and the turbulent intensity were increased by placing the sill, it is not possible to dedicate the erosion to the turbulent fluctuations only.

The tests showed that when a pile was placed in the flume, erosion of base material occurred. This while the base material was stable before the pile was placed. The pile introduces three different possible causes for the erosion of base material;

## | Test results

- Increased velocity. The pile limits the cross-section of the flume resulting in an increased velocity;
- Increased turbulent intensity. The structure introduces extra turbulence;
- Flow through the filter under the pile. The piles were placed directly on top of the filter material. Water flows under the pile through the porous filter layer.

Despite the increased velocity over the complete width of the flume, the erosion occurs mainly directly behind the pile. Behind the pile there is an upward flow through the filter as a result of the flow under the pile through (this flow can be prevented by placing a foundation, as was done in the case of the sill). Besides this flow, there are also vortexes created by the piles (increased turbulence level). Based on observations, the flow through the filter layer under the pile is considered as the most important reason for erosion of base material.

During the test, three different types of piles were used (see paragraph 4.6.4 for the dimensions of the piles). These piles had different shapes (round and rectangular) and different dimensions. When comparing the observations of the tests with those three different piles the following general conclusions can be drawn;

- More erosion of base material occurred in the case of rectangular piles (compared to round piles);
- Larger piles result in more erosion.

Rectangular piles are not so streamlined as round piles, resulting in heavier turbulent motions. Based on this observation, one can conclude that the erosion of base material is related to turbulent intensity.

Larger piles, resulted in more erosion. Larger piles are also blocking a larger part of the cross-section of the flume. As a result of the smaller cross-section the average velocity is increased. Also the pressure gradient is increased, resulting in an increased flow under the pile.

These first tests confirm that turbulent fluctuations have an influence on the stability of the material and that there should be additional research to get better insight into these effects.



**Figure 5-18 Turbulent motion and erosion behind a round pile**



**Figure 5-19 Erosion behind a round pile (red lines indicate the diverging turbulent motion)**



**Figure 5-20 Erosion behind a rectangular pile**

## 5.5 SOURCES OF ERRORS

In model tests, errors may be present. Errors can be caused by the lay-out of the model tests and by the measurements/measurement equipment. In this paragraph the errors and taken measurements to limit the effects of those errors are discussed.

### 5.5.1 MODEL LAY-OUT

Some of the limitations of the model test lay-out are discussed below. One is referred to appendix E for the design of the model test lay-out.

Errors as a result of boundaries;

- Acceleration of the flow at the end of the flume. To limit the effect of this strongly accelerating flow, no measurements are obtained from the last 50 cm of the flume;
- To prevent erosion of base material directly along the glass wall of the flume, the section filled with sand is slightly smaller than the layer of filter material on top of it;
- The fixed slabs of filter material are limited in size and are laid against each other. To prevent weak spots at those transitions, small holes were filled with loose filter material;

- Difference roughness of the glass-wall and the bed. Both roughness's are taken into account to determine a representative roughness of the flume.

The pressure tubes used to measure the pressure had to lead out of the flume. The tubes were attached to the wall, resulting in a discontinuity (Figure 5-21). To limit the effect of the tubes, the tubes were attached in such a way that the wall was as smooth as possible.



**Figure 5-21 Pressure tubes attached to the flume wall**

### 5.5.2 START-UP AND SETTINGS

At the start of each test the flume was slowly filled with water to prevent erosion as a result of the filling. After the situation was in rest, the zero-measurement was taken.

For each test situation the velocity had to be set manually. The velocity is related to the discharge and the water level. The discharge was regulated with a valve (left picture in Figure 5-22) and the water level with a weir (middle and right picture in Figure 5-22). Both had to be set manually, which made it impossible to create the exact velocity as determined beforehand. The discharge and weir are set manually in such a way that approximately the right velocity is set. For each following load condition the discharge and weir are set again to increase the velocity.

During each load condition the discharge and the water level were measured. From these measurements the velocity was determined. By measuring the discharge and water level during the test, the effect of the manually set velocity is excluded.

During the setting of a new load condition/velocity some start-up effects occurred. Those effects influenced the measurements in the first couple of minutes after setting the new condition. During the first five minutes, no discharge, pressure and velocity measurements were obtained. To limit the effect in the measured amount of transport, the test were run for (at least) one hour (to limit the influence of the transported material as a result of start-up effects).



**Figure 5-22** Left: Valve (discharge), Middle and right: Weir (manually)

### 5.5.3 MEASUREMENTS

Every measurement/measurement equipment has its limitations in accuracy.

The Vectrino (ADV) only measures velocities when the signal is reflected against a particle. So there have to be enough particles in the flow, besides the particles the settings are of importance. Even if there are plenty of particles in the water, sometimes bad measurements could occur in a measurement record. Those measurements have to be filtered out. Solutions are explained in paragraph 5.1.1.

The pressure measurements had some limitations which have already been explained in paragraph 5.3.

The largest uncertainties are in the measurement of the transport of materials. Some of the uncertainties:

- Two types of transport, winnowing and transport through the filter layer (paragraph 2.1 and 5.2);
- Material transported during the start of the test;
- Effect of the build-up of the layers (weak spots, etc.). Differing from test to test and resulting in a deviation of the measured transport;
- Sand that is partly transported during a test (this is not measured);
- Sand that was partly transported during an earlier load condition (and filtered out of the water during another condition).

The deviations of material transport measurements are investigated in appendix G. The determined deviations in appendix G are used to give a range of uncertainty for all the measurements.

For small amounts of sand transport, another inaccuracy becomes of importance. The filters filter not only the base material out of the water, but also all the particles and trash that are in the water that is circulated. When small amounts of material are collected within the sieve, the influence of trash and other particles can be significant.

To get a picture about the measured amount of base material transport; a handful of sand is about 100 gram.

# 6 ANALYSIS AND DISCUSSION

---

This chapter describes the analysis of the design formula and discusses the results found during the model tests executed in the laboratory by the author. Where possible, a link is made with other tests and reports.

The chapter starts with an extensive analysis of the design formula. Special attention is paid to the alpha value and the relative layer thickness. In paragraph 6.2 special attention is given to the effect of the turbulent motions.

Paragraph 6.3 explains the potentiality to use the design formula for multiple layered geometrically open filter structures.

Hoffmans [2012] and CUR [2010] made use of some simplifications, whether these simplifications are justified is explained in paragraph 6.4.

## 6.1 ANALYSIS ALPHA D AND RELATIVE LAYER THICKNESS

For the analysis of the design formula and the alpha value, four different representations of the design formula are used. The relative layer thickness is presented as a relation between the layer thickness and  $d_{f15}$  (equation [6.1] and [6.2]) respectively  $d_{f50}$  (equation [6.3] and [6.4]). In both cases the normal and simplified representations of the design formula are given (note: the alpha parameters in the following formulas have different values and are not exchangeable):

$$\frac{D_f}{d_{f15}} = \alpha_{d,1} \ln \left( \frac{d_{f50}}{d_{b50}} \right) \quad [6.1]$$

$$\frac{D_f}{d_{f15}} = \alpha_{d,2} \ln \left( \frac{d_{f50}}{d_{b50}} \frac{\Delta_f}{\Delta_b} \frac{\Psi_{c,f}}{\Psi_{c,b}} \frac{1 - \gamma V_{Gf}}{1 - \gamma V_{Gb}} \right) \quad [6.2]$$

$$\frac{D_f}{d_{f50}} = \alpha_{d,3} \ln \left( \frac{d_{f50}}{d_{b50}} \right) \quad [6.3]$$

$$\frac{D_f}{d_{f50}} = \alpha_{d,4} \ln \left( \frac{d_{f50}}{d_{b50}} \frac{\Delta_f}{\Delta_b} \frac{\Psi_{c,f}}{\Psi_{c,b}} \frac{1 - \gamma V_{Gf}}{1 - \gamma V_{Gb}} \right) \quad [6.4]$$

The alpha values in equation [6.1] and [6.2] are related to the alpha values in equation [6.3] and [6.4]:

$$\alpha_{d,3} = \alpha_{d,1} \frac{d_{f15}}{d_{f50}} \quad [6.5]$$

$$\alpha_{d,4} = \alpha_{d,2} \frac{d_{f15}}{d_{f50}} \quad [6.6]$$

This relation between the alpha values is valid for each individual test.

### 6.1.1 ALPHA VALUES MODEL TESTS VAN DE SANDE

The alpha values of the model tests corresponding to equation [6.1] to [6.4] are given in Table 6-1. The tests are ranked, based on corresponding alpha values (high to low). The tests with high alpha values (test To7 and To1) are tests where transport of filter material occurred before transport of base material occurred. The tests with low alpha values (test To2 and To5) are tests where transport of base material occurred before transport of filter material occurred. In between are the test with simultaneous erosion (test To3, To6 and To4). A nice distinction between the different types of results is visible in Table 6-1.

The colours in Table 6-1 (and also in Table 6-2 and Table 6-3) are corresponding with the different results as introduced in paragraph 4.1. Green represents test with a safe design (assuming that the filter layer is designed properly). Red represents badly designed filters (too thin) and orange represents optimal designs.

Test	$\alpha_{d,1}$	$\alpha_{d,2}$		$\alpha_{d,3}$	$\alpha_{d,4}$		Test result
		$\Psi_{c,}$ phase 1	$\Psi_{c,}$ phase 6		$\Psi_{c,}$ phase 1	$\Psi_{c,}$ phase 6	
To7	0.88	0.72	0.75	0.79	0.64	0.67	$u_{b,c} > u_{f,c}$
To1	0.81	0.66	0.71	0.70	0.57	0.61	$u_{b,c} > u_{f,c}$
To3	0.62	0.53	0.56	0.56	0.48	0.50	$u_{b,c} \approx u_{f,c}$
To6	0.62	0.50	0.53	0.55	0.45	0.47	$u_{b,c} \approx u_{f,c}$
To4	0.33	0.27	0.27	0.29	0.24	0.25	$u_{b,c} \approx u_{f,c}$
To2	0.27	0.23	0.24	0.25	0.21	0.22	$u_{b,c} < u_{f,c}$
To5	0.12	0.10	0.11	0.11	0.09	0.09	$u_{b,c} < u_{f,c}$

**Table 6-1 Alpha values (ranked from high to low), related to the model tests**

### 6.1.2 ALPHA VALUES FOR ALL THE MODEL TESTS

The results (Table 6-1) are extended with results obtained by other researches (appendix A). The alpha values for the complete set of model tests are given in Table 6-2 and Table 6-3. The ranked alpha values in Table 6-2 are based on the formulas with a relative layer thickness related to  $d_{f15}$ . In Table 6-3 the relative layer thickness is related to  $d_{f50}$ .

Information about some of the properties of the materials used in previous model tests (appendix A) is lacking. Especially information about the density of the used materials is lacking in a major part of the model tests. When information is lacking for a certain test it is indicated by a question mark in Table 6-2 and Table 6-3. The following assumptions are used when information about the parameters was not available:

$$\frac{\Delta_f}{\Delta_b} = 1 \qquad \frac{\Psi_{c,f}}{\Psi_{c,b}} = 1$$

These assumptions are the same as used by Hoffmans [2012] and CUR [2010]. These assumptions give on average, as mentioned in paragraph 6.4, a slight underestimation of the required layer thickness. When these

assumptions are used to determine the alpha values, it results in a slightly overestimated value for alpha.

As the relative layer thickness is known, an underestimation of the logarithmic part results in an overestimation of the alpha value;

$\frac{D_f}{d_{f15}} / \frac{D_f}{d_{f50}}$  is known, so if  $\ln\left(\frac{d_{f50}}{d_{b50}} \frac{\Delta_f}{\Delta_b} \frac{\Psi_{c,f}}{\Psi_{c,b}} \frac{1-\gamma V_{Gf}}{1-\gamma V_{Gb}}\right)$  is underestimated,

$\alpha_d$  is overestimated (the multiplication of the logarithmic part and the alpha value should result in the relative layer thickness).

The stability parameters for all the tests are determined with the dimensions of the materials and Figure 3-3.

Test	$\alpha_{d,1}$	$\alpha_{d,2}$		Test result	$\Delta_f/\Delta_b$	$(1-\gamma V_{Gf})/(1-\gamma V_{Gb})$
		$\Psi_{c,1}$ phase 1	$\Psi_{c,2}$ phase 6			
<b>M1012-T1</b> * <sup>1</sup>	2.17	2.09	2.16	$U_{b,c} > U_{f,c}$	1.12	0.90
<b>Lo1-Lo7</b> * <sup>2</sup>	2.07	1.80	1.97	$U_{b,c} > U_{f,c}$	1.09	1.04
<b>R460-T2</b> * <sup>1</sup>	1.75	1.70	1.75	$U_{b,c} < U_{f,c}$	?	?
<b>M633-d</b> * <sup>1,2</sup>	1.60	1.53	1.64	$U_{b,c} > U_{f,c}$	?	0.93
<b>M633-a2</b> * <sup>1</sup>	1.57	1.45	1.47	$U_{b,c} > U_{f,c}$	?	0.82
<b>M1012-T2</b> * <sup>1</sup>	1.30	1.26	1.30	$U_{b,c} \approx U_{f,c}$	1.12	0.90
<b>Q572-T5a,b,c</b>	1.02	0.98	1.02	$U_{b,c} > U_{f,c}$	?	1.01
<b>Lo8</b> * <sup>2</sup>	1.03	0.90	0.98	$U_{b,c} \approx U_{f,c}$	1.09	1.04
<b>Q572-T10</b> * <sup>1</sup>	0.95	0.93	0.97	$U_{b,c} \approx U_{f,c}$	?	0.92
<b>M1012-T3</b>	0.89	0.84	0.87	$U_{b,c} \approx U_{f,c}$	1.12	1.03
<b>R460-T1</b> * <sup>1</sup>	0.87	0.85	0.87	$U_{b,c} < U_{f,c}$	?	?
<b>Q572-T4</b>	0.85	0.82	0.85	$U_{b,c} > U_{f,c}$	?	0.98
<b>To7</b>	0.88	0.72	0.75	$U_{b,c} > U_{f,c}$	1.20	1.06
<b>M633-a3</b> * <sup>1</sup>	0.78	0.72	0.73	$U_{b,c} < U_{f,c}$	?	0.82
<b>To1</b>	0.81	0.66	0.71	$U_{b,c} > U_{f,c}$	1.00	1.05
<b>M633-g</b> * <sup>1</sup>	0.72	0.66	0.67	$U_{b,c} \approx U_{f,c}$	?	0.86
<b>To3</b>	0.62	0.53	0.56	$U_{b,c} \approx U_{f,c}$	1.00	1.07
<b>To6</b>	0.62	0.50	0.53	$U_{b,c} \approx U_{f,c}$	1.20	1.06
<b>Q572-T11</b>	0.55	0.52	0.54	$U_{b,c} \approx U_{f,c}$	?	1.05
<b>Q572-T6c</b>	0.54	0.45	0.46	$U_{b,c} \approx U_{f,c}$	?	1.00
<b>Q572-T2</b>	0.43	0.41	0.43	$U_{b,c} \approx U_{f,c}$	?	0.98
<b>Q572-T3</b>	0.43	0.41	0.43	$U_{b,c} \approx U_{f,c}$	?	0.98
<b>Q572-T6b</b>	0.47	0.38	0.40	$U_{b,c} \approx U_{f,c}$	?	1.42
<b>Q572-T9</b>	0.47	0.38	0.40	$U_{b,c} \approx U_{f,c}$	?	1.42
<b>Q572-T6a</b>	0.41	0.39	0.41	$U_{b,c} \approx U_{f,c}$	?	1.05
<b>Q572-T7</b>	0.41	0.39	0.41	$U_{b,c} < U_{f,c}$	?	1.05
<b>Q572-T1</b>	0.35	0.34	0.35	$U_{b,c} < U_{f,c}$	?	1.08
<b>To4</b>	0.33	0.27	0.27	$U_{b,c} \approx U_{f,c}$	1.07	1.05
<b>Q891-T2</b>	0.27	0.25	0.26	$U_{b,c} < U_{f,c}$	?	1.02
<b>Q891-T11</b>	0.27	0.25	0.26	$U_{b,c} < U_{f,c}$	?	1.02
<b>To2</b>	0.27	0.23	0.24	$U_{b,c} < U_{f,c}$	1.00	1.07
<b>Q891-T10</b>	0.24	0.21	0.23	$U_{b,c} < U_{f,c}$	?	1.08
<b>To5</b>	0.12	0.10	0.11	$U_{b,c} < U_{f,c}$	1.20	1.06

\*<sup>1</sup> Tests with wide graded filter material  
\*<sup>2</sup> Tests with an increased turbulent intensity  
? Unknown value, assumed to be 1.00

**Table 6-2 Alpha values (ranked from high to low) for all model tests, relative layer thickness:  $D_f/d_{f15}$**

Test	$\alpha_{d,3}$	$\alpha_{d,4}$		Test result	$\Delta_f/\Delta_b$	$(1-\gamma V_{Gf})/(1-\gamma V_{Gb})$
		$\Psi_{c,1}$ phase 1	$\Psi_{c,2}$ phase 6			
L01-L07*2	1.72	1.49	1.63	$U_{b,c} > U_{f,c}$	1.09	1.04
M1012-T1*1	1.34	1.29	1.34	$U_{b,c} > U_{f,c}$	1.12	0.90
M633-d*1,2	1.13	1.08	1.16	$U_{b,c} > U_{f,c}$	?	0.93
M633-a2*1	0.86	0.80	0.81	$U_{b,c} > U_{f,c}$	?	0.82
L08*2	0.86	0.75	0.82	$U_{b,c} \approx U_{f,c}$	1.09	1.04
M1012-T2*1	0.80	0.78	0.80	$U_{b,c} \approx U_{f,c}$	1.12	0.90
Q572-T5a,b,c	0.72	0.68	0.71	$U_{b,c} > U_{f,c}$	?	1.01
To7	0.79	0.64	0.67	$U_{b,c} > U_{f,c}$	1.20	1.06
M1012-T3	0.70	0.67	0.69	$U_{b,c} \approx U_{f,c}$	1.12	1.03
To1	0.70	0.57	0.61	$U_{b,c} > U_{f,c}$	1.00	1.05
R460-T2*1	0.59	0.58	0.59	$U_{b,c} < U_{f,c}$	?	?
Q572-T4	0.57	0.55	0.57	$U_{b,c} > U_{f,c}$	?	0.98
Q572-T10*1	0.56	0.55	0.57	$U_{b,c} \approx U_{f,c}$	?	0.92
To3	0.56	0.48	0.50	$U_{b,c} \approx U_{f,c}$	1.00	1.07
To6	0.55	0.45	0.47	$U_{b,c} \approx U_{f,c}$	1.20	1.06
M633-a3*1	0.43	0.40	0.40	$U_{b,c} < U_{f,c}$	?	0.82
M633-g*1	0.43	0.40	0.40	$U_{b,c} \approx U_{f,c}$	?	0.86
Q572-T11	0.41	0.39	0.41	$U_{b,c} \approx U_{f,c}$	?	1.05
Q572-T6c	0.40	0.34	0.35	$U_{b,c} \approx U_{f,c}$	?	1.00
Q572-T6b	0.35	0.28	0.30	$U_{b,c} \approx U_{f,c}$	?	1.42
Q572-T9	0.35	0.28	0.30	$U_{b,c} \approx U_{f,c}$	?	1.42
Q572-T6a	0.31	0.29	0.30	$U_{b,c} \approx U_{f,c}$	?	1.05
Q572-T7	0.31	0.29	0.30	$U_{b,c} < U_{f,c}$	?	1.05
R460-T1*1	0.30	0.29	0.30	$U_{b,c} < U_{f,c}$	?	?
Q572-T2	0.28	0.27	0.28	$U_{b,c} \approx U_{f,c}$	?	0.98
Q572-T3	0.28	0.27	0.28	$U_{b,c} \approx U_{f,c}$	?	0.98
Q572-T1	0.28	0.27	0.28	$U_{b,c} < U_{f,c}$	?	1.08
To4	0.29	0.24	0.25	$U_{b,c} \approx U_{f,c}$	1.07	1.05
To2	0.25	0.21	0.22	$U_{b,c} < U_{f,c}$	1.00	1.07
Q891-T2	0.21	0.19	0.20	$U_{b,c} < U_{f,c}$	?	1.02
Q891-T11	0.21	0.19	0.20	$U_{b,c} < U_{f,c}$	?	1.02
Q891-T10	0.21	0.18	0.19	$U_{b,c} < U_{f,c}$	?	1.08
To5	0.11	0.09	0.09	$U_{b,c} < U_{f,c}$	1.20	1.06

\*1 Tests with wide graded filter material  
\*2 Tests with an increased turbulent intensity  
? Unknown value, assumed to be 1.00

**Table 6-3 Alpha values (ranked from high to low) for all model tests, relative layer thickness:  $D_f/d_{f50}$**

### 6.1.3 DETERMINATION ALPHA VALUES, DETERMINISTIC APPROACH

For design purposes, the interest is in envelope curves bounding similar results (envelope curves are plotted in Figure 5-12 to Figure 5-15). Table 6-4 presents the alpha values for the envelope curves bounding the results. All the results beneath the lower boundary, are situations where base material eroded first (not desirable result). The upper boundary is a safe design value for  $\alpha_d$ .

Besides a lower and upper boundary a 90% boundary is determined, in this case the most extreme results are excluded. Especially for the equations where the relative layer thickness is related to  $d_{f15}$  the extreme values are wide spread. For a relative layer thickness related to  $d_{f50}$  the values are less spread, this can also be seen in Figure 6-1. Based on this observation it is better to use a relative

layer thickness related to  $d_{f50}$ . The reason for this wide spreading of alpha values can be found in the grading of the filter material used during the tests (explanation in paragraph 6.1.4).

		Lower boundary	90% lower	Upper boundary
$\alpha_{d,1}$	eq.[6.1]	0.33	1.03	1.75
$\alpha_{d,2}$	eq. [6.2]	0.27	0.98	1.75
$\alpha_{d,3}$	eq. [6.3]	0.28	0.70	0.86
$\alpha_{d,4}$	eq. [6.4]	0.24	0.69	0.82

**Table 6-4 Deterministic  $\alpha_d$  values**

Based on model tests of Klar [2005], where the damping of turbulent energy within a layer of granular material is measured, alpha values with a range from 0.85 to 1.35 are calculated (paragraph 3.2.6). These are alpha values for the design formula in which the relative layer thickness is related to  $d_{f15}$ . The 90% boundary of  $\alpha_{d,1}$  and  $\alpha_{d,2}$  is in accordance with the range based on the experiments of Klar [2005]. The upper boundary (Table 6-4), which is based on tests with wide graded filter material is out of the range. (Klar [2005] did not use wide graded filter material).

To be able to compare the alpha values based on the tests of Klar [2005] with  $\alpha_{d,3}$  and  $\alpha_{d,4}$ , the values have to be related to  $d_{f50}$ . For normal graded material the following relation can be used:  $d_{f50}/d_{f15} \approx 1.25$ . When relating the relative layer thickness to the median diameter, the alpha values based on the tests of Klar [2005] are ranged from 0.68 to 1.08. The design values for  $\alpha_{d,3}$  and  $\alpha_{d,4}$  (last two columns in Table 6-4) are in accordance with the alpha values calculated based on the tests of Klar [2005].

#### 6.1.4 WIDE GRADED MATERIAL

Especially the tests with wide graded filter material (indicated by a star (\*) in Table 6-2 and Table 6-3) are the cause of the wide spread calculated alpha values. When the relative layer thickness is related to  $d_{f15}$  the design thickness of the layer in the case of wide graded filter material becomes small in comparison with a similar normally graded material. By relating the relative layer thickness to  $d_{f15}$  the influence of the grading of the filter material becomes of huge importance. When the alpha values are calculated with a relative layer thickness related to  $d_{f50}$  (Table 6-3), the tests with wide graded filter material are more in line with the other tests.

This conclusion is based on a limited number of tests with wide graded filter material (tests from Bakker [1960], Haverhoek [1968], Wouters [1982] and Van Huijstee and Verheij [1991]). For a better substantiated conclusion more test with wide graded materials should be carried out.

The origin of the  $d_{f15}$  within the relative layer thickness is the damping length. The derivation of the design formula [3.13] is based on the damping of turbulent energy (the load) within the filter layer (step 2 of the derivation, paragraph 3.1.2). The damping of turbulent energy within a granular layer is related to the damping length ( $L_d$ ), equation [3.8]. Within the derivation the damping length is defined as:  $L_d = \alpha_d d_{f15}$ . The damping of turbulent energy is related to the size of the pores within the filter layer. The smaller particles of a

grading give a good approximation of the pore size. From this point of view it is logical to relate the damping length to the smaller particles ( $d_{f15}$ ).

Within the design formula the load is implicit taken into account by the median diameter of the filter material. Based on the load the required filter material is determined, resulting in a relation between filter and base material (this is the dominant relation within the logarithmic part of the equation). In this way the load indirectly determines the required relative layer thickness. If the relative layer thickness is related to  $d_{f15}$ , the grading is determining the absolute layer thickness ( $D_f$ ). This relation implicitly assumes that wide graded material requires smaller layer thicknesses. When an extreme is taken (extremely wide graded filter material) it can result in an extremely low required layer thickness (until nearly zero).

A problem with wide graded filter materials is the washing out of the small particles. The small particles cannot withstand the load conditions, so they will be washed out of the filter (especially in the top part of the filter layer). This results in larger pores than assumed during the design (the  $d_{f15}$  of the filter layer becomes larger because the smallest particles are washed away).

When the relative diameter is related to  $d_{f15}$  and a wide graded material is chosen instead of a normal graded material, it results in a drastically lower required layer thickness. Over time the small particles will be washed out of the filter layer, resulting in larger pores which results in less damping of turbulent energy. This can finally result in an insufficient layer thickness of the bed protection. When using the  $d_{f50}$  instead of the  $d_{f15}$ , this problem is covered. When the relative layer thickness is related to the  $d_{f50}$  it is also implicitly related to the load conditions.

### 6.1.5 INFLUENCE STABILITY PARAMETER

Breusers made a distinction between seven phases of transport (paragraph 3.2.4). The values of the stability parameters corresponding with the different phases of transport have been presented in Figure 3-3. During the analysis phase 1 and phase 6 are used to determine the stability parameters corresponding with the dimensions of the materials.

When e.g. the formula of Shields (equation [2.15]) is used to determine the required stones size, the influence of the chosen stability parameter is significant. When using the stability parameter corresponding with phase 6 ( $\psi_{c,f} = 0.055$ ) instead of phase 1 ( $\psi_{c,f} = 0.03$ ) it results in a 45% reduction of the required stone size.

The direct influence of the ratio of the stability parameters within the design formula for geometrically open filter structures is limited. Using stability parameters corresponding to phase 1 (for both base and filter material) (Figure 3-3) results in slightly thicker (safer) relative layer thickness (compared to phase 6). Using phase 1 instead of phase 6 results in an increase of the required relative layer thickness of only 4% (this percentage is the average difference based on the complete set of model tests).

The direct influence of the different phases that can be chosen for the stability parameters is limited. Indirectly the influence is significant, the

stability parameter has a significant influence on the design of the required stone diameter. The stone size has a direct influence on the ratio between the dimensions of the filter and base material resulting in different required relative layer thickness.

#### 6.1.6 DETERMINATION ALPHA VALUES, PROBABILISTIC APPROACH

With the use of the program Bestfit the distribution fitting the set of alpha-values is determined. The distribution fitting the alpha-values best is the log-normal distribution. This distribution (red lines) together with the set of alpha-values (blue bars) is plotted in Figure 6-1.

With Matlab the mean and variance of the distributions related to the set of alpha-values is determined. The mean and variance of the log-normal distributions of the alpha-parameter for the different representations of the design formula ([6.1] to [6.4]) are given in Table 6-5. In this table (as a comparison) also the mean and variance are given for the data-set represented as normal distributions. Comparing the variances of equation [6.1]/[6.2] with the variances of equation [6.3]/[6.4] it can be seen that the variances of the later two are smaller. This smaller variance is also clearly visible when comparing the top graphs with the bottom graphs in Figure 6-1. These figures indicate that the relative layer thickness is better represented when related to the  $d_{f50}$  (instead of the  $d_{f15}$ ). The spreading/variance is much smaller when the relative layer thickness is related to  $d_{f50}$ .

A complete set of properties of the log-normal distributions is given in Table 6-6.

The last column of Table 6-5 gives the mean alpha values of the relevant tests executed during this research. This average is based on three tests (test To3, To4 and To6). From a statistical point of view this average is not reliable. The mean values given in the last column (Table 6-5) are similar to the mean values of the complete dataset for  $\alpha_{d,3}$  and  $\alpha_{d,4}$ . For  $\alpha_{d,1}$  and  $\alpha_{d,2}$  the difference is larger.

The distribution of the alpha-factor can be used for probabilistic design.

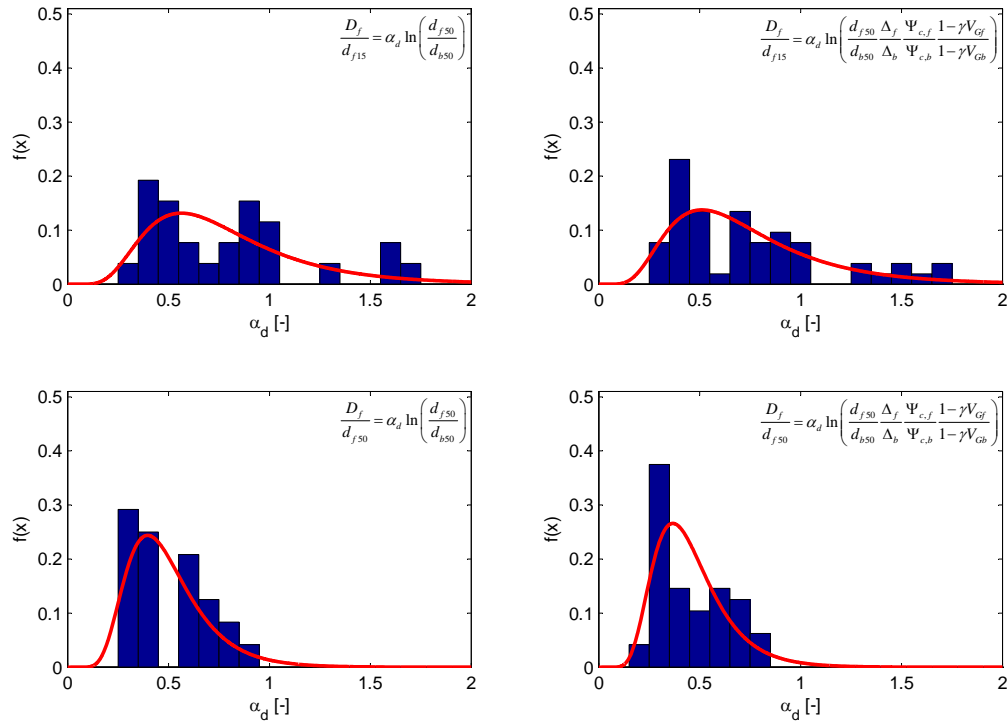


Figure 6-1 Distribution  $\alpha_d$  values (best-fit: log-normal distributions)

		Log-normal distribution		Normal distribution		Van de Sande [2012]
		$E(\alpha_d)$	$Var(\alpha_d)$	$E(\alpha_d)$	$Var(\alpha_d)$	$E(\alpha_d)$
$\alpha_{d,1}$	eq.[6.1]	0.80	0.17	0.80	0.16	0.52
$\alpha_{d,2}$	eq. [6.2]	0.75	0.16	0.75	0.16	0.44
$\alpha_{d,3}$	eq. [6.3]	0.50	0.04	0.50	0.04	0.47
$\alpha_{d,4}$	eq. [6.4]	0.46	0.03	0.46	0.04	0.40

Table 6-5 Distributions  $\alpha_d$  values

		Log-normal distribution			
		$E(\alpha_d)$	$Var(\alpha_d)$	$\mu$	$\sigma$
$\alpha_{d,1}$	eq.[6.1]	0.80	0.17	-0.34	0.48
$\alpha_{d,2}$	eq. [6.2]	0.75	0.16	-0.42	0.50
$\alpha_{d,3}$	eq. [6.3]	0.50	0.04	-0.78	0.38
$\alpha_{d,4}$	eq. [6.4]	0.46	0.03	-0.86	0.38

Table 6-6 Log-normal distributions  $\alpha_d$  values

## 6.2 EFFECT OF HIGHER TURBULENT INTENSITY

Turbulent fluctuations are a load condition. When the top-layer is designed properly by taking into account the turbulent fluctuations, the turbulence is indirectly included in the design of the filter layer thickness. E.g. when in a highly turbulent situation the turbulence level is included in the design of the top-layer, it results in a larger required stone diameter. Larger stones require a larger (relative) layer thickness, so indirectly the turbulent fluctuations are included in the design formula. Whether this increased layer thickness is enough to encounter the influence of the increased turbulence level is doubtful. Larger stones result in larger pores, which are easier to penetrate for eddies.

During test To6b and To6c situations with increased turbulent energy level were tested. In those situations winnowing was clearly visible. It was not

possible to attribute the transport of base material completely to the increased turbulence level but it is reasonable to assume that the turbulence level (and the penetration of eddies into the filter layer) have an influence on the stability of the base material/filter structure (e.g. a sill can be used to increase the level of turbulence).

Concluding, the turbulent fluctuations are partly implicitly included in the design formula by taking into account a properly designed top layer. Whether this is enough in the case of highly turbulent situations is doubtful. Additional research is needed to get better insight into the influence of turbulent fluctuations on the stability of geometrically open filter structures.

The turbulence level within the flow is related to the roughness, dimensions and shape of obstacles. In an open channel flow, the turbulent intensity is related to the roughness of the bed (and wall). In the case of piles, the turbulent motions are dominated by the dimensions and the shape of the pile. The dimension of the pile is normative for the dimension of the turbulent motions, while the shape influences the location of the detachment point.

### 6.2.1 DAMPING WITHIN THE FILTER LAYER

The design formula is based on damping of turbulent energy within the filter/granular layer (step 2 of the derivation of the design formula, paragraph 3.1.2).

No conclusions about the damping of turbulent motions within the filter layer could be drawn based on the pressure measurements (explanation in paragraph 5.3).

Van Os [1998] and Klar [2005] measured velocities within a granular layer. For both, the load was generated by a current parallel to the filter layer.

Van Os [1998] measured velocities within a granular structure with a Laser Doppler Anemometry (LDA). Based on his experiments he concluded that the reduction of flow velocity and velocity fluctuations (which are directly related to the turbulent motions) takes place in the first 1.5 times the nominal stone diameter thick layer of the filter.

Klar [2005] measured velocities within pores of a granular layer with an endoscope. According to data from Klar [2005], Figure 3-4, the damping of turbulent energy due to currents is effective until a layer with a dimension of 4 to 5 times the nominal stone diameter.

The difference between the thickness of the layer in which turbulent motions are damped when comparing the conclusion of Van Os [1998] with the conclusion based on the data of Klar [2005] cannot be explained. Additional measurements related to damping of flow and turbulent motions within granular layers can give better insights into the correctness of the thickness of the layer in which damping occurs.

Both the experiments of Van Os [1998] and Klar [2005] describe the damping logarithmically. The load is decreasing logarithmically until a certain threshold value. This threshold value is related to the dimensions of the pores within the filter layer.

Van Os described two types of turbulent eddies within the filter layer. Eddies with a low frequency (large eddies) and eddies with a high frequency (small eddies). The low frequency eddies are the eddies from the main flow penetrating into the filter layer. The high frequency eddies are small eddies which are a result of the detachment of the flow within the filter layer behind each stone. This last group of eddies is directly related to the dimensions of the pores. The low frequency eddies are damped within the filter layer logarithmically. When the low frequency eddies are damped completely, only the high frequency eddies remain.

Even though the load is damped to a certain layer thickness ( $1.5 d_{f50}$  according to Van Os [1998], 4 to 5  $d_{f50}$  according to test of Klar [2005]) a thicker filter layer results in less erosion of base material. This can be explained by the distance that a particle (base material) has to travel before it is through the filter layer. A thicker filter layer results in a longer distance a particle has to travel. Because fluctuations have short durations, it is possible that a particle comes in suspension but is not able to travel completely through the filter layer (when the load drops beneath the threshold of motion again the particle will settle).

The logarithmic damping of turbulent motions and the influence of the distance to travel for particles is confirming the logarithmic shape of the design formula. Up to a certain layer thickness, the load is damped logarithmically. Even thicker layers only result in a longer path to travel for a grain of base material.

In the case of a thin filter layer, an increased layer thickness will result in a reduction of the load on the base material and in an increased distance the particles (base material) have to travel (which can be compared with the steep part of the logarithm). When increasing the layer thickness of a thick filter layer, the load is not further reduced, only the damping length is increased (this can be compared with the rather flat part of the logarithm).

## 6.3 MULTIPLE LAYERED BED PROTECTIONS

To resist high load conditions large stones are required. A filter layer with large stones can require a rather thick layer thickness. From a cost perspective it can be more profitable to create a multiple layered geometrically open filter structure. Equation [3.13] is derived for single layered geometrically open filter structures only.

Equation [3.13] is based on the damping of the load in a granular layer. The load is reduced in the filter layer such that the layer beneath the top layer can resist the load. This principle can also be used for multiple layered filter structures (CUR, 2010).

The top layer is designed in such a way that the material can resist the load. A filter layer is chosen after which the required layer thickness for the top layer can be determined. The load has to be reduced such that the filter layer beneath the top layer is stable. The filter layer beneath the top layer is considered stable and represents the load condition at this location. Based on the ratio between the filter layer and the base material the required layer thickness of the filter layer is determined. This principle can be used for an endless number of layers. The layer thickness of each layer is determined based on the ratio between the

layer for which the required layer thickness is determined and the layer beneath this layer. This is repeated until the base layer is reached.

The principle of damping for multiple layered filter structures is schematized in Figure 6-2.

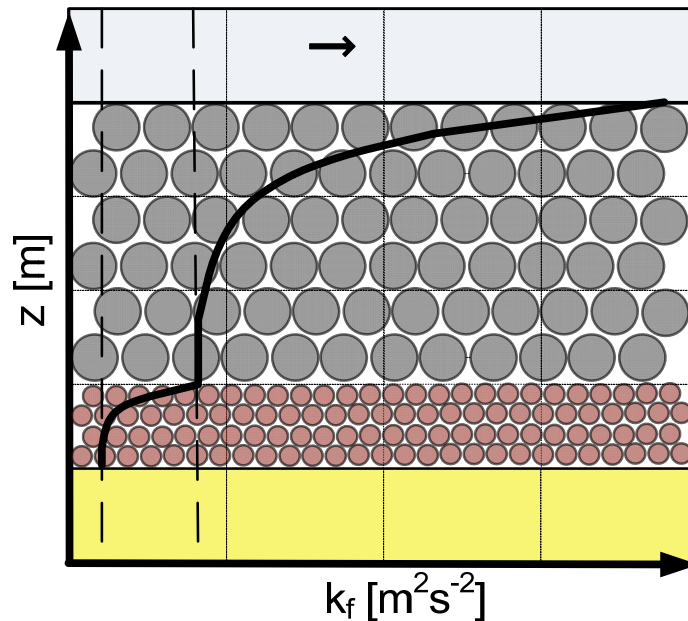


Figure 6-2 Damping in multiple layered geometrically open filter structures

## 6.4 JUSTIFICATION SIMPLIFICATIONS

Hoffmans [2012] and CUR [2010] derived simplified versions from their design formulas. These simplifications were based on the following assumptions;

$$\frac{\Delta_f}{\Delta_b} = 1 \qquad \frac{\Psi_{c,f}}{\Psi_{c,b}} = 1 \qquad \frac{1 - \gamma V_{Gf}}{1 - \gamma V_{Gb}} = 1$$

For different test series the values corresponding the mentioned ratios are calculated, the results are given in Table 6-7.

	Min. [-]	Mean [-]	Max. [-]	Based on
$\frac{\Delta_f}{\Delta_b}$	1.00	1.10	1.20	Van de Sande [2012], Haverhoek [1968], Van Velzen [2012]
$\frac{\Psi_{c,f}}{\Psi_{c,b}}$	1.00	1.41	2.00	Van de Sande [2012], Bakker [1960], Haverhoek [1968], Wouters [1982], Konter et al. [1990], Van Huijstee and Verheij [1991], Van Velzen [2012]
$\frac{1 - \gamma V_{Gf}}{1 - \gamma V_{Gb}}$	0.82	1.03	1.42	Van de Sande [2012], Bakker [1960], Haverhoek [1968], Konter et al. [1990], Van Huijstee and Verheij [1991], Van Velzen [2012]

Table 6-7 Relative density, stability parameter and shape factors.

The ratio relative density filter material to relative density base material is slightly larger than one. In general the density of stone/gravel is slightly larger than the density of sand, resulting in a ratio slightly larger than one.

For the ratio of the stability parameters an average value of 1,41 is found for the test given in the last column of Table 6-7. This value is in accordance with CUR [2010], where ratios of 1.3 to 1.5 are given as (most common) realistic ratios. The simplification of the ratio of stability parameters results in an underestimation of the required layer thickness.

For most tests the ratio between the shape parameters is almost equal to one. This simplification is justified when both materials are equally graded. When dealing with wide graded material the ratio becomes of importance and using the simplified version of formula [3.15] results in an under- or overestimation of the required layer thickness.

Determination of the average underestimation using the average values from Table 6-7:

$$\frac{D_f}{d_{f50}} = \alpha_d \ln \left( \frac{d_{f50}}{d_{b50}} \frac{\Delta_f}{\Delta_b} \frac{\Psi_{c,f}}{\Psi_{c,b}} \frac{1 - \gamma V_{Gf}}{1 - \gamma V_{Gb}} \right) \quad [6.7]$$

$$\frac{D_f}{d_{f50}} = \alpha_d \ln \left( \frac{d_{f50}}{d_{b50}} 1.10 \cdot 1.41 \cdot 1.03 \right) = \alpha_d \left( \ln \left( \frac{d_{f50}}{d_{b50}} \right) + \ln (1.60) \right)$$

Average underestimation of the required layer thickness:

$$D_f = \alpha_d \ln(1.60) \cdot d_{f50} = 0.47 \cdot \alpha_d d_{f50} \quad [6.8]$$

In the case of an  $\alpha_d$  parameter of 0.69 (explanation in paragraph 6.1), the average underestimation is approximately 1/3  $d_{f50}$ . This underestimation can also be seen as a shift in the values for  $\alpha_d$  in Table 6-1 (comparing column 2 with column 3 and 4 and column 5 with 6 and 7), Table 6-2 (comparing column 2 with column 3 and 4) and Table 6-3 (comparing column 2 with column 3 and 4).

A combination of the extremes (rather unrealistic), the maximum values for the different ratios given in Table 6-7 combined with  $\alpha_d = 0.82$  (Table 6-4), results in an underestimation of the required layer thickness of approximately 1  $d_{f50}$ .



# 7 DESIGN GUIDELINE

---

The design of a single layered geometrically open filter structure can be schematized in two steps;

- Firstly, determination of the required stone size that should be used for the top-layer;
- Secondly, determination of the layer-thickness of the filter/top-layer taking into account filter and base material characteristics.

## 7.1 DIMENSION TOP-LAYER MATERIAL

The top-layer should be stable and should be able to withstand the load.

The required stone diameter for flow conditions can be calculated with e.g. formulas based on Izbash [1930] or Shields [1936] (Schierreck, 2004). The design of a bottom protection loaded by a flow is described in paragraph 2.3. Two formulas to calculate the required stone diameter are the formulas of Shields (equation [7.1]) and Hoffmans (equation [7.2]):

$$d_{n50} = \frac{\bar{u}_c^2}{\Psi_c \Delta C^2} \quad [7.1]$$

$$d_{50} = 0.7 \frac{(r_0 \bar{u}_c)^2}{\Psi_c \Delta g} \quad [7.2]$$

## 7.2 REQUIRED LAYER-THICKNESS

With the formulas introduced in the previous paragraph the required stone diameter for a stable top-layer can be calculated. Based on this calculation the type of stones and the grading should be chosen.

Based on the parameters related to the chosen grading for the bed protection and the parameters related to the base material (the material to be protected) the layer thickness of the single layered geometrically open filter structure can be calculated with the following equation:

$$\frac{D_f}{d_{f50}} = \alpha_d \ln \left( \frac{d_{f50} \Delta_f \Psi_{c,f} (1 - \gamma V_{Gf})}{d_{b50} \Delta_b \Psi_{c,b} (1 - \gamma V_{Gb})} \right) \quad [7.3]$$

For  $\alpha_d$  in equation [7.3] the following values can be used;

- Deterministic approach:
  - $\alpha_d = 0.82$ , safe upper-limit;
  - $\alpha_d = 0.69$ , 90% confidence limit;
- Probabilistic approach; Log-normal distribution, with:
  - $\mu = -0.86$ ,  $\sigma = 0.38$ ;
  - $E(\alpha_d) = 0.46$ ;
  - $Var(\alpha_d) = 0.04$ .

When using a probabilistic approach one should use distributions for each of the parameters.

From a practical point of view one should never apply layers with a thickness less than two times the nominal diameter of the granular material.

### 7.3 INSUFFICIENT DATA

When making a (draft) design it might be that not all the properties of the materials are known. One should at least know the median diameter of the base and filter (i.e. top-layer) material to be able to calculate the required layer thickness.

The relative density of the filter material and the critical stability parameter are needed for calculating the required stone size (paragraph 7.1) and the required layer thickness (paragraph 7.2). When those parameters are unknown and assumptions are made, one should use the same assumptions for both, calculating the required stone size and calculating the required layer thickness.

When the density of the materials is unknown one can make an assumption. Table 3.2 of the Rock Manual (CIRIA, CUR, & CETMEF, 2007) gives a range of densities for the most commonly used types of rock. According to the Rock Manual (CIRIA, CUR, & CETMEF, 2007) the density of rock used in hydraulic engineering varies from 2300 kg/m<sup>3</sup> to 3600 kg/m<sup>3</sup>. In general rock is heavier than sand, resulting in a ratio ( $\Delta_f/\Delta_b$ ) slightly larger than one.

The stability parameters for the base and filter material can easily be determined with the median diameter of the material and Figure 7-1.

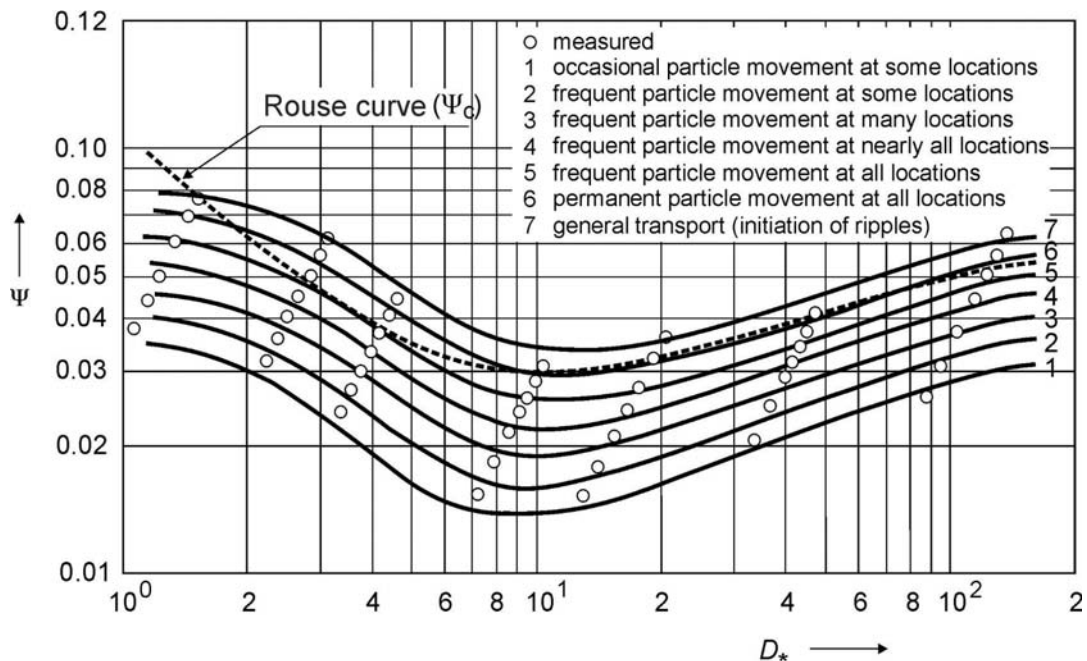


Figure 7-1 Stability parameter  $d^* = d_{50}(\Delta g/\nu^2)^{1/3}$  ( $\nu \approx 10^{-6} \text{ m}^2/\text{s}$ ) (CUR, 2010)

When the grading of the materials is unknown but both materials are approximately equally graded one can assume that the relation between the grading of filter and base material is approximately one

$\left(\frac{1-\gamma V_{Gf}}{1-\gamma V_{Gb}}\right) \approx 1$ ). This assumption should not be made when dealing with wide graded base or filter material.

When the densities and gradings of the materials are unknown and no reliable approximation can be made the following formula can be used:

$$\frac{D_f}{d_{f50}} = \alpha_d \ln \left( \beta \frac{d_{f50}}{d_{b50}} \frac{\Psi_{c,f}}{\Psi_{c,b}} \right) \quad [7.4]$$

In equation [7.4] the unknown densities and gradings are represented by the beta factor. The values for beta are based on the data from the model tests (Table 6-7):

$$E(\beta) = 1.13$$

$$Var(\beta) = 0.20$$

No safety factor is included within equation [7.4]. It is recommended to use a safety factor to take the uncertainties of the unknown parameters (which are represented by beta) into account. For deterministic calculations the following values for beta are proposed:

- $\beta = 1.39$ , 90% confidence limit (safety factor: 1.23);
- $\beta = 1.60$ , 99% confidence limit (safety factor: 1.42).

## 7.4 LIMITATIONS

According to Hoffmans [2012] the design formula is valid for current and wave loads. So far no tests have been performed that confirm the validity of the design formula in the case of waves. One is advised to use the formula only in situations loaded by currents.

There are still some uncertainties about the influence of turbulent motions on the stability of the base material beneath the filter layer. One should be careful when using the design formula for a situation with a high turbulence level (e.g. a protection loaded by a propulsion system (e.g. propeller or jet) of a vessel).

## 7.5 EXAMPLE

This paragraph gives a simple example for designing a bed protection. A geometrically closed and geometrically open filter structure are designed (using a deterministic approach) and compared.

For a canal with a width of 40 meter and a depth of 3 meter a bed protection has to be designed. The flow velocity in the canal is 2 m/s. The properties of the bed material (the material that has to be protected) are given in Table 7-1.

Several types of filter material are available for the project. The gradings of the different materials are given in Table 7-2. The different types of filter materials are based on existing gradings. The density of all the different types of filter materials is assumed to be the same,  $\rho = 2650 \text{ kg/m}^3$ .

Material	$d_{15}$ [mm]	$d_{50}$ [mm]	$d_{85}$ [mm]	$V_G$ [-]	$\rho$ [kg/m <sup>3</sup> ]
Base material	0.25	0.31	0.39	0.20	2630

Table 7-1 Properties bed material

Material	$d_{15}$ [mm]	$d_{50}$ [mm]	$d_{85}$ [mm]	$d_{n50}$ [mm]	$V_G$ [-]
Filter material 1	37.41	41.68	45.38	36.68	0.10
Filter material 2	22.45	25.01	27.23	22.01	0.10
Filter material 3	15.93	17.86	19.91	15.72	0.11
Filter material 4	10.70	12.80	14.98	11.26	0.16
Filter material 5	7.42	8.57	9.99	7.54	0.13
Filter material 6	5.19	6.50	7.81		0.20
Filter material 7	3.29	4.38	5.46		0.25
Filter material 8	2.11	3.00	3.89		0.30
Filter material 9	1.74	2.10	2.46		0.17
Filter material 10	1.21	1.50	1.89		0.19

Table 7-2 Available granular materials

### 7.5.1 DETERMINATION REQUIRED STONE DIAMETER

The first step in the design is the determination of the required stone diameter for the top layer. The formula of Shields will be used to determine the required stone size.

First the Chézy coefficient has to be determined. For the determination of the roughness of the bed it is assumed that filter material 1 will be used (Table 7-2).

$$C = 18 \log \left( \frac{12R}{k_r} \right) = 18 \log \left( \frac{12 \left( \frac{3 \cdot 40}{3 + 3 + 40} \right)}{2 \cdot 0.03668} \right) = 47.3 \quad (\text{with : } k_r = 2d_{n50}) \quad [7.5]$$

For the design of the bed protection we allow (almost) no transport of material, phase 1 in Figure 7-1. For the granular material phase 1 results in a stability parameter of 0.03. Determination of the required stone diameter:

$$d_{n50} = \frac{\bar{u}_c^2}{\Psi_c \Delta C^2} = \frac{2^2}{0.03 \cdot 1.65 \cdot 47.3^2} = 0.036 \text{ m} \quad [7.6]$$

Filter material 1 (Table 7-2) will be used as material for the top layer.

### 7.5.2 GEOMETRICALLY CLOSED FILTER STRUCTURE

According to the rules for geometrically closed filter structures the granular material required for the top layer cannot be placed directly on top of the base material, filter layers are required.

With the use of the rules for geometrically closed filter structures the filter layers can be determined.

$$\text{Stability: } \frac{d_{f15}}{d_{b85}} < 5 \quad \text{Int. Stability: } \frac{d_{60}}{d_{10}} < 10 \quad \text{Permeability: } \frac{d_{f15}}{d_{b15}} > 5$$

Bed protection using the principle of geometrically closed filter structures:

1. Top layer: filter material 1,  $d_{f50} = 41.68$  mm,  $D_f = 20$  cm
2. Filter layer: filter material 5,  $d_{f50} = 8.57$  mm,  $D_f = 20$  cm
3. Filter layer: filter material 10,  $d_{f50} = 1.50$  mm,  $D_f = 20$  cm
4. Base material:  $d_{b50} = 0.31$  mm

For granular layers a required layer thickness of at least two times the nominal diameter of the material is used. With a practical lower limit of 20 cm (regarding accuracy in construction).

### 7.5.3 GEOMETRICALLY OPEN FILTER STRUCTURE

With the use of paragraph 7.2 and the properties of base and filter material (determined in paragraph 7.5) the required filter layer thickness can be determined (the stability parameter is determined with Figure 7-1 (phase 1)):

$$\begin{aligned} \frac{D_f}{d_{f50}} &= \alpha_d \ln \left( \frac{d_{f50} \Delta_f \Psi_{c,f} (1 - \gamma V_{Gf})}{d_{b50} \Delta_b \Psi_{c,b} (1 - \gamma V_{Gb})} \right) \\ D_f &= \alpha_d d_{f50} \ln \left( \frac{d_{f50} \Delta_f \Psi_{c,f} (1 - \gamma V_{Gf})}{d_{b50} \Delta_b \Psi_{c,b} (1 - \gamma V_{Gb})} \right) \\ D_f &= 0.69 \cdot 0.04168 \cdot \ln \left( \frac{0.04168 \cdot 1.65 \cdot 0.03 \cdot (1 - 0.625 \cdot 0.10)}{0.00031 \cdot 1.63 \cdot 0.015 \cdot (1 - 0.625 \cdot 0.20)} \right) = 0.163 \text{ m} \end{aligned} \quad [7.7]$$

To give a comparison the similar calculation is made with the simplified representation of the design formula (when for example the grading was unknown this formula could be used):

$$\begin{aligned} \frac{D_f}{d_{f50}} &= \alpha_d \ln \left( \beta \frac{d_{f50} \Psi_{c,f}}{d_{b50} \Psi_{c,b}} \right) \\ D_f &= \alpha_d d_{f50} \ln \left( \beta \frac{d_{f50} \Psi_{c,f}}{d_{b50} \Psi_{c,b}} \right) \\ D_f &= 0.69 \cdot 0.04168 \cdot \ln \left( 1.39 \frac{0.04168 \cdot 0.03}{0.00031 \cdot 0.015} \right) = 0.170 \text{ m} \end{aligned} \quad [7.8]$$

Equation [7.7] and [7.8] give approximately the same result. For practical reasons the minimal layer thickness is 20 cm.

### 7.5.4 RESULTS

The different layers in the filter structure and the required layer thickness corresponding to a geometrically closed and a geometrically open filter structure are given in Table 7-3.

From a practical point of view it is hard to place granular layers with a small layer thickness (because of accuracy of placing). As a rule of thumb a layer

thickness of at least 20 cm is used. When multiple layers are required it results in rather thick filter structures.

In the case of geometrically open filter structures only one layer is required, which is more easy to construct. In this example the required total layer thickness is smaller for a geometrically open filter structure (this is not always the case).

	Geometrically closed filter structure		Geometrically open filter structure		
	$d_{50}$ [mm]	Theoretical $D_f$ [cm]	Practical $D_f$ [cm]	Theoretical $D_f$ [cm]	Practical $D_f$ [cm]
Top layer	41.68	9	20	17	20
Filter layer 1	8.57	2	20		
Filter layer 2	1.50	1	20		
Base layer	0.31				
<b>Total layer thickness</b>		<b>12</b>	<b>60</b>	<b>17</b>	<b>20</b>

Table 7-3 Results example

# 8 CONCLUSIONS AND RECOMMENDATIONS

---

The objective of this research as stated in the introduction:

*“Is the theoretically derived design formula for geometrically open filter structures (Hoffmans G. , 2012) in agreement with the test results for a situation where a single layered granular filter experiences a flow velocity parallel to the filter structure?”*

## 8.1 CONCLUSIONS

The model tests showed that the formula as proposed by Hoffmans [2012] (equation [8.1]) is in general valid for single layered geometrically open filter structures. His representation of the design formula is less suitable for wide graded filter materials.

$$\frac{D_f}{d_{f15}} = \alpha_d \ln \left( \frac{d_{f50}}{d_{b50}} \frac{\Delta_f}{\Delta_b} \frac{\Psi_{c,f}}{\Psi_{c,b}} \frac{1 - \gamma V_{Gf}}{1 - \gamma V_{Gb}} \right) \quad [8.1]$$

Two adjustments are proposed:

1. The relative layer thickness fits better with  $d_{f50}$  than with  $d_{f15}$
2. The alpha value proposed by Hoffmans [2012] is too high ( $\alpha_d=1.5$ )

New proposed design formula:

$$\frac{D_f}{d_{f50}} = \alpha_d \ln \left( \frac{d_{f50}}{d_{b50}} \frac{\Delta_f}{\Delta_b} \frac{\Psi_{c,f}}{\Psi_{c,b}} \frac{1 - \gamma V_{Gf}}{1 - \gamma V_{Gb}} \right) \quad [8.2]$$

With the following  $\alpha_d$  values;

- Deterministic approach;
  - $\alpha_d = 0.82$ , safe upper-limit
  - $\alpha_d = 0.69$ , 90% confidence bound
- Probabilistic approach; Log-normal distribution with;
  - $\mu = -0.86$ ;
  - $\sigma = 0.38$ ;
  - $E(\alpha_d) = 0.46$ ;
  - $Var(\alpha_d) = 0.04$ .

Limitations of the design formula (equation [8.2]);

- The formula has only been verified for flow conditions (currents);
- There are still some uncertainties about the damping of turbulent motions in the filter layer. One should be careful using the design

formula for situations with a high turbulence level (especially when dealing with extremes such as propulsion systems of vessels (propellers and jets)).

### 8.1.1 ANSWERS TO THE SUB-QUESTIONS

In the introduction four sub-questions were given. Each of the questions will be answered in this paragraph.

#### (1) What relevant tests were done in the past?

Research into previously performed model tests resulted in the following series of relevant researches;

- Bakker [1960]\*
- Haverhoek [1968]\*
- Wouters [1982]\*
- Wörman [1989]
- Konter et al. [1990]\*
- Van Huijstee and Verheij [1991]\*
- Dixen [2008]
- Van Velzen [2012]\*

The tests indicated with a star are used to create a larger data set and better substantiated conclusions.

#### (2) What are parameters of importance?

The determination of the relative layer thickness is based on a relation between the base and filter (i.e. top-layer) material. The ratios between the median diameters, densities, stability parameters and shape parameters of base and filter material are of importance.

The dominant ratio is the ratio between the dimensions of base and filter material.

Explanation of the different elements within the design formula:

- $d_{f50}$  The median sieve diameter of the filter material represents the load (the required dimensions of the filter material are determined with use of the load conditions);
- $\frac{\Delta_f}{\Delta_b} \frac{\Psi_{c,f}}{\Psi_{c,b}} \frac{1-\gamma V_{Gf}}{1-\gamma V_{Gb}}$  The ratios between the properties of the filter and base material translate the load which is related to the filter material to a load related to the base material (the properties of the filter material are used to determine the required nominal diameter of the filter material to withstand the load);
- $\frac{d_{f50}}{d_{b50}}$  The ratio between the median sieve diameters represents the difference in size. The size of the materials represents the resistance to the load. If the ratio is larger, the damping should be larger as well;

- $\alpha_d \ln(\dots)$       The load is damped logarithmically within the filter layer. The alpha value is a fitting parameter.

(3) *How is the flow velocity (load) related to the design formula?*

The load conditions are taken into account indirectly by means of the  $d_{f50}$  of the filter material (i.e. top layer). It is assumed that the top-layer has been designed properly.

The stability of the base layer is related to the damping of the load within the filter layer. During the derivation of the design formula it is assumed that velocities and turbulent motions are damped logarithmically within the filter layer. That velocity and turbulent motions are damped logarithmically is also shown by tests performed by Van Os [1998] and Klar [2005]. The damping is effective to a certain filter layer thickness. Thicker layers do not result in more effective damping of velocities and turbulent motions but they still increase the distance particles have to travel through the filter layer.

About the effective layer thickness for damping the load no clear conclusion can be drawn. Van Os [1998] reports that damping is effective up to a layer thickness of 1.5 times the nominal diameter of the filter material. Based on experiments of Klar [2005] the effective layer thickness for damping of turbulent energy is 4 to 5 times the nominal diameter of the filter material.

(4) *What is/are the value(s) of the coefficient  $\alpha_d$ ?*

Based on a large set of model tests (model tests performed during this research supplemented with older model tests (see answer sub-question 1)) the alpha values have been determined. The relevant alpha values for deterministic and probabilistic design purposes:

- Deterministic approach;  
 $\alpha_d = 0.82$ , safe upper-limit  
 $\alpha_d = 0.69$ , 90% confidence bound
- Probabilistic approach; Log-normal distribution with;  
 $\mu = -0.86$ ;  
 $\sigma = 0.38$ ;  
 $E(\alpha_d) = 0.46$ ;  
 $Var(\alpha_d) = 0.04$ .

The new alpha values are in accordance with the values calculated based on model tests of Klar [2005].

## 8.2 RECOMMENDATIONS

The recommendations are mainly focused on making the design formula applicable for a wider range of situations.

### 8.2.1 ADDITIONAL TESTS WITH WIDE GRADED MATERIAL

The adjustment to the design formula using a relative layer thickness related to  $d_{f50}$  instead of  $d_{f15}$  is based on a limited number of tests with wide graded material (tests performed by Bakker [1960], Haverhoek [1968], Wouters [1982] and Van Huijstee and Verheij [1991]).

To prove the use of  $d_{f50}$  instead of  $d_{f15}$  additional tests should be performed.

### 8.2.2 TURBULENCE

Test To6b and To6c showed the importance of turbulent motions on the transport of base material. No quantitative measurements were obtained during these tests and additional tests should be performed to get a better insight into the effect of turbulent motions on the stability of base material beneath a geometrically open granular filter. Additional test could prove the validity of the design formula for situations with an increased turbulence level. E.g. tests with a sill could be used to verify the validity of the design formula for turbulent situations (another source of turbulent motions that should be tested is a load generated by a propulsion system (propeller or jet) of a vessel).

### 8.2.3 WAVE LOAD

According to Hoffmans [2012] the design formula is also valid for wave loads. This research was focused on filter structures loaded by currents. Based on this research no conclusions can be drawn about the validity of the design formula for structures loaded by waves. Model tests should be used to prove or disprove the validity of the design formula for wave conditions.

Based on this research two adjustment are proposed (see paragraph 8.1). These adjustments are based on model tests were filter structures were loaded by currents. It is unknown whether these adjustments also apply in the case of waves.

### 8.2.4 PROTECTIONS ON A SLOPE

Additional tests should be performed to verify the validity of the design formula for protections on a slope. These tests could be combined with the tests for wave load conditions.

### 8.2.5 DAMPING

It is still unclear how velocity and turbulent motions are damped within a granular layer. According to Van Os [1998] the load is damped in a layer with a thickness of about 1.5 times the nominal diameter of the filter material. Based on the experiments of Klar [2005] the damping of turbulent energy (directly related to turbulent motions) occurs in a layer of 4 to 5 times the nominal diameter of the filter material.

To be able to add turbulent motions directly into the design formula, which may make the formula better applicable for highly turbulent situations,

additional research should be executed to get better insight into the penetration of the load (velocity and velocity fluctuations (turbulence)) into the filter.

Research into damping of velocity and turbulent motions into a granular layer can be combined with research into validity of the design formula for situations with a high turbulence level.

### 8.2.6 MULTIPLE LAYERED BED PROTECTIONS

When using the principle of geometrically open filters it can result in a large required layer thickness. From a practical/design point of view it could be interesting to use a geometrically open filter structure to protect the base material with on top a granular top-layer to withstand the load. Changing the design formula to a formula applicable for multiple layered geometrically open filter structures will be an useful improvement.

### 8.2.7 PRIORITY

Research into each of the topics mentioned in the recommendations increases the range of situations where the design formula is applicable.

One of the uncertainties which is of importance for the understanding of the effect of the influence of turbulent motions is the damping of velocity and turbulent fluctuations within the filter layer. Research into the effect of turbulent motions on the stability of base material can be tested with test situations with different levels of turbulent intensity. These tests can be combined with research into damping of turbulent fluctuations in granular layers.

When there is a better understanding of the influence of turbulent fluctuations and the damping of these fluctuations in a filter layer it can be used to improve the design formula and make it applicable for multiple layered filter structures.



# REFERENCES

---

- BAKKER, M.J. (1960), Onderzoek steenstortingen, Deel III, Uitspoeling van zand door een laag grind, *report M633, Waterbouwkundig Laboratorium*
- BATTJES, J.A. (2002), CT2100 Vloeistofmechanica, *Delft University of Technology*
- BOOIJ, R. (1998), Erosie onder een geometrisch open filter, *Delft University of Technology*.
- BOSBOOM, J. AND STIVE, M.J.F. (2011), Coastal Dynamics 1, *VSSD, Delft*
- BOSMA, C. (2001), Porositeit in breuksteenconstructies, *MSc. Delft University of Technology*
- CIRIA, CUR, CETMEF (2007), The Rock Manual, The use of rock in hydraulic engineering (2nd edition), *CIRIA, London*
- CUR (2010), CUR 233: Interface stability of granular filter structures, *Gouda*
- DE GUNST, M. (1999), Steenstabiliteit in een turbulente stroming achter een afstap, *MSc. Delft University of Technology*
- DEN ADEL, H., KOENDERS, M.A., & BAKKER, K.J. (1994), The analysis of relaxed criteria for erosion-control filters
- DETERT, M., WEITBRECHT, V., JIRKA, G.H. (2010, October), Laboratory Measurements on Turbulent Pressure Fluctuations in and above Gravel Beds, *Journal of hydraulic engineering*, 779-789.
- HAVERHOEK, F.J. (1968), Uitspoelen van zand door een laag van fosforslakken, *report M1012, Waterbouwkundig Laboratorium, Delft*
- HOAN, N.T. (2008), Stone Stability Under Non-uniform Flow, *PhD Delft University of Technology*
- HOAN, N.T., STIVE, M.J.F., BOOIJ, R., HOFLAND, B., VERHAGEN, H.J. (2007), Stone stability under non-uniform flow, *5th International Symposium on Environmental Hydraulics, Tempe*
- HOFFMANS, G.J.C.M. (2012), The Influence of Turbulence on Scour and Erosion, *Deltares Select Series, Delft*
- HOFFMANS, G.J.C.M., DEN ADEL, H., & VERHEIJ, H.J. (2008), Horizontal granular filters, *4th International Conference on Scour and Erosion, Tokyo*
- HOFLAND, B. (2005), Rock & Roll, Tubulence-induced damage to granular bed protections, *Febodruk b.v.*
- HUGHES, S.A. (1993), Physical Models and Laboratory Techniques in Coastal Engineering, *World Scientific Publishing Co. Pte. Ltd., Singapore*

- KIRONOTO, B.A AND GRAF, W.H. (1994, December), Turbulence characteristics in rough uniform open-channel flow, *Proc. Instn civ. Engrs Wat., Marit & Energy*
- KIRONOTO, B.A AND GRAF, W.H. (1995, December), Turbulence characteristics in rough non-uniform open-channel flow, *Proc. Instn civ. Engrs Wat., Marit & Energy*
- KLAR, M. (2005), Design of an endoscopic 3-D Particle-Tracking Velocimetry system and its application in flow measurements within a gravel layer, *PhD University of Heidelberg*
- KONTER, J.L.M., VERHELJ, H.J., DE JONG, R.J., BOUWMEESTER, J.H., VAN ZWOL, J. (1990), Haalbaarheid van de toepassing van niet-zanddichte bodemverdedigingen, report Q891, *Waterloopkundig laboratorium*
- LEIJENDECKERS, P.H.H., FORTUIN, J.B., VAN HERWIJNEN, F., SCHWIPPERT, G.A. (2005), Poly-Technisch Zakboek, Studenteditie, *Reed Business Information bv., Doetichem*
- NORTEK (2004), Vectrino velocimeter, User guide, *Nortek*
- NORTEK (2009), Vectrino velocimeter, User guide, *Nortek, Rud*
- OCKELOEN, W.J. (2007), Open filters in breakwaters with a sand core, *MSc. Delft University of Technology*
- PIETRZAK, J. (2010), Lecture notes CT5317: An Introduction to Oceanography for Civil and Offshore Engineers, *Delft University of Technology*
- SCHIERECK, G.J. (2004), Introduction to Bed, bank and shore protection, Delft University Press, Delft
- SCHIERECK, G.J. (2007), Concise overview of scale rules in coastal engineering, *Water Resources University, Hanoi*
- SCHOKKING, L.A. (2002), Bowthruster-induced Damage, *MSc. Delft University of Technology*
- SHIELDS, A. (1936), Anwendung der Aehnlichkeitsmechanik und der Turbulenzforschung auf die Geschiebebewegung, *Mitteilungen der Preußischen Versuchsanstalt für Wasserbau und Schiffbau, Berlin*
- SHIELDS, A. (1936), Application of Similarity Principles and Turbulence Research to Bed-load Movement, Translated by Ott, W.P. and Van Uchelen, J.C., *Mitteilungen der Preußischen Versuchsanstalt für Wasserbau und Schiffbau, Berlin*
- SUMER, B.M., COKGOR, S., & FREDSE, J. (2001, April), Suction Removal of Sediment from between Armor Blocks, *Journal of hydraulic engineering*, 293-306
- UELMAN, E.F. (2006), Geometrically Open Filters in Breakwaters, *MSc. Delft University of Technology*
- UIJTTEWAAL, W.S.J. (2011), Lecture notes CT5312: Turbulence in hydraulics, *Delft University of Technology*
- VAN BLAADEREN, E.A. (2006), Modelling bowthruster induced flow near a quay-wall, *MSc. Delft University of Technology*

- VAN DOORN, R. (2012), Bow Truster Currents at Open Quay Constructions on Piles, *MSc. Delft University of Technology*
- VAN HUIJSTEE, J.J.A. AND VERHEIJ, H.J. (1991), Verruiming ontwerpregels voor filters in bodemverdedigingen, *report Q572, Waterbouwkundig Laboratorium*
- VAN OS, P.P.A.M. (1998), Hydraulische belasting op een geometrisch open filterconstructie, *MSc. Delft University of Technology*
- VAN RIJN, L.C. (2011), Principles of Fluid Flow and Surface Waves in Rivers, Estuaries, Seas and Oceans, *Aqua Publications*
- VAN VELZEN, G. (2012), Flexible scour protection around circular piles, *MSc. Delft University of Technology*
- VERHEIJ, H.J., DEN ADEL, H., PETIT, H. (2000), Design formulas for granular filters, *report Q2629, WL | Delft Hydraulics*
- VERRUIJT, A. (2005), Grondmechanica, S. Van Baars (ed.), *VSSD, Delft*
- WATERBOUWKUNDIGE LABORATORIUM (1976), Inleiding fysisch modelonderzoek, *Waterbouwkundige laboratorium, Delft*
- WATERBOUWKUNDIGE LABORATORIUM (1998), Gedrag van een bodemverdedigingsrand bij een over- en langstreckende stroom, verslag modelonderzoek, *Waterbouwkundige laboratorium, Delft*
- WILCOCK, P.R. AND CROWE, J.C. (2003, February), Surface-based Transport Model for Mixed-Size Sediment, *Journal of Hydraulic Engineering*
- WOLTERS, G. (to be published), JIP Topfilter, *Deltares*
- WÖRMAN, A. (1989), Riprap protection without filters, *Journal of Hydraulic Engineering, 115 no.12*
- WOUTERS, J. (1982), Gedrag fosforslakken als bodembeschermingsmateriaal onder stroomaanval en verval, *report R460, Waterloopkundig laboratorium*

## PUBLICATIONS

---

- VERHEIJ, H.J., HOFFMANS, G., DORST, K., VAN DE SANDE, S.A.H. (2012), Interface stability of granular filter structures under currents, *6<sup>th</sup> International Conference on Scour and Erosion, Paris*



# APPENDICES

---



# A DATA PREVIOUS MODEL TESTS

---

The issue of geometrically open filter structures has been a topic of interest for a long time and several researchers have performed model tests to get better insight into the physics of geometrically open filter structures.

Previously performed model tests are taken into account for two reasons, firstly to be able to base conclusions and recommendations on a larger data set, secondly to give a complete overview of the research carried out so far.

The following series of model tests have been taken into account;

- Bakker [1960]
- Haverhoek [1968]
- Wouters [1982]
- Wörman [1989]
- Konter et al. [1990]
- Van Huijstee and Verheij [1991]
- Dixen [2008]
- Van Velzen [2012]

Each of the above mentioned test series will be explained briefly within the next paragraphs. Also the most important parameters of those tests will be given. But first some general assumptions will be explained.

## A.1 GENERAL ASSUMPTIONS

Not all the properties of importance for this research, of the used materials during the tests mentioned within this appendix, could be obtained.

When the right information could not be obtained from the reports of previous researches the following assumptions were made to determine the relative density and/or grading;

$$\frac{\Delta_f}{\Delta_b} = 1$$

$$\frac{1 - \gamma V_{Gf}}{1 - \gamma V_{Gb}} = 1$$

These assumptions are corresponding to the simplifications made by Hoffmans [2012] and CUR [2010], when they derived the simplified formulations from their design formulas (equations [3.13] and [3.14]).

The stability parameters for all the tests mentioned within this appendix are based on the dimensions of the materials and Figure 3-3.

## A.2 BAKKER [1960]

Bakker [1960] performed model tests in a three-meter-wide flume. The flume was split in two parts by a wooden plate (resulting in two, 1.5 m wide, flume sections). Within this flume several model tests were performed with different kinds of filter material. The properties of the base material (which is used for all the tests) are given in Table A-1 and those of the filter material in Table A-2.

Two different kinds of load conditions were used;

- Uniform flow conditions, flow parallel to the bed protection;
- Non-uniform flow conditions, a turbulent flow was created by placing a wooden bulkhead in the flume (the bulkhead blocked a part of the flow profile).

The situations were not all tested until base or filter material transport occurred and not for each test a conclusion could be drawn.

$d_{b15}$ [mm]	$d_{b50}$ [mm]	$d_{b85}$ [mm]
1.00	1.25	1.70

Table A-1 Base material used for all the tests (Bakker, 1960)

Test number	$D_f$ [mm]	$d_{f15}$ [mm]	$d_{f50}$ [mm]	$d_{f85}$ [mm]	High turbulence level	Conclusion
<b>M633-a1</b>	300	33	60	90	No	Not mentioned in the results*1
<b>M633-a2</b>	200	33	60	90	No	$U_{b,c} > U_{f,c}$
<b>M633-a3</b>	100	33	60	90	No	$U_{b,c} < U_{f,c}$
<b>M633-b</b>	200	33	60	90	Yes	No conclusion could be drawn
<b>M633-c1</b>	50	12	17	30	No	Base and filter material stable
<b>M633-c2</b>	30	12	17	30	No	Base and filter material stable
<b>M633-d</b>	50	12	17	30	Yes	Base and filter material stable $U_{b,c} > U_{f,c}$ *2
<b>M633-e</b>	100		Unknown		No	Base and filter material stable $U_{b,c} > U_{f,c}$ *2
<b>M633-f</b>	100		Unknown		Yes	Base and filter material stable $U_{b,c} > U_{f,c}$ *2
<b>M633-g</b>	150	50	83	128	No	$U_{b,c} \approx U_{f,c}$

\*1 It can be assumed that filter material was instable before base material became instable, this is based on the result of test M633-a2 were the filter layer was thinner and this result was obtained.  
\*2 Conclusions drawn were not directly seen during the tests.

Table A-2 Data model tests Bakker [1960], colours in the right column are corresponding to situations as explained in paragraph 4.1

## A.3 MODEL TESTS HAVERHOEK [1968]

In 1968, Haverhoek did research at WL Delft (currently Deltares) into erosion of base material that was covered with a layer of phosphorus slag.

Three tests were performed in a flume in laboratory “de Voorst”. The data of the model tests are given in Table A-3.

Test results:

- M1012-T1: Top layer started to erode first;
- M1012-T2: Simultaneous erosion of base and top material;
- M1012-T3: Simultaneous erosion of base and top material.

Test number	$D_f$ [mm]	$d_{b15}$ [mm]	$d_{b50}$ [mm]	$d_{b85}$ [mm]	$d_{f15}$ [mm]	$d_{f50}$ [mm]	$d_{f85}$ [mm]	$\rho_f$ [kg/m <sup>3</sup> ]
<b>M1012-T1</b>	250	0.105	0.140	0.180	21	34	54	2800
<b>M1012-T2</b>	150	0.105	0.140	0.180	21	34	54	2800
<b>M1012-T3</b>	150	0.150	0.140	0.180	30	38	60	2800

Table A-3 Data model tests Haverhoek [1968]

## A.4 WOUTERS [1982]

In 1982, Wouters, like Haverhoek [1968], did research at WL Delt (currently Deltares) into erosion of base material that was covered with a layer of phosphorus slag.

The conclusions given in Table A-4 are taken from Van Huijstee and Verheij [1991].

Test number	$D_f$ [mm]	$d_{b50}$ [mm]	$d_{f15}$ [mm]	$d_{f50}$ [mm]	Conclusion
<b>R460-T1</b>	100	0.135	19	56	$u_{b,c} < u_{f,c}$
<b>R460-T2</b>	200	0.135	19	56	$u_{b,c} < u_{f,c}$

Table A-4 Model tests Wouters [1982], colours in the right column are corresponding to the situations as explained in paragraph 4.1

## A.5 WÖRMAN [1989]

Bridge piles or in general piles influencing the flow, result in a more turbulent flow. The increase in turbulence intensity result in scour. Bed protections are commonly used to prevent the bed behind bridge piles from eroding. Wörman [1989] performed tests with geometrically open filter structures around bridge piles to create a design rule/formula to design protections around (bridge) piles.

The tests executed by Wörman are presented in Table A-5. Within his experiments Wörman did not make a distinction between simultaneous and non-simultaneous erosion of base and filter material. Because of the lack of this information no conclusions related to the validation of formula [3.13] can be made based on the model tests of Wörman.

Test number	$D_f$ [mm]	$d_{b50}$ [mm]	$d_{f15}$ [mm]	$d_{f50}$ [mm]
1	50	0.78	36	45
2	70	0.78	36	45
3	90	0.78	36	45
4	100	0.36	36	45
5	30	0.78	18	23
6	70	0.78	18	23
7	50	0.36	18	23
8	80	0.17	18	23
9	40	0.78	12.4	16
10	30	0.78	9	11.3
11	30	0.78	9	11.3
12	30	0.36	9	11.3
13	10	0.17	5.6	7.5
14	40	0.78	18	23
15	40	0.36	18	23
16	30	0.36	9	11.3

Table A-5 Model tests Wörman [1989](Wörman, 1989)

## A.6 KONTER ET AL. [1990]

Konter et al. [1990] tested geometrically open filter structures. Thirteen tests were performed. For all the tests the same base material was used, see Table A-6.

$d_{b15}$ [mm]	$d_{b50}$ [mm]	$d_{b85}$ [mm]
0.163	0.216	0.277

Table A-6 Base material used for all the tests (Konter et al., 1990)

The model tests can be split up in three categories;

- The first test (T0) was a test without bed protection. This test was performed to measure the development of erosion in an unprotected situation;
- Test T1, T2, T10, T11 and T12 were tests under uniform flow conditions;
- Test T3 till T9, were tests with a pile-construction detached to the wall.

The tests can be separated into tests with normal and test with increased levels of turbulent intensities. The pile-construction which was attached to the glass wall of the flume during tests T3 - T9 resulted in an increased level of turbulence.

Not all the results obtained by the measurements by Konter et al. [1990] could be translated into the three categories as mentioned in paragraph 4.1. For some tests no transport of base or filter material was measured and for some of the tests the right information was not available. The tests for which a conclusion could be drawn are given in Table A-7. Those conclusions are based on the conclusions drawn by Van Huijstee and Verheij [1991].

Test number	$D_f / d_{f50}$ [mm]	$d_{f15}$ [mm]	$d_{f50}$ [mm]	$d_{f85}$ [mm]	Pile	Conclusion
<b>Q891-T2</b>	1	18	23	30	No	$U_{b,c} < U_{f,c}$
<b>Q891-T10</b>	1	24	28	32	No	$U_{b,c} < U_{f,c}$
<b>Q891-T11</b>	1	18	23	30	No	$U_{b,c} < U_{f,c}$

**Table A-7 Model tests Konter et al. [1990], colours in the right column are corresponding to situations as explained in paragraph 4.1**

## A.7 VAN HUIJSTEE AND VERHEIJ [1991]

Van Huijstee and Verheij [1991] performed tests on geometrically open filter structures loaded with a flow parallel to the filter layer in the laboratory of the WL Delft (currently Deltares). The tests are very similar to the tests performed during this research.

Van Huijstee and Verheij [1991] observed the movement of base and filter material visually. Movement for both base and filter material was split up in four different categories. Those categories were based on the seven stages of transport defined by Breusers (see also paragraph 3.2.4).

The four phases used for the determination of movement of the filter material (Van Huijstee & Verheij, 1991);

1. No movement at all (stable);
2. Shaking stones, a single stone rolls;
3. Some stones are rolling;
4. Movement at all locations (unstable).

The four phases for the determination of horizontal movement of the base material (Van Huijstee & Verheij, 1991);

1. No movement at all (stable);
2. Small, “countable” number of grains are in motion, usually locally and not regularly;
3. Number of moving grains could not be counted anymore, no noticeable material transport;
4. Grains in motion, noticeable material transport (unstable).

The four phases for the determination of vertical movement of the base material (Van Huijstee & Verheij, 1991);

1. No movement at all (stable);
2. Occasionally a cloud of sand is transported through the filter layer;
3. Regularly a cloud of sand is transported through the filter layer;
4. Constant movement of sand through the filter layer. Clearly vertical movement/transport (unstable).

Based on the observations and the phases of transport as described above each test is classified as a situation with simultaneous or non-simultaneous erosion of base and filter material (categorized based on the three categories defined in paragraph 4.1). The tests performed by Van Huijstee and Verheij [1991] are given in Table A-8.

The density of the materials used by Van Huijstee and Verheij [1991] was not determined. They made the following assumption (which has also been adopted in this report):  $\Delta_f = \Delta_b = 1.65$

Test number	$D_f$ [mm]	$d_{b15}$ [mm]	$d_{b50}$ [mm]	$d_{b85}$ [mm]	$d_{f15}$ [mm]	$d_{f50}$ [mm]	$d_{f85}$ [mm]	Conclusion
Q572-T1	70	0.104	0.151	0.265	35	44	59	$U_{b,c} < U_{f,c}$
Q572-T2	45	0.104	0.151	0.265	20	30	48	$U_{b,c} \approx U_{f,c}$
Q572-T3	45	0.104	0.151	0.265	20	30	48	$U_{b,c} \approx U_{f,c}$
Q572-T4	90	0.104	0.151	0.265	20	30	48	$U_{b,c} > U_{f,c}$
Q572-T5a	30	0.104	0.151	0.265	7	10	15	$U_{b,c} > U_{f,c}$
Q572-T5b	30	0.104	0.151	0.265	7	10	15	$U_{b,c} > U_{f,c}$
Q572-T5c	30	0.104	0.151	0.265	7	10	15	$U_{b,c} > U_{f,c}$
Q572-T6a	30	0.104	0.151	0.265	15	20	28	$U_{b,c} \approx U_{f,c}$
Q572-T6b	30	0.100	0.285	0.650	15	20	28	$U_{b,c} \approx U_{f,c}$
Q572-T6c	30	0.360	0.480	0.565	15	20	28	$U_{b,c} \approx U_{f,c}$
Q572-T7	30	0.104	0.151	0.265	15	20	28	$U_{b,c} < U_{f,c}$
Q572-T8	100	0.104	0.151	0.265	7	10	15	*
Q572-T9	30	0.100	0.285	0.650	15	20	28	$U_{b,c} \approx U_{f,c}$
Q572-T10	45	0.104	0.151	0.265	10	17	33	$U_{b,c} \approx U_{f,c}$
Q572-T11	40	0.104	0.151	0.265	15	20	28	$U_{b,c} \approx U_{f,c}$

\* No observations were made during test Q572-T8

**Table A-8 Model tests Van Huijstee and Verheij [1991], colours in the right column are corresponding to situations as explained in paragraph 4.1**

In their report Van Huijstee and Verheij [1991] made a survey of previously performed model tests by “Waterloopkundig laborototium” (WL Delft, currently Deltares). The results of the following reports of model tests were added to the report by Van Huijstee and Verheij [1991];

- Bakker [1960]
- Haverhoek [1968]
- Wouters [1982]
- Konter et al. [1990]

All those tests have already been mentioned in previous paragraphs in this appendix.

## A.8 DIXEN [2008]

Like Van Huijstee and Verheij [1991] Dixen [2008] did research at geometrically open filter structures loaded by a uniform flow.

Dixen’s tests focused on thin filter layers. Most of the tests were with a filter layer thickness of only one time the nominal stone diameter. With the exception of test 151 and 154 (Table A-9), were filter layers of respectively two and three times the nominal stone diameter were used.

Test number	$D_f$ [mm]	$d_{b50}$ [mm]	$d_{f15}$ [mm]	$d_{f50}$ [mm]
66	100	0.147	100	100
S32	16	0.200	16	16
S34	25	0.200	25	25
S36	39	0.200	39	39
S39	100	0.200	100	100
151	77	0.147	39	39
154	116	0.147	39	39

**Table A-9 Model tests Dixen [2008]**

## A.9 MODEL TESTS VAN VELZEN [2012]

Van Velzen [2012] has done experimental research into flexible scour protection around cylindrical piles. The focus of her research was on edge failure (see Figure 2-1).

Eight different lay-outs were tested. For all the situations the same base and filter materials were used. The properties of the used materials are given in Table A-10. Variations in the lay-out were made in the following elements (Van Velzen, 2012);

- Extension of the protection;
- Thickness of the protection;
- Sill height.

As edge failure is outside the scope of this research, the variation in sill height and the extension of the protection is not of importance to this research.

$d_{b15}$ [mm]	$d_{b50}$ [mm]	$d_{b85}$ [mm]	$d_{f15}$ [mm]	$d_{f50}$ [mm]	$d_{f85}$ [mm]	$\Delta_b$ [-]	$\Delta_f$ [-]	$\Psi_{c,b}$ [-]	$\Psi_{c,f}$ [-]
0.139	0.180	0.243	11.2	13.5	15.7	1.65	1.65	0.05	0.03

**Table A-10 Material properties model tests Van Velzen [2012]**

Van Velzen’s research focused on edge failure, therefore the layer thickness of the protection was designed in such a way that no transport of base material from under the filter layer would occur. This resulted in a layer thickness of 100 mm. This layer thickness is used in the first seven lay-outs.

For lay-out LO8 a thinner layer of filter material was used. This resulted in a situation where winnowing could occur. During the test with lay-out LO8 winnowing occurred close to the pile at ray 1 and ray 2 (see Figure A-1). This is in front and at the side of the pile in an area with accelerating flow. Behind the pile, where the velocity is lower but the turbulent intensity is higher no winnowing was observed. Based on this observation one can conclude that the transport of base material is mainly related to the flow velocity.

Test number	$D_f$ [mm]
<b>L01 – L07</b>	100
<b>L08</b>	50

**Table A-11 Model tests Van Velzen [2012]**

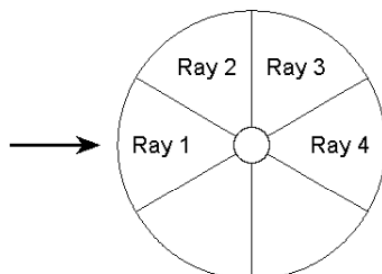


**Figure A-1 Sections as used within report Van Velzen [2012], the inner circle represents the pile, the outer circle the bed protection and the black arrow indicates the flow direction (Van Velzen, 2012)**

The following conclusions can be drawn from the model tests of Van Velzen [2012];

- Tests with lay-out L01-L07: Transport of filter material occurs before transport of base material occurs;
- Test with lay-out L08: Transport of filter and base material starts at approximately the same critical velocity.

## B MATERIAL PROPERTIES

Five different materials were used during the tests, two types of base material (sand) and three types of filter material (gravel). The properties and grading of each material are given in this appendix. Figure B-1 gives an overview of the sieve curves.

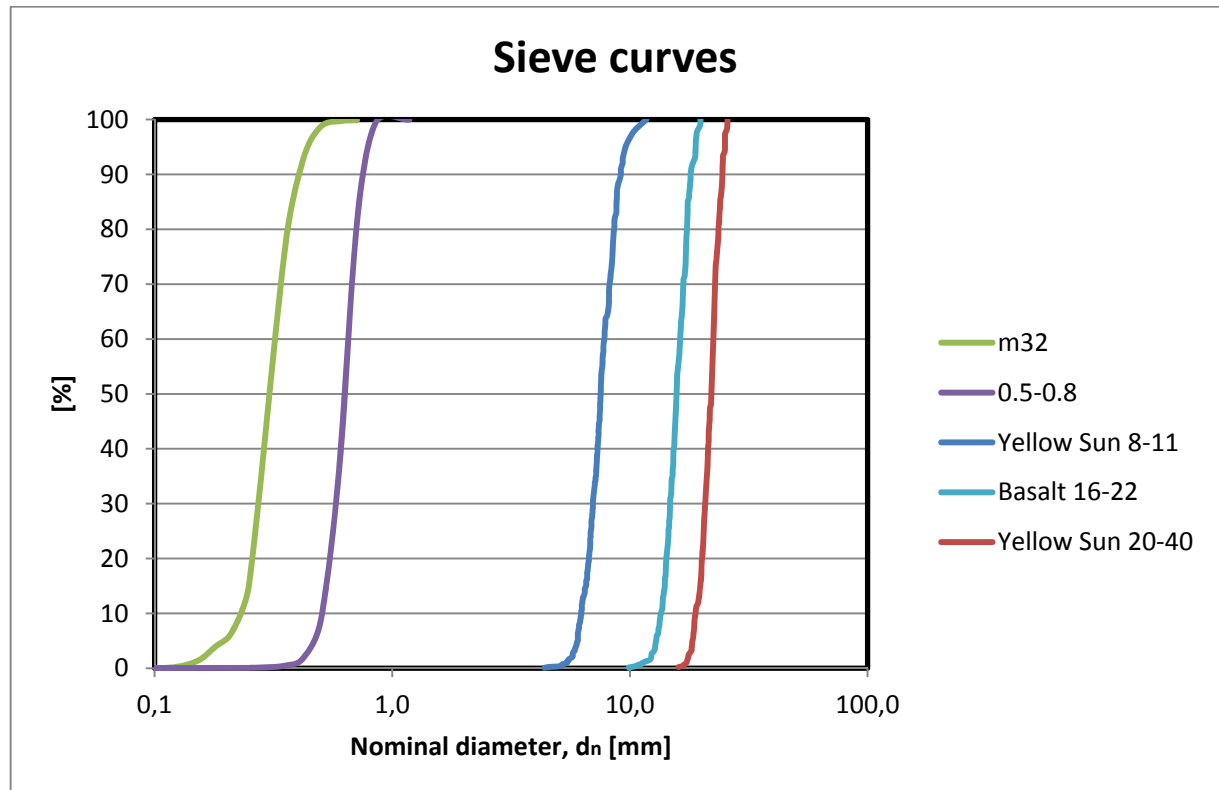


**Figure B-1 Sieve curves base and filter material**

### B.1 BASE MATERIAL

#### Dimensions of the base material

The sieve curves of the base material were determined in the lab using a series of sieves. The amount of sand that was collected by each sieve was weighed, resulting in a percentage of the material that is larger than the diameter of the openings in the sieve. The used sieves and the amount of sand collected in each sieve are given in Table B-1 (base material m32) and Table B-2 (base material 0.50-0.80).

Sieve [mm]	Amount of sand [gram]	Amount of sand [%]	Percentage larger than the sieve diameter [%]
<b>0.710</b>	1.39	0.1%	0.1%
<b>0.600</b>	1.58	0.2%	0.3%
<b>0.500</b>	10.07	1.0%	1.3%
<b>0.425</b>	54.59	5.4%	6.8%
<b>0.355</b>	160.64	16.0%	22.8%
<b>0.250</b>	618.16	61.7%	84.5%
<b>0.212</b>	88.28	8.8%	93.3%
<b>0.180</b>	27.57	2.8%	96.1%
<b>0.150</b>	26.69	2.7%	98.7%
<b>0.112</b>	11.94	1.2%	99.9%
<b>0</b>	0.82	0.1%	100.0%

Table B-1 Results sieving base material: M32

Sieve [mm]	Amount of sand [gram]	Amount of sand [%]	Percentage larger than the sieve diameter [%]
<b>1.180</b>	0.06	0.0%	0.0%
<b>0.850</b>	6.40	0.7%	0.7%
<b>0.710</b>	177.83	18.1%	18.7%
<b>0.600</b>	436.08	44.4%	63.1%
<b>0.500</b>	278.08	28.3%	91.4%
<b>0.425</b>	65.03	6.6%	98.0%
<b>0.355</b>	14.98	1.5%	99.5%
<b>0.250</b>	3.93	0.4%	99.9%
<b>0.212</b>	0.23	0.0%	100.0%
<b>0</b>	0.41	0.0%	100.0%

Table B-2 Results sieving base material: 0.50-0.80

#### Density of the base material

Besides the dimensions of the grains, the density of the material is determined. The determination of the density is done in two steps;

- Material is weighed dry;
- Relative weight is measured by weighing the same amount of sand under water.

The difference in weight is equal to the displaced amount of water. As the density of water is known, the volume of the sample can be determined with the difference in weight between the measurement of the dry sand and the underwater measurement.

The density of the sample can be determined by dividing the weight of the sample by the volume of the sample. This test was repeated three times for both types of base material, resulting in the densities given in Table B-3.

	Density M32 [kg/m <sup>3</sup> ]	Density 0.50-0.80 [kg/m <sup>3</sup> ]
Measurement 1	2631	2549
Measurement 2	2632	2594
Measurement 3	2626	2439
<b>Average</b>	<b>2630</b>	<b>2527</b>

**Table B-3 Density base material**

Based on the data of Table B-1, Table B-2 and Table B-3 the sieve curves (Figure B-1) and main properties of the base materials are determined (Table B-4).

Type	$d_{15}$ [ $\mu\text{m}$ ]	$d_{50}$ [ $\mu\text{m}$ ]	$d_{85}$ [ $\mu\text{m}$ ]	$\rho_b$ [kg/m <sup>3</sup> ]
<b>A<sub>b</sub></b> m32	248	309	389	2630
<b>B<sub>b</sub></b> 0.50-0.80	523	633	739	2527

**Table B-4 Main properties base material**

## B.2 FILTER MATERIAL

### Dimensions of the filter material

The nominal diameter of the filter material was determined by measuring the weight of 200 stones. Each stone was weighed individually. With the use of equation [B.1] the size of each stone is determined (where the size is represented as a side of a cube with a volume equivalent to the volume of the weighed stone).

$$d_n = \left( \frac{W}{\rho_f} \right)^{\frac{1}{3}} \quad [\text{B.1}]$$

With the 200 measurements a distribution of the dimensions was made, resulting in a sieve curve for each type of filter material. The nominal diameters are given in Table B-5.

The sieve diameters of the materials have been determined using the relation between nominal and sieve diameters prescribed by (CIRIA, CUR, & CETMEF, 2007);

$$d_n = F_s^{\frac{1}{3}} d \quad [\text{B.2}]$$

In formula [B.2]  $F_s$  is a conversion factor. According to the Rock Manual (CIRIA, CUR, & CETMEF, 2007) the conversion factor ( $F_s$ ) for model-scale armour materials used in the hydraulics laboratory ranges from 0.66 to 0.70. For the determination of the sieve diameters of the material used in the model tests performed within this research a conversion factor ( $F_s$ ) of 0.68 is assumed. This results in the following relation between the nominal diameter and the sieve diameter of the material;

$$d_n = 0.88 d \quad [\text{B.3}]$$

Type	$d_{15}$ [mm]	$d_{50}$ [mm]	$d_{85}$ [mm]	$d_{90}$ [mm]	$d_{n15}$ [mm]	$d_{n50}$ [mm]	$d_{n85}$ [mm]	$d_{n90}$ [mm]
<b>A<sub>f</sub></b> Yellow Sun 8-11	7.42	8.57	9.99	10.41	6.53	7.54	8.79	9.16
<b>B<sub>f</sub></b> Basalt 16-22	15.93	17.86	19.91	20.47	14.02	15.72	17.52	18.02
<b>C<sub>f</sub></b> Yellow Sun 20-40	22.45	25.01	27.23	27.83	19.75	22.01	23.96	24.49

Table B-5 Dimensions filter material

Density of the filter material

The density of the filter material is determined in the same way as the density of the base materials. Grading A<sub>f</sub> and C<sub>f</sub> (Table B-5) are the same type of material (both Yellow Sun) and have logically the same density.

The density of the Yellow Sun is based on 15 measurements and the density of the Basalt is based on 10 measurements. The measurements are given in Table B-6.

	Density Yellow Sun [kg/m <sup>3</sup> ]	Density Basalt [kg/m <sup>3</sup> ]
Measurement 1	2687	2974
Measurement 2	2612	2963
Measurement 3	2595	2964
Measurement 4	2660	2962
Measurement 5	2628	2966
Measurement 6	2640	2974
Measurement 7	2595	2971
Measurement 8	2613	2945
Measurement 9	2651	2946
Measurement 10	2666	2937
Measurement 11	2647	
Measurement 12	2587	
Measurement 13	2611	
Measurement 14	2652	
Measurement 15	2656	
<b>Average</b>	<b>2633</b>	<b>2960</b>

Table B-6 Density filter material

Porosity of the filter layers

One could imagine that winnowing is related to the dimensions of the pores and the amount of pores within the filter layer. The percentage of pores is determined for each situation executed with slabs of filter material (filter material glued together with elastocast).

Each slab of filter material was weighed. The weight ( $W$ ) is used to calculate the volume of stones. Because the dimensions, and with this, the volume ( $I$ ) of each slab is known, the percentage of the volume that is filled with stones can be determined. When the percentage of stones is known, the percentage of pores is also known.

$$n = 1 - \frac{W}{\rho_f \cdot I}$$

[B.4]

The volume of a slab is given by:

$$I = D_f \cdot b \cdot l - \text{correction} \quad [\text{B.5}]$$

For the volume a correction has to be applied to take the contact with the walls into account. Bosma [2001] gives the following relation for a correction of the volume in case of calculating the porosity for a granular filter against a wall:

$$\text{correction} = A \cdot K \cdot d_{85} \quad [\text{B.6}]$$

Where  $A$  is the contact area with the wall. As the slabs were made in moulds, the sidewalls, bottom and top surfaces can be seen as contact area of filter layer and wall.

With the corrected volume of a slab and its weight the porosity is determined.

For each test, four slabs of filter material were used. The average percentage of pores for each set of four slabs of filter material is given in Table B-7.

	n [-]
Yellow Sun 8-11 $D_f = 20 \text{ mm}$	0.43
Basalt 16-22 $D_f = 40 \text{ mm}$	0.38
Basalt 16-22 $D_f = 57 \text{ mm}$	0.40
Yellow Sun 20-40 $D_f = 27 \text{ mm}$	0.31
Yellow Sun 20-40 $D_f = 61.5 \text{ mm}$	0.32

**Table B-7 Pores, filter layer**



## C DIMENSIONS ELASTOCOAST SLABS

Figure C-1 gives a schematic representation of a slab lifted. The slab is lifted at both ends. The slab bends because of its own weight.

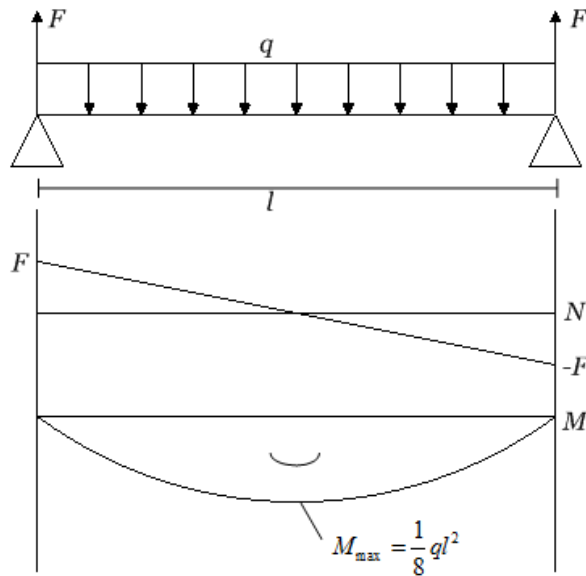


**Figure C-1 Schematic representation of a lifted slab of filter material**

The tensile strength within the material can be given by:

$$\sigma_s = \frac{M}{W} \quad [\text{C.1}]$$

$M$  = moment [Nm]

$W$  = modulus [ $m^3$ ]

The maximum moment:

$$M = \frac{1}{8} q l^2 \quad [\text{C.2}]$$

Where the distributed load is the own weight of the slab of filter material:

$$q = b_f D_f (1-n) \rho_s g \quad [\text{C.3}]$$

The slab can be schematised as a beam with holes. The modulus for this beam is given by (Leijendeckers et al., 2005):

$$W = \frac{b_f D_f^3 - n b_f (n D_f)^3}{6 D_f} = \frac{1}{6} (1-n^4) b_f D_f^2 \quad [\text{C.4}]$$

The maximum length of the slab (whereby a safety factor of 1.5 is taken into account for the distributed load) can be given by:

$$\sigma_s = \frac{M}{W} = \frac{\frac{1}{8} 1.5 b_f D_f (1-n) \rho_s g l^2}{\frac{1}{6} (1-n^4) b_f D_f^2} = \frac{9 (1-n) \rho_s g l^2}{8 (1-n^4) D_f} \Rightarrow l_{\max} = \sqrt{\frac{8 (1-n^4) D_f}{9 (1-n) \rho_s g} \sigma_s} \quad [\text{C.5}]$$

The tensile strength of stones (CIRIA, CUR, & CETMEF, 2007):

$$\sigma_s = 2 \cdot 10^6 \text{ N/m}^2$$

The normative material parameters for Yellow Sun are;

$$\rho_s = 2633 \text{ kg/m}^3$$

$$n = 0.31$$

For the Basalt stones, the normative material parameters are;

$$\rho_s = 2960 \text{ kg/m}^3$$

$$n = 0.38$$

The maximum lengths of the slabs of filter material are given in Table C-1.

$D_f$ [cm]	$l_{\max}$ (Yellow Sun) [cm]	$l_{\max}$ (Basalt) [cm]
2.0	141	139
3.0	172	170
10.0	314	311

**Table C-1 Maximum length filter material slabs**

# D VELOCITY METERS

This appendix is divided in two parts, the first part explains generally the different types of velocity meters. The second part gives more details about the used velocity meter, the Acoustic Doppler Velocimeter.

## D.1 TYPES OF VELOCITY METERS

Four frequently used types of measurement equipment will be introduced briefly. All four types of equipment are single point measurement systems. Single point means that the velocity is measured at a single point. These type of measurements give no information about the instantaneous flow field. By measuring at many different positions the mean flow field and its statistics can be obtained.

The four types which will be introduced briefly (the most important properties are given in Table D-1):

- Pitot tube;
- Electromagnet flow meter (EMS);
- Acoustic Doppler Velocimeter (ADV);
- Laser Doppler Anemometry (LDA).

Type	Measuring method	Fine particles needed?	Sampling rate [Hz]	Probing volume [m <sup>3</sup> ]
Pitot tube	Pressure difference	No		
Electromagnetic flow meter (EMS)	Potential difference	No	10	~10 <sup>-5</sup>
Acoustic Doppler Velocimeter (ADV)	Sound, Doppler shift	Yes	25	~10 <sup>-7</sup>
Laser Doppler Anemometry (LDA)	Light, Doppler shift	Yes		~10 <sup>-9</sup>

**Table D-1 Velocity meters**

### Pitot tube

The Pitot tube is based on the Bernoulli equation. The Bernoulli equation consist of a piezometric head and a velocity height.

A Pitot tube has two water intakes, an impact tube (opening in the direction of the flow) and a static tube (opening perpendicular to the flow direction). Since both tubes are located at the same position, the equality of Bernoulli states that the measured pressure difference is equal to the velocity height. So the velocity can be obtained from this pressure difference:

$$p_t - p_s = \frac{1}{2} \rho_w u^2 \quad [\text{D.1}]$$

Where  $p_t$  is the pressure measured with the tube in the flow direction and  $p_s$  is the pressure measured with the static tube.

The Pitot tube can be used to determine the main flow velocity. It is not possible to determine the turbulent properties of the flow with this type of instrument.

#### Electromagnetic flow meter (EMS)

The EMS measures velocities based on a potential difference. The technique is based on the induction law of Faraday. The law states that a charge moving in a magnetic field will create a potential difference which is proportional to the velocity of the charge carried by the flow (Uijtewaal, 2011).

The signal is obtained from the volume directly underneath the probe (where the electrodes are mounted). The probe gives a small disturbance of the flow. With a proper calibration the electrodes allow to measure with a frequency of maximal 10 Hz (Uijtewaal, 2011).

#### Acoustic Doppler Velocimeter (ADV)

The ADV measures velocities based on a Doppler shift of an acoustic signal. The acoustic signal is reflected by particles in the water. The water motion causes a Doppler shift in the ultrasound frequency proportional to the velocity (Uijtewaal, 2011). From the received signal, the instantaneous velocity is determined.

The frequency of the ADV is high enough to measure turbulent motions in the flow.

Because the measurement volume is located a certain distance from the probe, the influence of the probe is limited.

#### Laser Doppler Anemometry (LDA)

Just like the ADV the LDA uses the Doppler shift to measure the velocity. Lasers and receivers are used to determine the velocity. The lasers are placed at one side of the glass flume wall and the receivers on the other side of the flume (positioning is extremely important and has to be done very accurately). The point where the laser beams cross is the measuring point (at least two beams are required, more when velocities in more directions are wanted). The crossing of the beams results in an interference pattern. Particles passing through the sampling volume will result in a Doppler shift of the scattered light, from this the velocity is obtained (Uijtewaal, 2011).

Since placing an LDA is an extremely accurate work it is not easy to measure at multiple locations.

## D.2 ACOUSTIC DOPPLER VELOCIMETER

The ADV measures the flow velocity of the fluid based on the velocity of the particles it transports. The instrument emits a sonic pulse. This pulse reflects on a particle in the sampling volume (Figure D-1). The reflected sonic wave is received by the sensors (sensors are located at the end of the legs, Figure D-1). The reflected signal has a Doppler-shift that determines the velocity. By receiving the signal on different locations, the velocity in different directions can be measured. The ADV measures velocities in three dimensions (x, y and z

direction). The ADV is generally placed in such a way that the x-direction is the direction of the flow.

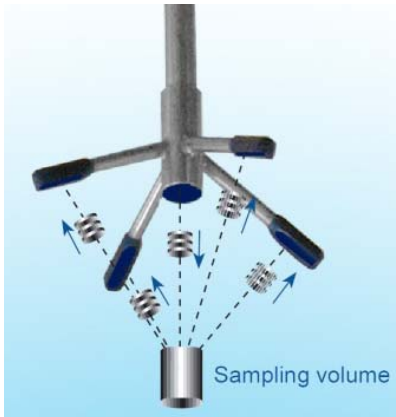


**Figure D-1 Measuring, Vectrino (ADV) (Nortek, 2009)**

### Doppler shift

The Doppler shift is the change in frequency of a wave (or other periodic event) for an observer moving relative to its source. It is commonly heard when a vehicle sounding a siren approaches, passes, and recedes from an observer. The received frequency is higher (compared to the emitted frequency) during the approach, it is identical at the instant of passing by, and it is lower during the recession (Wikipedia).

The relative changes in frequency can be explained as follows. When the source of the waves is moving toward the observer, each successive wave crest is emitted from a position closer to the observer than the previous wave. Therefore each wave takes slightly less time to reach the observer than the previous wave. Therefore the time between the arrival of successive wave crests at the observer is reduced, causing an increase in the frequency. While they are travelling, the distance between successive wave fronts is reduced. Conversely, if the source of waves is moving away from the observer, each wave is emitted from a position farther from the observer than the previous wave, so the arrival time between successive waves is increased, reducing the frequency. The distance between successive wave fronts is increased, so the waves spread out (Wikipedia).

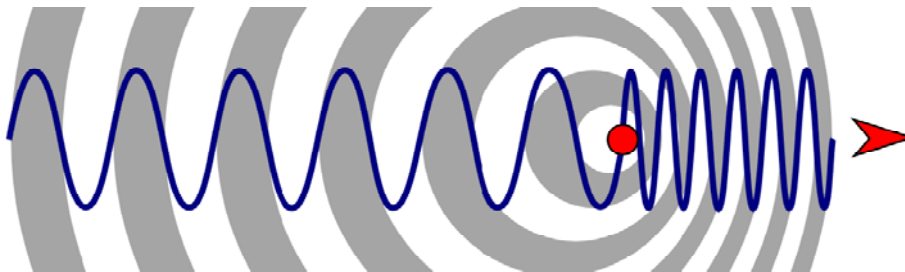


**Figure D-2 Doppler shift (Wikipedia)**

### Particles

As stated earlier, the instrument needs particles to be able to measure a velocity. The particles in the fluid reflect the sound pulse needed for measuring. The type of material is unimportant, as long as it is capable of producing an

echo of the sound pulse. It is possible to use sediment, microorganisms and bubbles as seeding material (Van Blaaderen, 2006).

The ADV does not measure directly the velocity of the flow but measures the velocity of the particles suspended in the flow. It is assumed that the particles have the same velocity as the fluid. When particles have a relative velocity to the flow, due to sinking or buoyancy, this assumption is not longer true and the measurements are not usable. The particles should not be too heavy (sinking) or light (buoyancy), they should be in suspension.

For the measurements during this research Kaolinite (also known as Chinese Clay) is used. This is very fine material:  $d_{50} = 2 \sim 3 \mu\text{m}$ . This very fine material is even suspended in the flow during very low velocities. During the measurement Kaolinite is added continuously to the water at the beginning of the flume.

The amount of Kaolinite that had to be added to the water per unit of time was based on test measurements. One of the outputs of the ADV meter is the number of reflections measured. According to the manufacturer this number should be at least 70 to produce a reliable measurement (Nortek, 2004). The amount of Kaolinite added to the flow was adjusted to an amount that results in reliable measurements.

#### ADV with sideward looking probe

The Environmental Fluid Mechanic Laboratory at Delft University of Technology has two ADV's, an ADV with a downward looking probe (Figure D-1) and one with a sideward looking probe (Figure D-3). During the research the ADV with the sideward looking probe was used. The reason for using the ADV with the sideward looking probe instead of the ADV with the downward looking probe can be found in the measurements close to the bed. If the ADV with the downward looking probe would be used, the ADV could receive acoustic waves reflected by the bed. This results in a lot of noise on the measuring signal. When the ADV with the sideward looking probe is used the influence of the bed is much smaller.

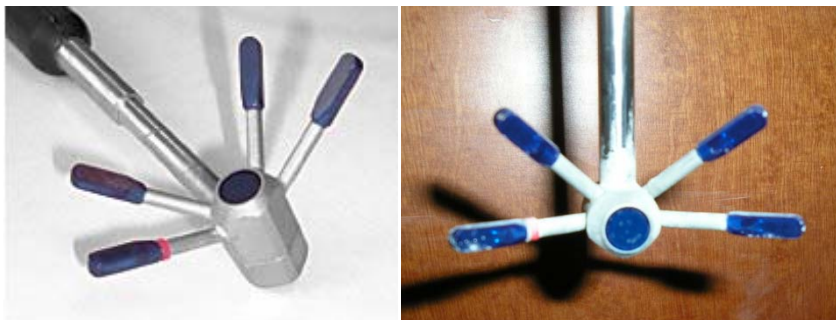


**Figure D-3 Sideward looking ADV (left picture (Nortek, 2009))**

#### Settings

The settings used during the measurements are presented in Table D-2.

For the sampling rate the maximum frequency is used. High frequencies make it possible to measure turbulent fluctuations in the flow.

An important setting is the nominal velocity range. The nominal velocity range is used by the program of the ADV to filter out unreliable data. The receivers receive reflected signals, this include reflections from inside and outside the measuring volume. The reflections obtained from outside the measuring volume are resulting in strange values. By indicating a nominal velocity range the program filters out values that are out of the scope of the nominal velocity. For the setting of the nominal velocity a couple of pre-set values can be used (available setting;  $\pm 0.01$  m/s,  $\pm 0.1$  m/s,  $\pm 0.3$  m/s,  $\pm 1$  m/s,  $\pm 2$  m/s,  $\pm 4$  m/s). Which setting was used was determined for each measurement. The setting was chosen in such a way that it was approximately the average velocity of the flow (local).

The other settings:

- Transmit length: pulse length;
- Sampling volume: the sampling volume has the shape of a cylinder, the height of the cylinder can be set;
- Power level: strength of the signal (decibel);
- Coordinate system: XYZ, where x was negative in the direction of the flow.

Sampling rate	25 Hz	
Nominal velocity range*	0.30 m/s	1.00 m/s
Transmit length	2.4 mm	
Sampling vol.	9.1 mm	
Power level	HIGH	
Coordinate system	XYZ	
<i>* The setting of the nominal velocity is based on the velocity of the test situation</i>		

**Table D-2 Used settings, Vectrino (ADV)**

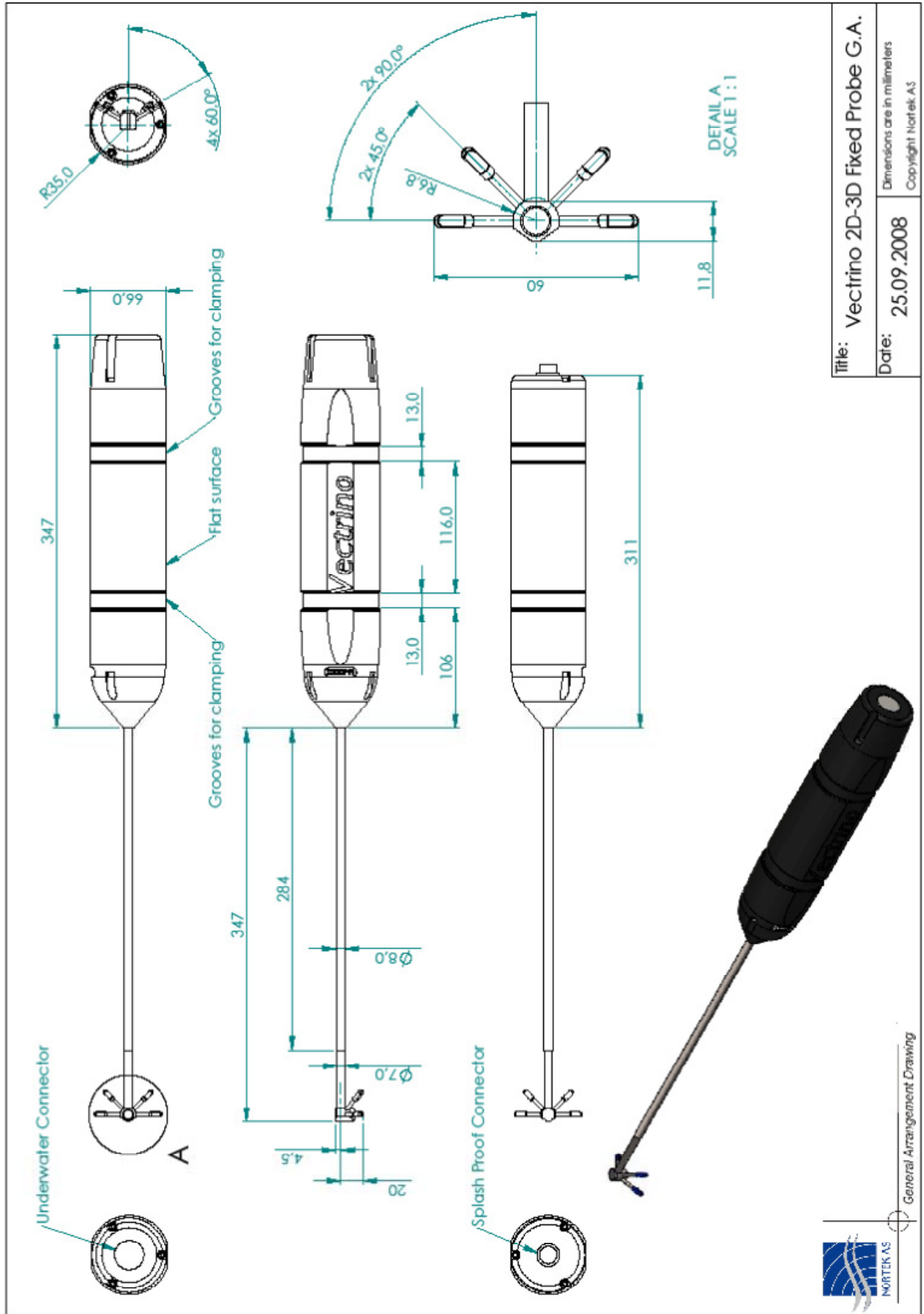


Figure D-4 Detailed drawing of the Vectrino (Nortek, 2009)

# E TEST FACILITY

---



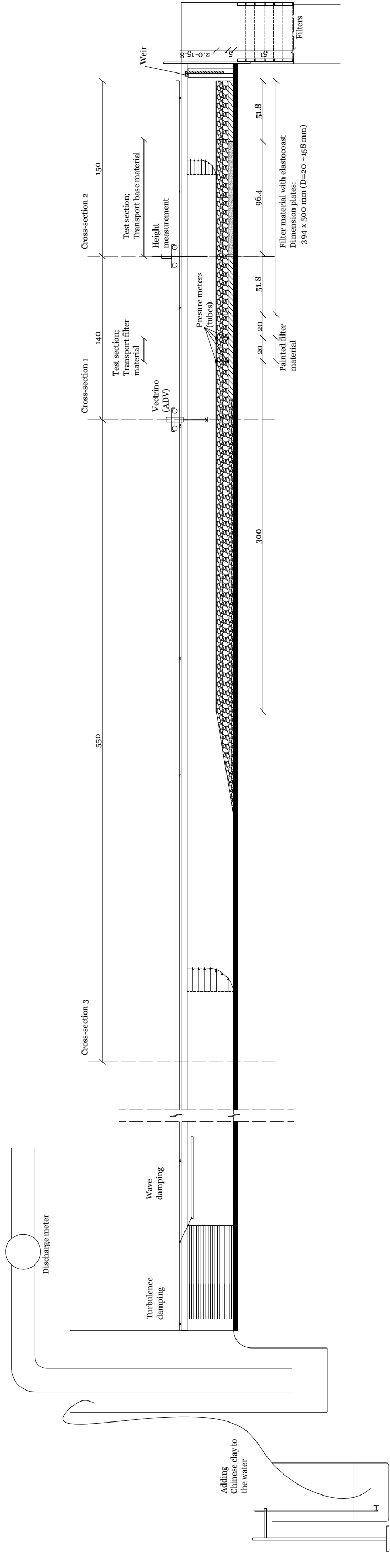


Figure E-1 Design model test (dimensions in cm)



# F RESULTS MODEL TESTS

In this appendix the results of each test are briefly presented.

## F.1 TEST T01

The first test was a test with relatively small filter material (in relation to the other tests), resulting in the smallest ratio between filter and base material. This lay-out was tested with five different load conditions. With an increasing discharge from condition one to five.

After the series of load conditions clear transport of filter material was visible (see Figure F-1), while hardly any transport of base material was measured. The measurements of base and filter material transport are given in Figure F-2.

To create a situation with simultaneous erosion a filter layer with a smaller layer thickness should be created. But from a practical point of view it was not possible to create filter layers with a layer thickness smaller than 20 mm.

Test T01	
Base material	m32
Filter material	Yellow Sun 8-11
$D_f$	20 [mm]
$D_f / d_{f15}$	2.70 [-]
$D_f / d_{f50}$	2.33 [-]
$d_{f50} / d_{b50}$	27.73 [-]
$\frac{d_{f50}}{d_{b50}} \frac{\Delta_f}{\Delta_b} \frac{\Psi_{c,f}}{\Psi_{c,b}} \frac{1 - \gamma V_{Gf}}{1 - \gamma V_{Gb}}$	45.63 – 58.08*1 [-]
$u_{c,b}$	> 1.00 [m/s]
$u_{c,f}$	~ 0.65 [m/s]

\*1: The upper and lower limit, determined by the stability parameter for phase 1 and phase 6 (see paragraph 3.2.4, Figure 3-3)

**Table F-1 Data test T01**



**Figure F-1 Transported filter material, test T01 (black arrow indicates main flow direction)**

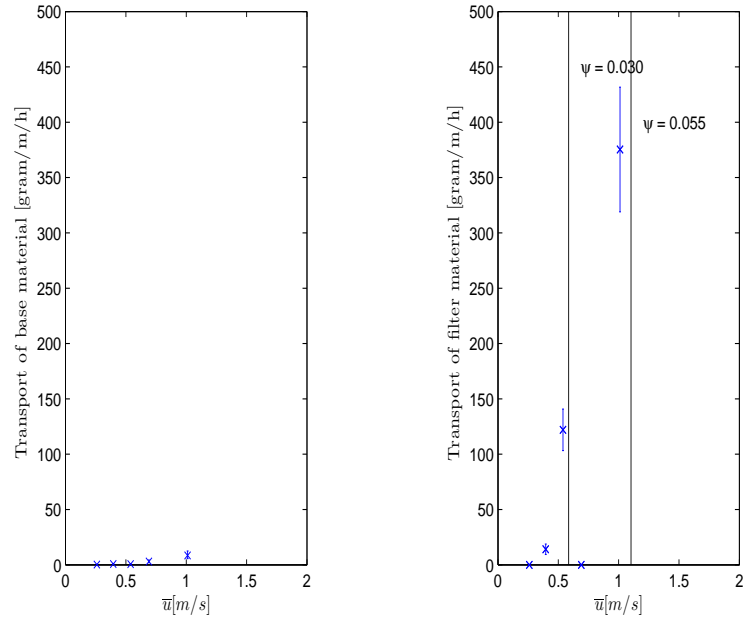


**Figure F-2** Transport of base/filter material vs. average velocity, T01

## F.2 TEST T02

Test T02 is a test with a relative thin filter layer (only 1.44 times the  $d_{f15}$ ). This lay-out was tested twice, where the only difference is the use of elastocoast;

- T02a: the stones above the test section for base material transport are glued together with elastocoast;
- T02b: all the stones are loosely placed (no elastocoast is used).

The results of both tests are given in Figure F-4. In both situations transport of base material is clearly visible, while there is no transport of filter material at all.

Near the weir there is an increased velocity (accelerating flow). The velocity near the bed at this location is significantly larger than in the rest of the flume. Normally the stones are fixed at this location, but during test T02b no elastocoast was used. The stones closest to the weir were washed away, resulting in a retreating filter protection (Figure F-3). Because of this retreating filter construction the filter layer became weaker, which possibly influenced the sediment transport.

Because of the retreating filter protection only four load conditions were tested during test T02b.

Test T02	
Base material	m32
Filter material	Yellow Sun 20-40
$D_f$	27 [mm]
$D_f / d_{f15}$	1.20 [-]
$D_f / d_{f50}$	1.08 [-]
$d_{f50} / d_{b50}$	80.94 [-]
$\frac{d_{f50}}{d_{b50}} \frac{\Delta_f}{\Delta_b} \frac{\Psi_{c,f}}{\Psi_{c,b}} \frac{1-\gamma V_{Gf}}{1-\gamma V_{Gb}}$	136.06 – 173.17*1 [-]
$u_{c,b}$ (test T02a)	~ 0.65 [m/s]
$u_{c,b}$ (test T02b)	~ 0.60 [m/s]
$u_{c,f}$ (test T02a)	> 0.80 [m/s]
$u_{c,f}$ (test T02b)	> 0.60 [m/s]
*1: The upper and lower limit, determined by the stability parameter for phase 1 and phase 6 (see paragraph 3.2.4, Figure 3-3)	

**Table F-2 Data test T02**



Figure F-3 Left: Retreating filter layer test T02b (black arrow indicates main flow direction), Right: Base layer after the test (after removing the filter layer, test T02a)

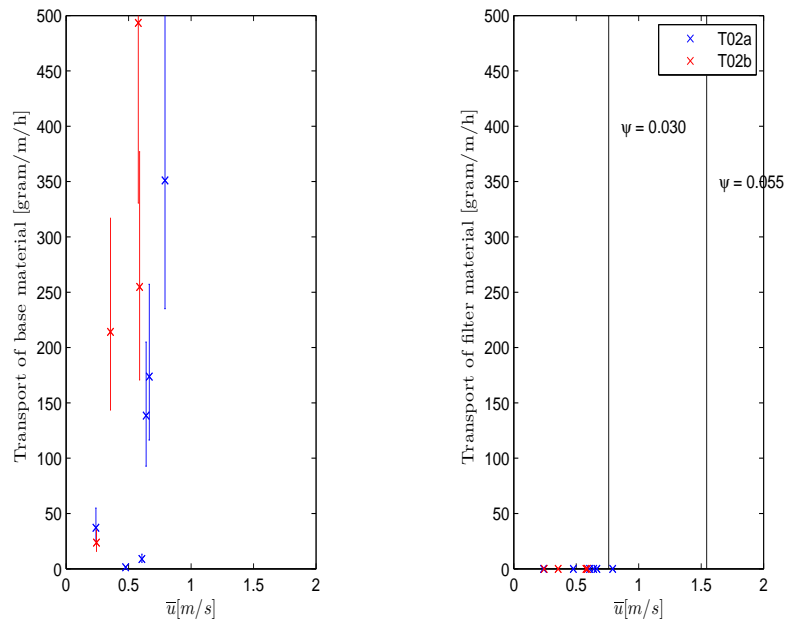


Figure F-4 Transport of base/filter material vs. average velocity, test T02a and T02b

### F.3 TEST T03

For test T03 the same materials were used as for T02, only the layer thickness for T03 was larger. A thicker layer is resulting in a larger damping of load (see chapter 3). This is also visible when the results of T02 (Figure F-4) and T03 (Figure F-5) are compared. The start of base material transport starts at a higher velocity in test T03.

The velocities for which the lay-out is tested are also higher in comparison with test T02. During test T03, both, base and filter material transport was measured. The start of base material and filter material transport starts at almost the same velocity.

Test T03	
Base material	m32
Filter material	Yellow Sun 20-40
$D_f$	61.5 [mm]
$D_f / d_{f15}$	2.74 [-]
$D_f / d_{f50}$	2.46 [-]
$d_{f50} / d_{b50}$	80.94 [-]
$\frac{d_{f50}}{d_{b50}} \frac{\Delta_f}{\Delta_b} \frac{\Psi_{c,f}}{\Psi_{c,b}} \frac{1 - \gamma V_{Gf}}{1 - \gamma V_{Gb}}$	136.06 – 173.17*1 [-]
$u_{c,b}$	~ 0.85 [m/s]
$u_{c,f}$	~ 0.85 [m/s]

\*1: The upper and lower limit, determined by the stability parameter for phase 1 and phase 6 (see paragraph 3.2.4, Figure 3-3)

Table F-3 Data test T03

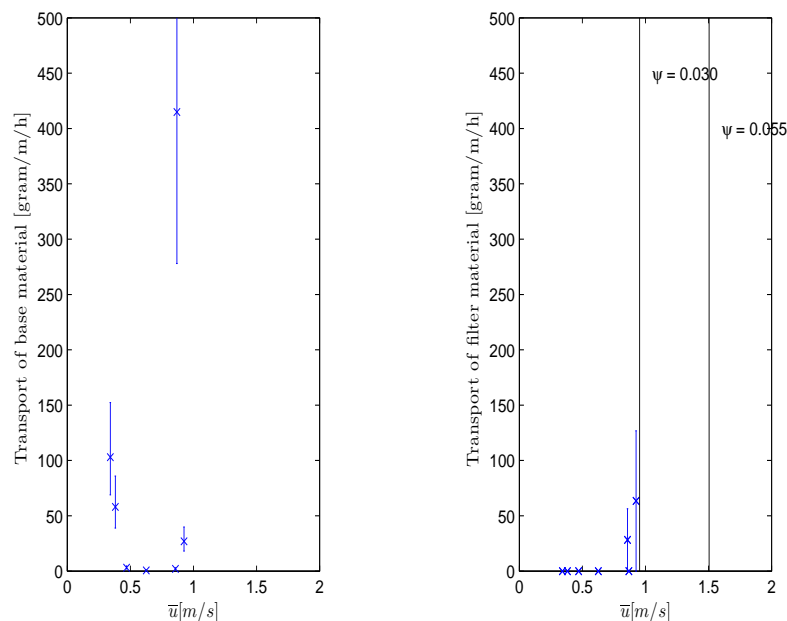


Figure F-5 Transport of base/filter material vs. average velocity, test T03

## F.4 TEST T04

For test T04 a coarser type of sand was used as base material. This in combination with the same filter layer as used in test T02a.

In Figure F-6, both, transport of base and filter material is visible. No large amounts of transport are measured. Because of limitations of the flume the velocity could not be increased any further. This resulted in a final result without significant amounts of transported material.

Test T04	
Base material	0.50 – 0.80
Filter material	Yellow Sun 20-40
$D_f$	27 [mm]
$D_f / d_{f15}$	1.20 [-]
$D_f / d_{f50}$	1.08 [-]
$d_{f50} / d_{b50}$	39.51 [-]
$\frac{d_{f50}}{d_{b50}} \frac{\Delta_f}{\Delta_b} \frac{\Psi_{c,f}}{\Psi_{c,b}} \frac{1 - \gamma V_{Gf}}{1 - \gamma V_{Gb}}$	81.34 – 88.73 <sup>*1</sup> [-]
$u_{c,b}$	~ 0.90 [m/s]
$u_{c,f}$	~ 0.90 [m/s]

<sup>\*1</sup>: The upper and lower limit, determined by the stability parameter for phase 1 and phase 6 (see paragraph 3.2.4, Figure 3-3)

Table F-4 Data test T04

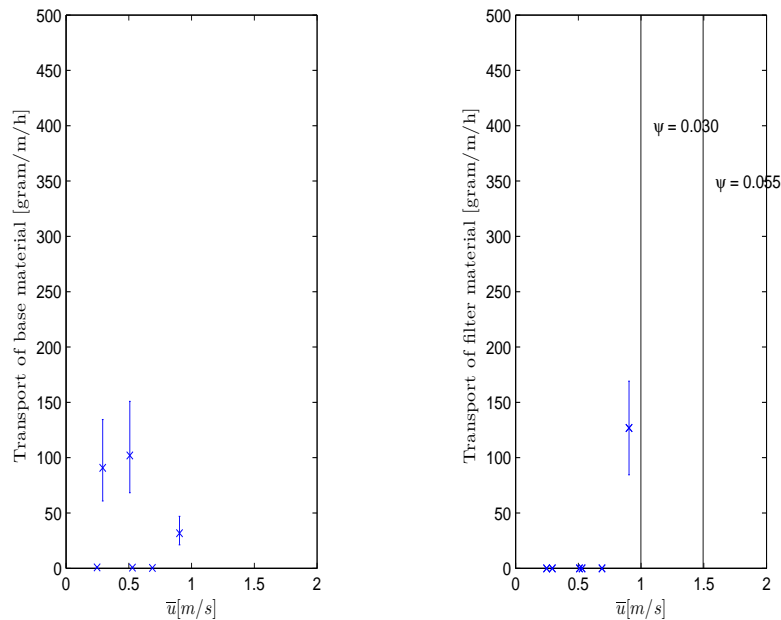


Figure F-6 Transport of base/filter material vs. average velocity, test T04

## F.5 TEST T05

During tests T05 no measurements were obtained. Conclusions are drawn based on visual observations.

For the lay-out of test T05, T06 and T07 the heavy (high density) basalt stones were used. The relative weight of this type of stone is significantly larger compared with the Yellow Sun (see appendix B.2).

As one can imagine, it is hard to create a filter layer with a thickness of about  $0.5 d_{f50}$ . The filter layer thickness was created by filling the filter with sand in such a way that about  $0.5 d_{f50}$  of the filter layer was above the sand material. Within this situation there was no clear distinction between the base and the filter layer. It was more a mixture of sand and stones, which makes this test somewhat out of the scope of this research. When analysing this kind of sand-gravel mixtures other kind of phenomena are playing a role. More information about the behaviour/erosion of sand-gravel mixtures can be obtained from (for example) the research of Wilcock and Crowe [2003].

Within the test it was clearly visible that the filter layer was too thin and erosion of sand (base material) was occurring at a large scale.

Test 05	
Base material	m32
Filter material	Basalt 16-22
$D_f$	8 [mm]
$D_f / d_{f15}$	0.50 [-]
$D_f / d_{f50}$	0.45 [-]
$d_{f50} / d_{b50}$	57.80 [-]
$\frac{d_{f50}}{d_{b50}} \frac{\Delta_f}{\Delta_b} \frac{\Psi_{c,f}}{\Psi_{c,b}} \frac{1-\gamma V_{Gf}}{1-\gamma V_{Gb}}$	116.16 – 147.84*1 [-]

\*1: The upper and lower limit, determined by the stability parameter for phase 1 and phase 6 (see paragraph 3.2.4, Figure 3-3)

**Table F-5 Data test T05**



**Figure F-7 Winnowing (in large quantities) during test T05**

## F.6 TEST T06

The lay-out of test T06 was used for three different tests. The first one (T06a) is a test situation with load conditions comparable with the other tests, the other two (T06b and T06c) are tests with high turbulence levels.

Test T06 resulted in simultaneous erosion of base and filter material. The measured transport is given in Figure F-8.

### High turbulence levels

During the tests T06b (with a sill) and T06c (with piles), erosion of base material occurred after the object had been placed. De results and observations made during test T06b and T06c are described in detail in paragraph 5.4.

Test o6	
Base material	m32
Filter material	Basalt 16-22
$D_f$	40 [mm]
$D_f / d_{f15}$	2.51 [-]
$D_f / d_{f50}$	2.24 [-]
$d_{f50} / d_{b50}$	57.80 [-]
$\frac{d_{f50}}{d_{b50}} \frac{\Delta_f}{\Delta_b} \frac{\Psi_{c,f}}{\Psi_{c,b}} \frac{1 - \gamma V_{Gf}}{1 - \gamma V_{Gb}}$	116.16 – 147.84*1 [-]
$u_{c,b}$ (test T06a)	~ 0.90 [m/s]
$u_{c,f}$ (test T06a)	~ 0.90 [m/s]

\*1: The upper and lower limit, determined by the stability parameter for phase 1 and phase 6 (see paragraph 3.2.4, Figure 3-3)

Table F-6 Data test T06

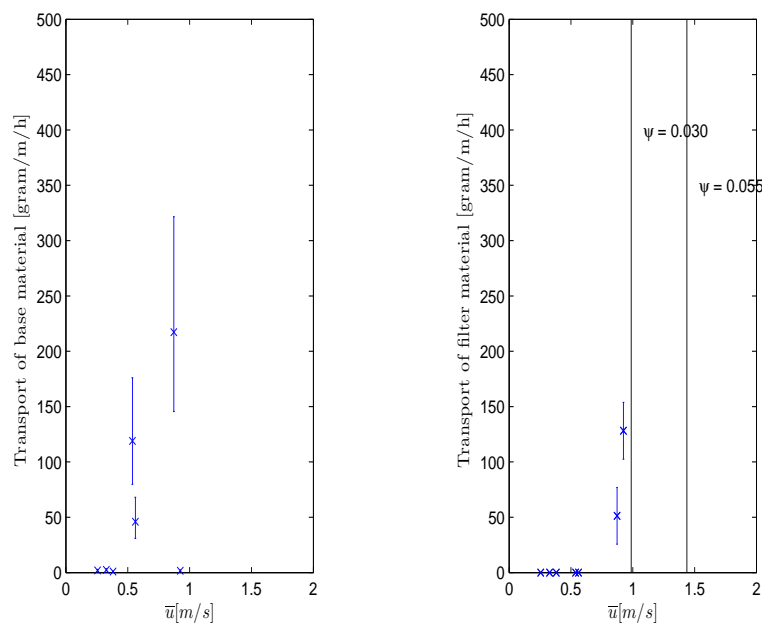


Figure F-8 Transport of base/filter material vs. average velocity, test T06a

## F.7 TEST T07

Test T07 is almost equal to test T06a. During test T07 a thicker filter layer was tested. Whereas during test T06a simultaneous erosion occurred, transport of filter material occurred first during test T07 (see Figure F-9).

Test T07		
Base material	m32	
Filter material	Basalt 16-22	
$D_f$	57	[mm]
$D_f / d_{f15}$	3.58	[-]
$D_f / d_{f50}$	3.19	[-]
$d_{f50} / d_{b50}$	57.80	[-]
$\frac{d_{f50}}{d_{b50}} \frac{\Delta_f}{\Delta_b} \frac{\Psi_{c,f}}{\Psi_{c,b}} \frac{1-\gamma V_{Gf}}{1-\gamma V_{Gb}}$	116.16 – 147.84*1 [-]	
$u_{c,b}$	> 0.95	[m/s]
$u_{c,f}$	~ 0.80	[m/s]
*1: The upper and lower limit, determined by the stability parameter for phase 1 and phase 6 (see paragraph 3.2.4, Figure 3-3)		

Table F-7 Data test T06

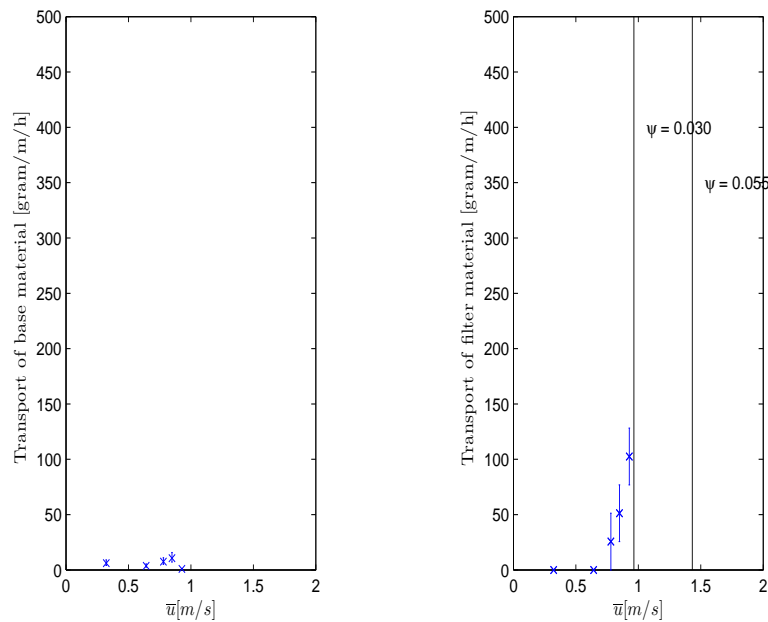


Figure F-9 Transport of base/filter material vs. average velocity, test T07



# G DEVIATION OF TRANSPORT MEASUREMENTS

---

When a certain situation with a certain load condition is tested multiple times, slightly different measurements will be obtained. There are various reasons for this differences. Some reasons;

- The bed/filter layers are not exactly the same. Individual grains are in a (slightly) different position;
- The load condition has a certain deviation;
- Movement of a grain is or is not measured; movement of filter material within the test section is not measured and neither is bed material that is transported but not collected within the sieve (not completely transported till the end of the flume).

Since every combination of test situation and load condition was tested only once, no distribution and mean value of transport can be calculated. The measured amount of transported material can be a mean value or a relatively high or low value. This has to be kept in mind. The measured amounts of transported material should be handled with care.

To take care of the uncertainties within the measurements, deviations in the form of a lower and upper boundary are taken into account. The determination of these boundaries is explained in the next paragraphs.

## G.1 BASE MATERIAL

To determine the deviations of the measurements, one test was repeated multiple times. For this the lay-out of test situation TO2a was used (see Table 4-4).

The repetition of the test was done for two different load conditions. During each of the conditions the flow velocity was kept the same all the time. To prevent deviations within the load conditions the flow was not shut down between the measurements, instead the sieves were placed on top of each other (in the same way it was done during the normal tests (see chapter 4)).

For the determination of the lower and upper limit it is of interest how far away each measurement is from the lowest and highest measured amount of base material transport. The difference is relative to the measurement and can be described by;

$$\sigma = \frac{|A - q|}{q} \quad \text{[G.1]}$$

$\sigma$  : relative difference [%]

$q$  : measured amount of transport

$A$  : mean/min/max value of the measurements

The results of the two series of tests are given in Table G-1 and Table G-2. For both, the situation with the low velocity and the situation with the high velocity, the relative difference between the highest and the lowest measured value is the same. The lowest measured amount of transport is 67% of the highest measured amount. The highest measured amount of transport is equal to 1,48 times the lowest measured amount.

Transport of base material [gram]	Relative difference in comparison with		
	Mean	Min	Max
0.32	9%	9%	34%
0.36	3%	19%	19%
0.43	19%	33%	0%
0.35	0%	17%	23%
0.29	21%	0%	48%

**Table G-1 Deviation of transported base material (average velocity = 0.35 m/s)**

Transport of base material [gram]	Relative difference in comparison with		
	Mean	Min	Max
70.69	22%	0%	48%
84.17	3%	16%	25%
104.81	17%	33%	0%

**Table G-2 Deviation of transported base material (average velocity = 0.65 m/s)**

When in a single measurement a certain amount of sediment transport is measured, it is not possible to determine if this is a relatively low or a relatively high value. So the measurement should be handled as if it is a high measured value to determine the lower boundary and as if it is a low measured value to determine the upper boundary.

Based on the results presented in Table G-1 and Table G-2 the lower and upper boundaries are determined. The boundaries used as a deviation of the measurements are;

- The lower boundary is recorded at 67% of the measured value;
- The upper boundary is recorded at 148% of the measured value.

## G.2 FILTER MATERIAL

The uncertainties about the transport of filter material are much smaller than those of the base material. Within the determination of the lower and upper boundaries a standard deviation of 15% of the measured value is used.

For small amounts of stone transport this deviation can be significantly larger (e.g. between one or two transported stones). To take this into account the determined value for the deviation of filter material transport is rounded up to a whole number of stones.

# H SPECTRAL ANALYSIS

---

The average dimension of the vortexes in the water can be estimated with an autocorrelation of the velocity measurements. The autocorrelation function measures the correlation between observations at different time steps.

A vortex is transported by the average water velocity. As long as the correlation between several lags ( $k$ ) is positive, the fluctuations in those steps have a similar direction. During the time of positive correlation the vortex passes a certain point with a velocity equal to the mean flow velocity.

The size of the vortex can be estimated by multiplying the average velocity with the time the vortex is measured:

$$\lambda = \bar{u} \cdot T \quad [\text{H.1}]$$

The autocorrelation coefficient can be calculated by computing the series of covariance coefficients ( $c_k$ ). The covariance coefficients can be calculated by:

$$c_k = \frac{1}{N} \sum_{t=1}^{N-k} (x_t - \bar{x})(x_{t+k} - \bar{x}) \quad [\text{H.2}]$$

The autocorrelation coefficient ( $r_k$ ) is given by:

$$r_k = \frac{c_k}{c_0} = \frac{\frac{1}{N} \sum_{t=1}^{N-k} (x_t - \bar{x})(x_{t+k} - \bar{x})}{\frac{1}{N} \sum_{t=1}^N (x_t - \bar{x})^2} \quad [\text{H.3}]$$

Within equation [H.2] and [H.3],  $k$  represents the lag. The lag is defined in measurement steps. The velocity is measured with a frequency of 25 Hz, so the length of one time step ( $k=1$ ) equals 0.04 s.

If the autocorrelation coefficient ( $r_k$ ) is calculated for every lag ( $k=0$  to  $k=(\text{length of the signal} - 1)$ ) Figure H-1 can be derived.

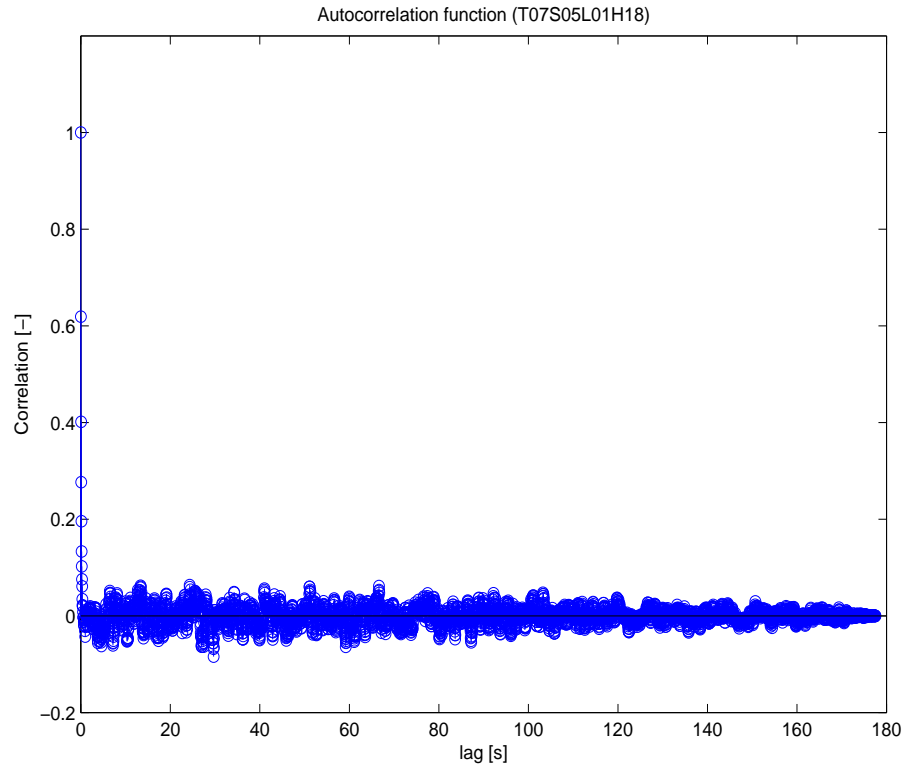


**Figure H-1 Autocorrelation velocity measurement**

At  $k=0$  the autocorrelation coefficient ( $r_k$ ) equals 1 (by definition). Each measurement is always correlated to itself.

If regular sinusoids could be detected it would say something about the sizes of the vortices (e.g. if regular waves would be recognised in the correlation pattern). From Figure H-1 no regular sinusoids could be detected (no regular patterns could be found with Fourier analysis).

Two alternative methods are used to determine the time scale of the vortices (with the time scale of the eddies the average length can be determined (equation [H.1])). The red lines in Figure H-2 represent the two methods.

#### Method 1

This method as described beneath is also used by Schokking [2002] and Van Doorn [2012] to estimate the average size of the vortices.

This first method uses the first two points of the autocorrelation to determine the average duration of an eddy. The gradient through the first two points of the autocorrelation is extrapolated until it crosses the x-axis (Schokking, 2002). This method is visualised with a red line (the red line indicated with method 1) in the more detailed visualisation of the autocorrelation (Figure H-2). The red line from Figure H-2 can be described with the following equation:

$$r = 1 - (r_0 - r_1)k \quad [\text{H.4}]$$

The vortex period is related to the crossing with the x-axis ( $r=0$ ) and can be calculated with the following equation:

$$T = \frac{1}{r_0 - r_1} \cdot \frac{1}{f} \quad [\text{H.5}]$$

### Method 2

A better method is integrating the autocorrelation function. The time scale of large turbulent structures is determined by the integration of the autocorrelation function (Uijtewaal, 2011):

$$T = \int_0^{\infty} r(k) dk \quad [\text{H.6}]$$

The first part of the autocorrelation function is the interesting part. The part with larger lags is of less interest and can result in unwanted deviations in the determination of the time scale. To eliminate the influence of the part with a large lag an exponential function is plotted through the autocorrelation function (red line, indicated by method 2, in Figure H-2). This function has the following shape:

$$r = \alpha e^{-\beta \frac{k}{f}} \quad [\text{H.7}]$$

Integration of this function results in:

$$T = \int_0^{\infty} r(k) dk = \int_0^{\infty} \alpha e^{-\beta \frac{k}{f}} dk = \left[ -\frac{\alpha f}{\beta} e^{-\beta k} \right]_0^{\infty} = \frac{\alpha f}{\beta} \quad [\text{H.8}]$$

The alpha and beta factor in equation [H.7] are different for each analysed measuring signal. These parameters are determined using point  $r_1$  and  $r_2$  (autocorrelations with a lag of 1 and 2 time steps). The function is fitted through those two points.  $r_0$  is not used because of the noise of the instrument that is included in the measuring signal. The noise is correlated to itself but is no longer visible after one time step. By excluding  $r_0$  and normalising the signal to point  $r_1$  the noise is eliminated. Fitting the exponential function, using  $r_1$  and  $r_2$  results in the following representations of alpha and beta parameters;

$$\alpha = \frac{r_1^2}{r_2} \quad [\text{H.9}]$$

$$\beta = -\ln\left(\frac{r_2}{r_1}\right) f$$

With equation [H.8] and the alpha and beta factor [H.9] the time scale is represented by:

$$T = \frac{\alpha f}{\beta} = \frac{\frac{r_1^2}{r_2} f}{-\ln\left(\frac{r_2}{r_1}\right) f} = \frac{r_1^2}{-r_2 \ln\left(\frac{r_2}{r_1}\right)} \quad [\text{H.10}]$$

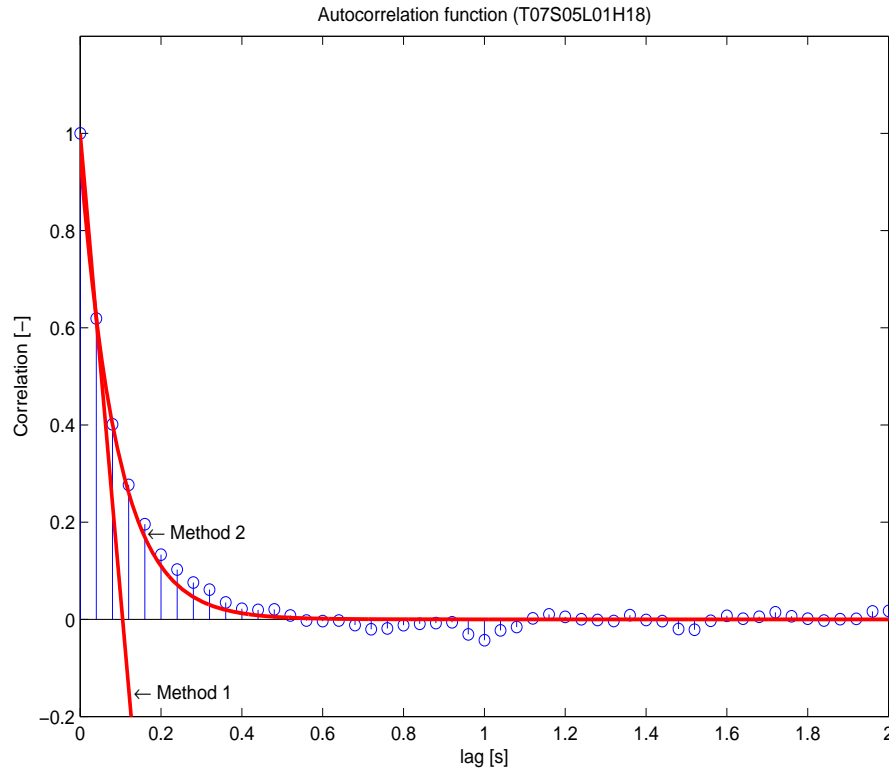


**Figure H-2 Autocorrelation velocity measurement**

With the average velocity of the signal and the period calculated with equation [H.5] or [H.10] the average length of the vortices can be calculated with equation [H.1].

The average length of the vortices is calculated for each measurement record. The distribution of the calculated lengths of the vortices of each measurement signal (excluding test T06b and T06c) is given in Figure H-3 (method 1) and Figure H-5 (method 2). The common length scale of the vortices is about a couple of centimetres. Most of the vortices are in the range from 1 to 10 cm. It is important to keep in mind that these are averaged vortex sizes of a measured dataset and that there are larger and smaller vortices in the flow.

A similar distribution is made for the situations with high turbulence intensities. This distribution is given in Figure H-4 (method 1) and Figure H-6 (method 2) and is based on the measurements downstream of the weir of test T06b. The amount of data available for situations with high turbulence levels is limited and the information within the figures should be handled with care. When assumed that this limited amount of data is a good representation of the real situation, one can conclude that the length scale of the vortices is in the same order of magnitude as the height of the weir (which was 6,5 cm).

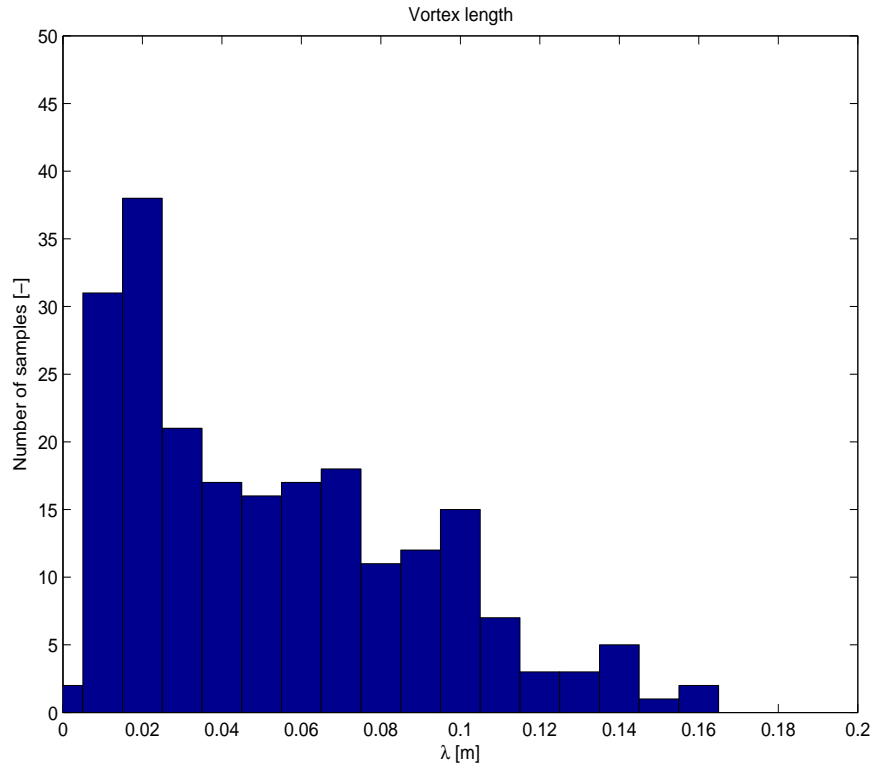


**Figure H-3 Distribution of the length scale, method 1 (based on 219 measurements)**

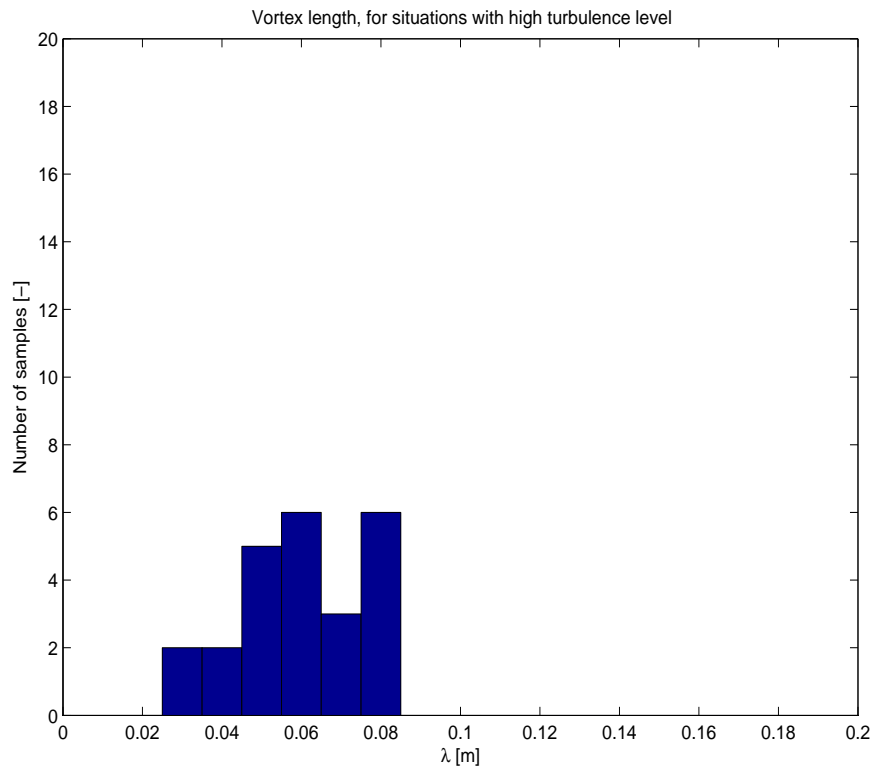


**Figure H-4 Distribution of length scale for situations with high turbulence levels, method 1 (based on 24 measurements)**

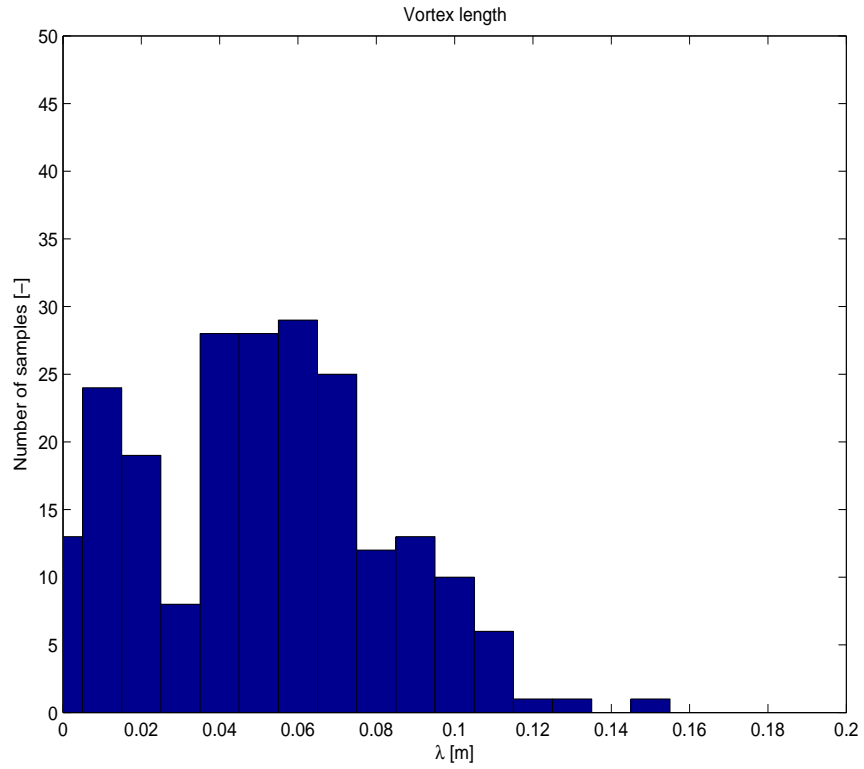


**Figure H-5 Distribution of the length scale, method 2 (based on 219 measurements)**

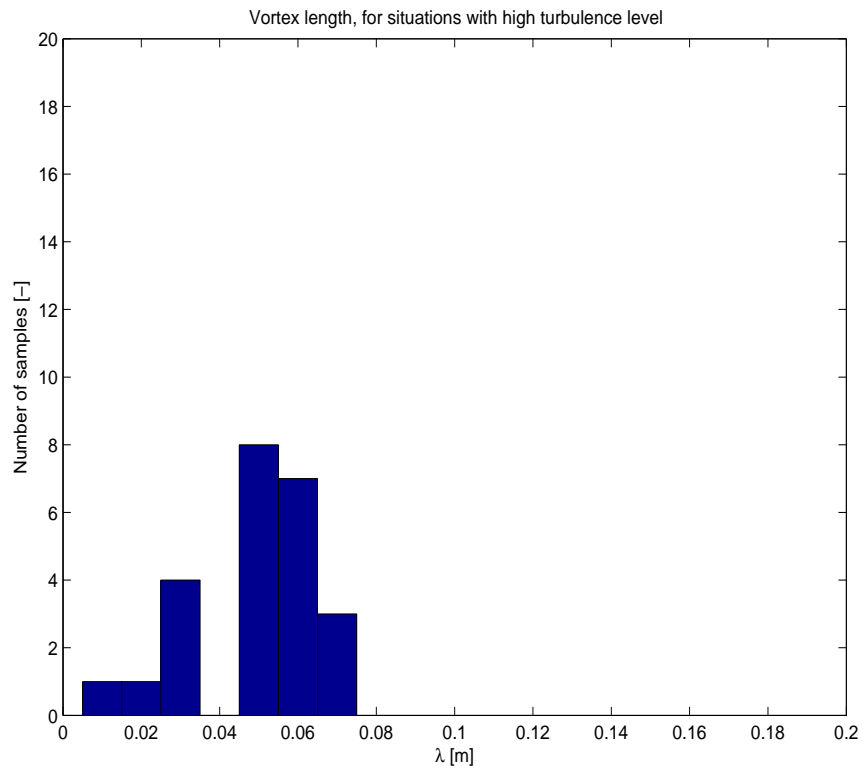


**Figure H-6 Distribution of length scale for situations with high turbulence levels, method 2 (based on 24 measurements)**



**2012**

**Stefan van de Sande**

---

